The Dissertation Committee for Victoria Phuong Le Certifies that this is the approved version of the following Dissertation:

Syndecan-1 in Vascular Mechanosensing

Committee:

Aaron B. Baker, Supervisor

Ernst-Ludwig Florin

Jeanne Stachowiak

Laura Suggs

John Wallingford

Syndecan-1 in Vascular Mechanosensing

by

Victoria Phuong Le

Dissertation

Presented to the Faculty of the Graduate School of

The University of Texas at Austin

in Partial Fulfillment

of the Requirements

for the Degree of

Doctor of Philosophy

The University of Texas at Austin

August 2019

Dedication

For my husband.

Acknowledgements

I would like to thank my mom and stepdad for their immeasurable support and encouragement throughout my academic endeavors. I thank my best friend and husband, Luís, for his love, companionship and unwavering belief in me. I thank my mentor, Dr. Aaron Baker, for welcoming me to his lab and giving me such unique research opportunities. I also thank Dr. Ernst-Ludwig Florin, Dr. Jeanne Stachowiak, Dr. Laura Suggs and Dr. John Wallingford, who have generously shared their time with me as members of my dissertation committee. They have been instrumental to the progress of my research. Also deserving of recognition and thanks for sharing their expertise are Ms. Chi Zhao, Dr. David Busch, along with the heroic undergraduate students who helped me along the way (Varun Koneru, Colton Edwards, Ameya Bhat, Estela Rojas and Sebastian Salvador). My colleagues in Dr. Baker's lab, past and present, deserve much praise for their camaraderie and senses of humor. Dr. Jessica Wagenseil, my first mentor: thank you so much for helping me find my voice. Finally, I would like to express gratitude to Laika (my Starry Messenger) for being a constant example of how to find joy in discovering the little things.

Abstract

Syndecan-1 in Vascular Mechanosensing

Victoria Phuong Le, Ph.D.

The University of Texas at Austin, 2019

Supervisor: Aaron B. Baker

The cells of vascular tissues are subject to biophysical and biochemical cues from their microenvironment. These cues are relayed to cells via adhesion receptors on the cell surface to components of the extracellular matrix, cytoskeleton-linked proteins and stretch-sensitive ion channels. These cues can influence cell alignment, morphology, proliferation and differentiation. A major challenge in engineering materials for vascular grafts is to understand and harness the mechanosensory mechanisms of cells to develop more effective therapies. Syndecan-1 is a transmembrane cell surface proteoglycan that has been shown to play a role in flow sensation in the glycocalyx of arteries, affecting endothelial cell proliferation and phenotype. Because of its interactions with cytoskeletal and focal adhesion associated proteins, it may serve as a mechanosensor for substrate-mediated cues. To date, the mechanisms of mechanical environment sensation through syndecan-1 are not well understood. This work tests the hypothesis that syndecan-1 is a key molecule in vascular cell mechanosensing and phenotype switching. We examine how cellular mechanosensing and adaptation to surfaces of various stiffness and nanotopography are

affected by syndecan-1. We determine what players of cytoskeletal rearrangement and nanotopography sensation are affected by syndecan-1 in this context. We also developed FRET-based syndecan-1 tension sensors to visualize syndecan-1 activation during mechanosensation and determine what domains of syndecan-1 are important to its mechanosensory function in vitro. Our findings demonstrate that syndecan-1 tension is modulated by substrate- and shear-stress-mediated cues.

Table of Contents

List of Tables

List of Figures

Chapter 1. Introduction

1.1 MOTIVATION

A major challenge in engineering biomaterials is to create substrates that are designed to produce desired behaviors and phenotypes in endogenous or delivered cells. Vascular bypass grafting, which is performed in approximately 600,000 patients per year in the US, is an important area for the application of engineered biomaterials. In situations where autogenous vascular substitutes are unsuitable, unavailable or risky for the patient, artificial grafts have been utilized, but the materials used for these grafts generally perform poorly for vascular grafts of diameters less than 6 mm. Such grafts are often at risk for thrombosis or differ too greatly in mechanical behavior compared to endogenous vessels.(Abbott, Megerman, Hasson, L'Italien, & Warnock, 1987; Greisler, 1990) When synthetic vascular grafts are implanted, endogenous endothelial cells interact with the biomaterials to colonize the vascular graft and re-endothelialize the blood-graft interface.(Dixit, Hern-Anderson, Ranieri, & Schmidt, 2001) The biophysical cues provided by the biomaterials profoundly alter the cells behavior and can lead endothelial cells to adopt a dysfunctional and inflammatory phenotype.(Wood et al., 2011)

The cells of vascular tissues are subject to biophysical and biochemical cues that serve as powerful regulators of homeostasis and disease processes.(Hahn & Schwartz, 2009; Lu & Kassab, 2011) These mechanical cues are sensed by many mechanisms including cell surface receptors, stretch sensitive ion channels and cytoskeleton-linked proteins.(Luo, Mohan, Iglesias, & Robinson, 2013) In therapeutic applications, a key

challenge is the development of engineered materials that can harness the curative effects of endogenous or delivered cells to enable the maximal therapeutic benefit from the implanted material. It is increasingly recognized that mechanical cues including substrate rigidity(Discher, Janmey, & Wang, 2005; Engler, Sen, Sweeney, & Discher, 2006; Swift et al., 2013) and the presence of nanotopological features(Dalby, Gadegaard, & Oreffo, 2014; D. H. Kim, Provenzano, Smith, & Levchenko, 2012b) in the cell microenvironment can profoundly alter cell behavior and differentiation. The main motivation of this work is to contribute to the understanding of how vascular cells sense and respond to mechanical cues, including those presented by engineered materials. Our hope is that the findings of this research contribute to the scientific understanding of the mechanobiology of cell-biomaterial interactions and provide some insights into how materials can be designed to use these effects to enhance therapies including synthetic vascular grafts.

Previous work from our group demonstrated that syndecan-1 (SDC1) has a role in controlling endothelial phenotype in response to hemodynamic forces and vascular smooth muscle cell differentiation.(Voyvodic et al., 2014) (Chaterji, Lam, Ho, Proske, & Baker, 2014) However, our knowledge of how SDC1 is involved in sensing these forces, what these forces are and how the absence of SDC1 affects the cell's sensation of its environment is very limited. The first objective of this research was to examine the role of SDC1 in sensing substrate stiffness and nanotopography of engineered materials. The second objective was to develop a FRET-based SDC1 tension sensor that could be used to investigate the response of SDC1's extracellular domain during cellular interactions with

substrates, utilizing the TSMod FRET tension sensing module.(Grashoff et al., 2010a) We developed a SDC1 tension sensor (SDC1-TS) and three mutant versions of the SDC1-TS to investigate the roles of the SDC1 ectodomain, glycosaminoglycan chains and cytoplasmic domain in SDC1 tension propagation. Our work demonstrated that tension on SDC1 decreases in response to decreased substrate compliance and that tension on SDC1 is higher in regions of cellular adhesion. Additionally, we found that tension on SDC1 can be modulated by nanotopography and that the ectodomain plays an important role in this response. Finally, the third objective was to elucidate the mechanisms of SDC1 tension propagation. Our work indicates that the αV integrins influence SDC1 tension and that SDC1 is responsive to shear stress.

1.2 THESIS ORGANIZATION

In Chapter 1, the motivation for this dissertation study was discussed. The background and previous work that informed this research is discussed in Chapter 2. Chapter 3 describes the role of SDC1 in mechanosensing substrate cues. Chapter 4 describes the design and validation of a FRET-based SDC1 tension sensor, as well as an exploration of SDC1 tension in response to engineered substrates. The tension sensors developed in Chapter 4 are used to elucidate the mechanisms of SDC1 tension propagation and the response of SDC1 tension during shear stress, described in Chapter 5. Conclusions resulting from this research and an exploration of potential future work are discussed in Chapter 6.

Chapter 2. Background

2.1 Overview of Cellular Mechanotransduction

Cells are constantly bombarded with biophysical cues. These cues are converted into biochemical signals that affect a number of processes, from development and cellular homeostasis to cardiovascular disease and cancer progression.(Hahn & Schwartz, 2009; Lu & Kassab, 2011; N. Wang, 2017) Cues from the extracellular matrix (ECM), in particular, can influence cell alignment, morphology, proliferation and differentiation (Kim, Provenzano, Smith, & Levchenko, 2012). Much interest exists in the identification of the players in mechanotransduction. To date, cell surface receptors, stretch sensitive ion channels and proteins linked to the cytoskeleton have been identified, but for many of these putative mechanosensors, little is understood about the mechanisms through which they transmit mechanical signals into cells to affect signaling and gene expression.(Luo et al., 2013)

At the onset of integrin interactions with the ECM, integrins are activated and cluster, recruiting focal adhesion kinase (FAK). During integrin activation, conformational changes occur on integrins, whose identity and specificity come from the combination of various α and β subunits. Mechanical cues received by the integrins are then relayed to the cytoskeleton via proteins such as talin, vinculin and paxillin. From there, actin assembly is regulated.(Martino, Perestrelo, Vinarsky, Pagliari, & Forte, 2018) Adding to the complexity of focal adhesions are the transmembrane proteins, such as the syndecans, that associate with both integrins and the ECM on the extracellular side.

2.2 SYNDECAN-1

Syndecans, from the Greek *syndein* "to bind together," are single-pass transmembrane proteins known for their binding of growth factors, interactions with the cytoskeleton and direct binding of the extracellular matrix via covalently bonded proteoglycans.(Bernfield et al., 1992) The syndecans share a number of characteristics. They possess a short cytoplasmic domain, comprised of two conserved regions and one variable region. The highly conserved transmembrane domain is followed by an ectodomain, which varies in size and composition with syndecan type.(Woods, 2001) Attached to the core ectodomain are glycosaminoglycan (GAG) chains: heparan sulfate chains (found on syndecans 1, 2, 3 and 4) and chondroitin/dermatan sulfate (found on syndecans 1 and 3). The four syndecans are believed to be present in all tetrapods.(Chakravarti & Adams, 2006)

Syndecan-1 (SDC1) is found on endothelial cells,(Voyvodic et al., 2014) vSMCs(Chaterji, Lam, et al., 2014), epithelial cells(Hayashida, Johnston, Goldberger, & Park, 2006) and macrophages.(Angsana et al., 2015) It is one of the most numerous proteins that comprise the endothelial glycocalyx, along with Syndecan-4.(B. M. Fu & Tarbell, 2013) The GAG chains present on SDC1's extracellular domain bind members of the ECM directly via the heparin-binding domains present on the ECM. SDC1possesses a docking site for integrins αVβ3 and αVβ5, which it can activate.(Mattson, Turcotte, & Zhang, 2017; Rapraeger, 2013) The consequences of such activation include cell spreading and migration.(Morgan, Humphries, & Bass, 2007)

Syndecan-1 has been implicated in a number of normal processes, as well as disease processes. Interactions of its GAG chains with growth factors and extracellular adhesion proteins are known to be involved in development.(Jenkins, Horst, Lancaster, & Mythreye, 2018) SDC1 has also been identified as having contradictory roles in cancer, suppressing and inducing apoptosis in cancer cells, and regulating other processes, including angiogenesis, metastasis and proliferation.(Khotskaya et al., 2009; Mythreye & Blobe, 2009) Soluble SDC1 (sSDC1) can deliver growth factors to neighboring cells upon proteolytic cleavage of the ectodomain. This was observed in cultured myeloma cells, in which sSDC1 in the culture medium transported growth factors to the nucleus of stromal cells (Stewart, Ramani, & Sanderson, 2015)

2.3 VASCULAR SMOOTH MUSCLE CELL MECHANOTRANSDUCTION

Vascular smooth muscle cells (vSMCs) form aligned, helical layers within the medial layer of blood vessels. Normal vSMCs have high expression levels of contractile proteins, such as calponin and SM22α, and reduction of their expression is indicative of maladaptive vSMC dedifferentiation into a more migratory and proliferative state. vSMC contractility contributes to arterial contraction and relaxation. They are also influenced and remodeled by circumferential stretch, shear stress, transmural pressure and biophysical cues relayed from the extracellular matrix.(Ahmad, Osborne, & Bendeck, 2007; Haga, Li, & Chien, 2007; Wolinksy & Glagov, 1967; Ye, Nesmith, & Parker, 2014). Cumulatively, these cues activate signaling pathways that control the behavior of vSMCs, with cyclic stretch has the greatest impact. Loss of vSMC contractility has potentially catastrophic

consequences for the aorta, such as weakening of the aortic wall, followed by aortic dissection.(Huang et al., 2010; Lesauskaite et al., 2001)

Integrins play a major role in the mechanotransduction of cyclic stretch in vSMCs, mediating activation of the JNK pathway.(Katsumi, Naoe, Matsushita, Kaibuchi, & Schwartz, 2005) Stretch has also been shown to affect the affinity of integrins. For example, integrin αVβ3 affinity for ECM binding in response to stretch.(Katsumi et al., 2005) Substrate stiffness is known to increase the presence of F-actin bundles in the focal adhesions of vSMCs and substrate topography has been shown to influence vSMC alignment.(Chaterji, Kim, et al., 2014; Peyton & Putnam, 2005).

2.4 Endothelial Shear-Mediated Mechanotransduction

In the vascular system, endothelial cells are found in the intimal layer, forming the endothelium, which interfaces directly with blood flow. The movement of blood through blood vessels produces fluid shear stress parallel to the intimal layer, which can be laminar or oscillatory in nature. While endothelial cells are subject to shear stress that is normal to their function, aberrant hemodynamic flow can contribute to disease states, such as atherosclerosis, which arise from the maladaptive response of endothelial cells. Regions of the vascular tree that tend to experience more oscillatory flow, such as the branch points of the aorta, are prone to developing atherosclerotic plaques, and in animal models of atherosclerosis, atherosclerotic plaque formation has been induced by the surgical perturbation of blood flow. These findings suggest that endothelial cells perceive shear stress via a mechanosensor or several.

To date, the glycocalyx, of which SDC1 is a part, has been suggested as possessing a shear stress mechanosensation role, but other proteins have been implicated, as well. Platelet endothelial cell adhesion molecule-1 (PECAM-1), which is involved in the junctional interactions between endothelial cells, have been shown to respond to shear stress, mediating alignment, and Akt phosphorylation.(Tzima et al., 2005) PECAM-1 and ERK phosphorylation have been induced following direct force exertion onto PECAM-1 via magnetic bead experiments.(Osawa, Masuda, Kusano, & Fujiwara, 2002) Additionally, when endothelial cells expressing a PECAM-1 tension sensor were exposed to shear stress, tension was found to increase on PECAM-1 at the cell-cell junctions, while non-junctional PECAM-1 tension was unchanged.(Conway et al., 2013)

VE-Cadherin has also been identified as a potential mechanosensor or at least an adaptor to a mechanosensor of shear stress. Loss of VE-Cadherin leads to the abolishment of integrin activation under shear stress and direct force application on VE-Cadherin via magnetic beads leads to changes in the actin cytoskeleton and increased cell stiffness.(Barry, Wang, & Leckband, 2015; Tzima et al., 2005) A VE-Cadherin FRET tension sensor demonstrated that under static conditions, junctional VE-Cadherin tension is higher within cell-cell junctions than elsewhere on the cell and decreases in response to shear stress.(Conway et al., 2013) VEGFR3 has been suggested as a mechanosensor of shear stress magnitude. Endothelial cells vary in their sensitivity to shear stress, depending on their location in the vascular tree, and some evidence exists for VEGFR2 and VEGFR3 in tuning this sensitivity.(Baeyens et al., 2015)

What senses shear stress at the surface of an endothelial cell? As a component of the flow-interfacing glycocalyx, SDC1 is an appealing candidate. Our group found that knockout of *SDC1* reduced the shear-stress-induced phosphorylation of Akt and spatial distribution of paxillin phosphorylation in endothelial cells. Knockout of *SDC1* also reduced the shear-stress-induced activation of RhoA.(Voyvodic et al., 2014) A criticism of previous efforts to identify SDC1 as a mechanosensor is that the signaling pathways affected by loss of SDC1 are also downstream of integrin activation, necessitating the parsing of SDC1 and integrin roles.(Givens & Tzima, 2016) However, SDC1's direct association with the cytoskeleton via its cytoplasmic domain suggests that forces exerted on SDC1 could be transmitted to the cytoskeleton. More than one shear stress mechanosensor may exist.

2.5 MICRO- AND NANOPATTERNED SUBSTRATES

In vivo, topography is presented to the cells via ECM proteins of the basement membrane and encompasses a range of sizes.(Gray & Stroka, 2017) Collagen fibrils, which possess diameters of 20-200 nm , can direct the migration and polarity of cells.(H. N. Kim et al., 2013) Collagen fibrils can also organize into collagen fibers, which are several microns in diameter. Thus, significant interest exists in tissue engineering to design nano- and microtopography that maintains or induces desired behaviors in cells. Engineered materials featuring micro- and nanotopography have been employed to manipulate cell adhesion, migration, differentiation, morphology, and a host of other characteristics, with the underlying aim of improving engineered tissues. A number of material variables can

be adjusted to achieve these influences: stiffness, chemistry, ECM coatings, feature size and others. Many geometries are possible, from pits and pillars to fibers, grooves to dots, to name a few.

In the medial layer of blood vessels, vascular smooth muscle cells are surrounded by elastin and collagen and elongated in a helical pattern. The elongation of smooth muscle cells is important not only for their contractility, but also the maintenance of the inner diameter of blood vessels and blood pressure.(H. N. Kim et al., 2013) Nanogrooved poly(methyl methacrylate) and poly(dimethylsiloxane) substrates were shown to induce the alignment and elongation of smooth muscle cells while reducing their proliferation.(E. Yim et al., 2005) Work from our own group found that the combination of increased substrate stiffness and nanopatterning upregulated the expression of RhoA, Rock1 and Rock2. Nanopatterning in the absence of a substrate with optimal stiffness increased vascular smooth muscle cell contractility. In general, nanopatterning also downregulated the expression of inflammatory markers.(Chaterji, Kim, et al., 2014)

Nanopatterns have been shown to impart more physiologically-relevant mechanical properties to vascular cells. vSMCs were cultured on poly(N-isopropylacrylamide) nanogrooves to induce alignment and then detached as a sheet. They demonstrated a maximum tensile stress similar to that of blood vessels, while cells cultured on flat substrate markedly lower maximum tensile stress.(Zorlutuna, Elsheikh, & Hasirci, 2009) Nanogrooved collagen films aligned endothelial cells and also improved their adherence under 10-20 dynes/cm2 shear stress.(Zorlutuna et al., 2009)

2.6 FRET TENSION SENSORS

Forster Resonance Energy Transfer (FRET) has become an important tool for the study of mechanotransduction, enabling the creation of molecular-scale tension sensors. Here, single-molecular fluorescence force spectroscopy will be discussed. In general, intramolecular FRET tension sensors consist of a pair of fluorophores joined by a connector of characterized force sensitivity. The fluorophores overlap in excitation and emission spectra such that excitation of the donor fluorophore results in the resonant transfer of energy to the acceptor fluorophore. As a consequence, the acceptor fluorophore emits light upon excitation of the donor in a manner that scales with the distance between the two fluorophores.(Aoki, Kamioka, & Matsuda, 2013) In theory, a FRET tension sensor of the appropriate force sensitivity can be introduced into a protein of interest to measure the forces exerted on that protein. As the distance between the fluorophores increases, the efficiency of FRET decreases, implying tension on the sensor.

The foundation of an intramolecular FRET tension sensor is the linker that joins the donor and acceptor fluorophores, as it is the force sensitivity of the linker that is used to measure force within the protein containing the module. Another characteristic that is relevant to the performance of FRET linkers is their resistance to hysteresis. Two FRET linkers that have been used in existing FRET tension sensors include stFRET (a coiled-coil spring) and TSMod (a random coil flagelliform) of TSMod. The random coil flagelliform of TSMod consists of 40 amino acids [$(GPGGA)_8$] and is derived from spider silk protein. This linker was characterized using optical tweezer calibration to have 1-6 pN sensitivity. In some works, “TSMod” refers to any tension-sensing module. In this dissertation,

"TSMod" refers to the specific random coil flagelliform used by Grashoff and colleagues. TSMod was also used in the talin, E-Cadherin, PECAM-1, β-spectrin and mucin-1 tension sensors, as well as the SDC1 tension sensor developed in this work. (Borghi et al., 2012; Conway et al., 2013; Grashoff et al., 2010a; Kumar et al., 2016a, 2016b; Paszek et al., 2014)

Another consideration that is important to the design of a FRET tension sensing module is the selection of a pair of fluorophores. The donor emission and acceptor excitation spectra of the fluorophores must overlap strongly.(Day, Booker, & Periasamy, 2008) The fluorophores should be photostable, possess sufficient brightness and have minimal direct effects on the health of the cells that express them. Additionally, the Förster radius (radius at which 50% FRET occurs) should be low. The need for those characteristics has led to the identification of cyan fluorescent protein (CFP) and yellow fluorescent protein (YFP), and their derivatives, as a highly suitable FRET pair in living cells.(Bajar, Wang, Zhang, Lin, & Chu, 2016) One example of an optimized derivative of CFP is teal fluorescent protein (mTFP1).(Ai, Henderson, Remington, & Campbell, 2006) mTFP1. Compared to ECFP, mTFP1 has a narrower emission profiler, reducing bleed-through. Other desirable characteristics include its high quantum yield and decreased sensitivity to photobleaching, compared to ECFP.(Ai et al., 2006) Mutations in YFP leading to improved acid sensitivity and quenchability by chloride ions led to the development of Venus.(Nagai et al., 2002) A mutation in Venus conferred a reduction in the dimerization of Venus and resulted in Venus A206K.(Zacharias, Violin, Newton, &

Tsien, 2002) mTFP1 and Venus are the donor-acceptor FRET pair used in TSMod.(Grashoff et al., 2010a)

Several tension sensors have been developed for use as molecular force transducers, including stFRET and sstFRET, which are coiled-coil springs and TSMod, a random coil flagelliform. TSMod is the sensor used in the vinculin, talin tension sensor, as well as the SDC1 tension sensor developed in this work. (Grashoff et al., 2010a; Kumar et al., 2016a, 2016b)

A number of techniques can be used to measure FRET. In fluorescence lifetime imaging (FLIM), the lifetime of the donor fluorophore is measured. As the donor is quenched by the presence of the acceptor, its lifetime is affected; close proximity between the donor and acceptor results in a shortened donor lifetime.(Swift et al., 2013) This method is considered the most quantitative method. Sensitized emission, the method used in this work, is intensity-based. In this technique, the intensity of the acceptor's emission under donor excitation is influenced by its proximity to the donor. This method requires evaluation of the direct excitation of the acceptor by the donor's excitation using bleed-through (acceptor-only and donor-only) controls.(Hachet-Haas et al., 2006) The main shortcoming of this method is the fact that it is intensity-based. Intensity-based imaging is subject to the influence of the concentration of fluorophores. However, it has been shown that FRET efficiencies obtained from sensitized emission are similar to those obtained using FLIM.(Krieg, Dunn, & Goodman, 2014)

2.7 SYNDECAN-1 KNOCK-OUT MICE

Vascular smooth muscle cells were harvested from the aortae of wild-type and syndecan-1 knockout (S1KO) littermates from a C57BL/6J background. Early characterization of S1KO mice revealed that loss that SDC1 did not cause morphological defects, although impaired would healing was observed.(Alexander et al., 2000; Stepp et al., 2002) S1KO mice have been utilized by our group in the past for study of SDC1 in the context of vSMCs and endothelial cells, (Chaterji, Lam, et al., 2014; Voyvodic et al., 2014) as well as in the work discussed in Chapter 4 of this dissertation.(Le et al., 2018)

Chapter 3. Syndecan-1 in Mechanosensing of Nanotopological Cues in Engineered Materials

3.1 INTRODUCTION

Cell therapies have great potential to improve the quality of life of countless patients with incurable diseases or severe injury. By their active nature, cell therapeutics can adapt and integrate into host tissues to perform functions not possible with drugs or protein therapeutics. A major component of enabling effective cell therapies is the use of scaffolds or delivery systems that support the function and phenotype of the cells once delivered.(Chan & Leong, 2008) In such engineered scaffolds, a key challenge is the development of engineered materials that can potentiate the curative effects of endogenous or delivered cells to enable the maximal therapeutic benefit from the implanted material.(Dang & Leong, 2007) Such instructive scaffolds or templates can recapitulate the cell-cell, cell-ECM, and cell-soluble factor signaling to orchestrate a therapeutic effect.(Lutolf & Hubbell, 2005) Only when facilitated by such an appropriate scaffold or carrier can cell-based therapies, such as those used in osteoarthritis(Diekman & Guilak, 2013) or in cardiac or vascular repair,(Lin et al., 2012) truly transform the landscape of tissue engineering.(Hill, Boontheekul, & Mooney, 2006; Karp & Langer, 2007) While there is much information on the use of chemical and biochemical signals to enhance engineered biomaterial function, the effects of physical forces and the mechanisms of

---

Le, V., Lee, J., Chaterji, S., Spencer, A., Liu, Y. L., Kim, P., Yeh, H.C., Kim, D.H., Baker, A. B. (2018). Syndecan-1 in mechanosensing of nanotopological cues in engineered materials. *Biomaterials, 155*, 13-24. Victoria Le performed the majority of the research and analysis and authored a proportion of the manuscript.

mechanosensing of nanomechanical cues remain poorly defined and have begun to emerge as critical parameters in nanomaterial design.

In particular, vascular tissue engineering has made great strides towards recreating artificial blood vessels to treat a variety of cardiovascular conditions, ranging from myocardial infarction and ischemia to peripheral vascular disease and wound healing after vascular injury.(Hoenig, Campbell, Rolfe, & Campbell, 2005; Lesman, Gepstein, & Levenberg, 2010; Patterson et al., 2012; Shin'oka, Imai, & Ikada, 2001) In the bench to bedside translation of engineered blood vessels, the importance of vascular integrity and the ability of vascular smooth muscle cells (vSMCs) to impart long-term stability to the engineered vessels is a key factor.(Frontini et al., 2011; Murakami & Simons, 2009; Samuel et al., 2013) The vSMCs populate the medial layer of blood vessels and are present in multiple layers embedded in the basement membrane, which consists of fibrillar collagens and elastin.(Ahmad et al., 2007; Wolinksy & Glagov, 1967) The cells are organized in an aligned helical pattern around the blood vessel circumference with the successive vSMC layers demonstrating alternating pitch directions.(Isenberg & Wong, 2006) Within this structure, organized extracellular matrix (ECM) molecules provide mechanical stability to the cells as well as biophysical and biochemical cues within the vascular "niche."(Nikolova, Strilic, & Lammert, 2007) On a biophysical level, the underlying ECM in the blood vessel provides nanotopological cues with feature sizes from tens to several hundreds of nanometers.(G. Abrams, Schaus, Goodman, Nealey, & Murphy, 2000; G. A. Abrams, Bentley, Nealey, & Murphy, 2002; Farhadian, Contard, Sabri,

Samuel, & Rappaport, 1996; Hedin, Roy, Tran, Lundmark, & Rahman, 2000; Kalluri, 2003) The nanotopographical cues can regulate the function of many cells types.(Bettinger, Langer, & Borenstein, 2009; D. H. Kim, Provenzano, Smith, & Levchenko, 2012a) We and others have shown that vSMCs respond to nanotopographical cues that can regulate their alignment and phenotype.(Chaterji, Kim, et al., 2014; Hu, Yim, Reano, Leong, & Pang, 2005; Y. Wang et al., 2014; E. K. Yim et al., 2005; Zhou et al., 2015) While the effects of these physical cues are now widely accepted, the mechanisms of nanotopographically-stimulated regulation remain largely unknown. Previous studies have implicated Rac1 GTPase as a sensory mechanism and basis for directional alignment of cells on nanopatterned surfaces.(Xia et al., 2008) In addition, knockdown of focal adhesion kinase leads to increased cell alignment of corneal epithelial cells with nanopatterns and regulated gene expression of nesprin-1 and -2.(Dreier, Raghunathan, Russell, & Murphy, 2012) In vSMCs, nanopatterning led to a significant increase in RhoA ROCK1 and ROCK2, implicating these pathways as potential mediators of mechanotransduction to nanopatterned surfaces.(Chaterji, Kim, et al., 2014) Further, several studies have also found regulation of integrins, Src, p130Cas and actin reorganization in response to nanopatterned substrates.(Arnold et al., 2004; Arnold et al., 2009; Dreier et al., 2013)

In this work, we examined the role of syndecan-1 (SDC1) in mechanosensing of nanopatterned substrates and material rigidity by vSMCs. Syndecan-1 (SDC1) is a transmembrane cell surface proteoglycan that is found on endothelial cells,(Voyvodic et al., 2014) vSMCs(Chaterji, Lam, et al., 2014) and macrophages(Angsana et al., 2015) in

the vascular system, as well as on many other cell types. Our group has recently shown that SDC1 regulates the inflammatory state of endothelial cells in response to shear stress(Voyvodic et al., 2014) and several studies have implicated heparan sulfate proteoglycans as key molecules in mechanosensing.(Baeyens et al., 2014; B. M. Fu & Tarbell, 2013; Tarbell, Simon, & Curry, 2014) In this study, we created materials with nanoscale contact guidance cues using ultraviolet (UV)-assisted capillary force lithography (CFL), a versatile molding technology for imparting nanoscale architecture to tissue scaffolds over large surface areas.(Suh, Park, & Kim, 2009) We grew vSMCs with genetic knockout of SDC1 and wild type phenotype on nanopatterned materials to explore mechanosensing and activation of the cells by nanotopographical cues. Our analyses support that SDC1 is a key molecule in regulating the vSMC response to nanopatterned substrates and alters mechanosensitive signaling pathways including those involving Yap/Taz, Smad2/3 and cytoskeletal regulators Rock1, Rac-1 and integrin-linked kinase (ILK).

3.2 Materials and Methods

3.2.1. Nanopatterned materials

Nanopatterned substrates were fabricated from a polyurethane acrylate (PUA) precursor, as described previously.(D. H. Kim et al., 2009) Briefly, an adhesion promoter (Minuta Tech) was applied to the glass coverslips by spin coating at 2000 rpm for 20 seconds and the coverslips were then baked at 65°C for 20 min. A PUA-based polymer of commercially characterized stiffness (6.7 MPa or 2.4 GPa) was then spin coated onto the

glass substrate and a PDMS mold with nanogrooves having an 800:800 nm groove:gap ratio with a 400 nm groove depth was placed on top of the PUA precursor layer. For nonpatterned surfaces, a mold with no features was placed on the polymer layer. Through capillary action, the polymer fills the mold and a nanopatterned surface is obtained. The patterns were UV cured using a wavelength of 365 nm for 60 seconds. The substrates were then placed into well plates and plasma coated to facilitate protein adsorption. The substrates were then coated with a solution of 11% (w/v) type I collagen overnight to facilitate cell attachment.

3.2.2. Cell isolation and culture

Aortae were harvested from 6-10 week old male syndecan-1 knockout (S1KO) and wild type (WT) mice. Following harvest, the aortae were minced and a glass coverslip was placed over the tissue fragments. The cells were then cultured in MCDB-131 culture medium (Life Technologies) with 20% fetal bovine serum (FBS), L-glutamine and antibiotics. The vSMCs migrated out of the tissue and were allowed to proliferate. After the first passage, the cells were grown in MCDB-131 with 10% FBS, L-glutamine and antibiotics. The vSMCs were seeded onto the substrates at 50% confluence. For long-term drug treatment experiments, cells were seeded onto the substrates and treated 24 hours later with 1% DMSO, 10 μM Y-27632 (Sigma), or 10 μM Verteporfin (Tocris) in culture medium for 48 hours. For short-term drug treatment experiments, cells were seeded onto the substrates and treated 24 hours later with 0.1% DMSO, 10 μM Y-27632 (Sigma), 10

μM Verteporfin (Tocris), 1 μM Latrunculin A (Abcam) or 10 μM Nocodazole (Abcam) in culture medium for 2 hours.

3.2.3. Immunostaining and image analysis

Following the treatments, the cells were washed with PBS at 37°C and fixed with 4% paraformaldehyde for 10 min. The cells were then washed three times with PBS and permeabilized with 0.2% Triton X-100 for 5 min. The cells were blocked with 1% BSA in PBS for 40 min and stained with primary antibody diluted in PBS with 1% BSA overnight. The primary antibodies and dilution used in the study are shown in **Table 3.1**. The cells were then rinsed PBS for 10 min three times. Secondary antibodies conjugated to fluorophores were added at 1:1000 dilution in 1% BSA in PBS containing 1 μg/ml of DAPI for nuclear staining. After 75 min of incubation at room temperature, the cell were rinsed extensively with repeated PBS washes. The cells were mounted and coverslipped in anti-fade mounting media (Vector Laboratories, Inc.).

Table 3.1. Antibodies used for immunostaining

Antibody Target	**Dilution**	**Vendor**	**Catalog**
ILK	1:50	BD Biosciences	611803
Paxillin	1:50	Santa Cruz	H-114
Phospho-MLC	1:50	VWR	PA517726
Phospho-Smad2	1:50	Thermo	44-244G
Phospho-Smad2/3	1:50	Cell Signaling, Inc.	8828S
Phospho-Smad3	1:100	Abcam	ab52903
Rac1	1:50	Life Technologies	PA1-091
Rock1	1:100	Life Technologies	PA5-22262
Smad2/3	1:50	BD Biosciences	610842
Smad2/3	1:50	Santa Cruz	Sc-133098
Yap/Taz	1:50	Cell Signaling, Inc.	8418S

The cells were imaged using an epifluorescent microscope (Axio Observer microscope, Carl Zeiss, Inc.). For each coverslip, ten images were taken at randomly selected areas. The same imaging exposure time and illumination intensity was used for all groups that were compared to each other following analysis. The cells and nuclei were selected and analysis was performed using computer-assisted morphometry with Metamorph 7.0 (Molecular Devices, LLC) or ImageJ. Measurements were made of the elliptical form factor (EFF; defined as the major axis divided by minor axis) and shape factor (defined as $4\pi[Area]/[Perimeter]^2$). For the quantification of cell alignment, the perimeters of the cells were traced and the angle of the cells calculated from the major axis of the cell area and compared to the angle of the nanogrooves in the substrate. For measurements of cell intensity, mean immunofluorescence intensities were measured in the selected areas using ImageJ. Background intensity outside the cell areas was subtracted from the measurements of mean cytoplasmic and nuclear intensity.

3.2.4. Flow cytometric analysis of cells

Cells were seeded onto coverslips of engineered substrates at 30% confluency. For all of the procedure, the buffers were supplemented with 2 mM sodium orthovanadate and 50 mM NaF to prevent alterations in the phosphorylation state of proteins. After 48 hours, the adherent vSMCs were washed with PBS and treated with Accutase (Millipore) for 5 minutes at 25°C. A cell scraper was used to ensure cell detachment from the engineered substrates. Cells were centrifuged at 8°C for six minutes at 400g, and the supernatant was aspirated. The pellet was resuspended and incubated in fixation/permeabilization buffer

(BD Pharmigen) at 4°C for 50 minutes. Permeabilization/wash buffer (BD Pharmigen) was added to cells, and the cells were again centrifuged and the supernatant aspirated. For intracellular staining, cells were incubated with antibodies against Rock1, ILK, Smad2/3 and p-Smad2/3 in permeabilization/wash buffer, as outlined in **Table 3.2**. The cells were next rinsed twice with permeabilization/fixation buffer, centrifuged and the supernatant was aspirated. The cells were resuspended in stain buffer (BD Pharmigen) and flow cytometry was performed using the LSRFortessa flow cytometer (BD). Flow cytometry data was analyzed using Flowjo software.

Table 3.2. Antibodies used for **flow cytometry**

Antibody Target	**Fluorochrome**	**Vendor**	**Catalog**
Rock1	Alexa 488	Abcam	ab205432
ILK	PE	Santa Cruz	sc-20019PE
Smad2/3	Alexa 647	BD	PE-CF594
p-Smad2/3	PE-CF594	Thermo	44-244G
Rabbit IgG (Control)	Alexa 488	Abcam	ab199091
Mouse IgG2b (Control)	PE	Santa Cruz	sc-2868
Mouse IgG2a (Control)	Alexa 647	Santa Cruz	sc-24637
Mouse 1gG1κ (Control)	PE-CF594	BD	562292

3.2.5. Measurement of cell mechanics using micropipette aspiration

Micro-capillary tubes were pulled using a micropipette puller and then the tip was cut and smoothed with a microforge. The micropipette was then filled with PBS using a MicroFil needle. Smooth muscle cells were trypsinized and resuspended in MCDB-131 media. The cell suspension was pipetted between two coverglasses and positioned on the microscope. Cells were suctioned onto the micropipette with a small suction force, no

greater than 50 Pa, and moved away from the coverglass. Pressure was increased by 100 Pa and images were captured at 10 second intervals for 100 seconds. This process was repeated four times for each cell while recording the precise pressure differences.

3.2.6. Particle-tracking microrheology

Cells were seeded on 35 mm tissue culture dishes and grown to ~80% confluence before ballistic injection of red fluorescent 100 nm carboxylated polystyrene particles (Thermo Scientific). The ballistic injection was conducted using a Biolistic® PDS-1000/He particle delivery system (Bio-Rad) as previously described.(Wu et al., 2012) In brief, nanoparticles were dialyzed against ethanol and deposited onto microcarriers and allowed to dry for 40 min. Rupture disks of 900 psi were used for single-microcarrier adaptor. After ballistic injection, cells were gently washed twice with 1X PBS and fresh cell culture medium. These cells were incubated in an incubator for at least 4 h to allow cells to recover from ballistic injection. Particle-injected cells were then reseeded into a chambered coverglass to grow overnight before observation on a microscope. Staining with Hoechst 33258 (Thermo Fisher) and CellMask Deep Red (Thermo Fisher) was performed of the nuclear DNA and plasma membrane. Cells were then treated with 60 mM KCl in cell culture media for 10 min to induce contraction(Peng, Wang, Lu, & Ran, 2010) and fluorescent particle tracking was again performed. Following tracking of the contracted cells, the media containing KCl was aspirated, and the cells rinsed twice with PBS. The cells were then treated with 10 μM of the Rock inhibitor Y-27632 (Sigma) for 15 min to induce relaxation in the cells(X. Fu, Gong, Jia, Somlyo, & Somlyo, 1998) before the

initiation of testing. All of the treatments and particle tracking were performed at 37ºC. Treatments remained present for the duration of testing. To probe the rheological properties within cells, we tracked ballistically injected particles and extracted the viscoelastic moduli using a frequency-dependent Stokes-Einstein equation.(Mason, Ganesan, van Zanten, Wirtz, & Kuo, 1997; Xu, Viasnoff, & Wirtz, 1998) A custom-built, two-photon 3D tracking microscope, termed TSUNAMI (Tracking of Single particles Using Nonlinear And Multiplexed Illumination), was used to track fluorescent particles for 60 s. The scheme of the TSUNAMI system has been previously reported and its use for tracking biomolecules in living cells has been demonstrated.(Perillo et al., 2015) Here, we used a Ti:sapphire laser output at 20 mW and 825 nm for tracking experiments. TSUNAMI can achieve localization accuracy as good as 17 nm in xy and 35 nm in z-direction. The temporal resolution of these particle-tracking experiments is 5 ms.(Perillo et al., 2015)

The detailed protocol for particle-tracking microrheology has been reported.(Wu et al., 2012) In brief, the trajectories were analyzed by custom software in MATLAB (The MathWorks, Natick, MA) to calculate the time-averaged *mean squared displacement* (MSD):

$$\mathrm{MSD}(\tau) = \langle [x(t+\tau) - x(t)]^2 + [y(t+\tau) - y(t)]^2 \rangle$$

where τ is the time lag and t the is elapsed time. The local creep compliance of the microenvironment around tracked particles was derived from MSD curves:

$$\mathrm{J}(\tau) = \left(\frac{3\pi a}{2k_B T}\right) * \mathrm{MSD}(\tau)$$

where k_B is the Boltzmann constant, T is the absolute temperature, and a is the radius of the particle. The creep compliance is a measure of the deformability of the cytoplasm.

The generalized Stokes-Einstein equation was then used to calculate the frequency-dependent viscoelastic modulus, $G^*(\omega)$:

$$G^*(\omega) = \left(\frac{2k_BT}{3\pi a}\right)\frac{1}{\mathrm{MSD}(\tau)\Gamma((1+\alpha(\tau))(1+\beta(\tau))/2)}$$

where $\omega = 1/\tau$, a is the radius of the particle, Γ is the gamma function, $\alpha(\tau)$ and $\beta(\tau)$ are the first derivative and second derivative of the logarithm MSD-time lag curve, respectively. The $G^*(\omega)$ curves were fitted with third-order polynomial in the logarithmic space, and then the first derivative, $\alpha_G(\omega)$, and the second derivative, $\beta_G(\omega)$, were directly calculated from the fitted polynomial function. The following two equations were used to calculate the frequency-dependent elastic modulus $G'(\omega)$, and viscous modulus, $G''(\omega)$ of the specimen:

$$G'(\omega) = \frac{G^*(\omega)}{1+\beta_G(\omega)}cos\left[\frac{\pi\alpha_G(\omega)}{2} - \beta_G(\omega)\alpha_G(\omega)\left(\frac{\pi}{2}-1\right)\right]$$

$$G''(\omega) = \frac{\mathrm{G}^*(\omega)}{1+\beta_G(\omega)}sin\left[\frac{\pi\alpha_G(\omega)}{2} - \beta_G(\omega)(1-\alpha_G(\omega))\left(\frac{\pi}{2}-1\right)\right]$$

3.2.7. Statistical analysis

All results are shown as mean ± standard error of the mean, unless otherwise specified. Comparisons between only two groups were performed using a two-tailed Student's t-test with differences were considered significant at $p<0.05$. Multiple comparisons between groups were analyzed by two-way ANOVA followed by a Tukey post-hoc test. A two-tailed *p*-value of less than 0.05 was considered statistically significant. For nonparametric data, a Kruskal-Wallis test was used followed by the Conover-Iman test to compare between multiple groups.

3.3 RESULTS

3.3.1. Syndecan-1 knockout reduces cellular alignment with nanogrooves under TNF-α treatment

Cellular alignment to nanogrooves has been observed for many cell types and occurs on surfaces with nanoscale features beyond 35 nm in dimension.(Loesberg et al., 2007) To examine the effect of SDC1 knockout on the ability of vSMCs to align to a nanopattern, we created PUA materials with nanogrooves (800 nm grooves) using UV assisted capillary force lithography and confirmed the nanopatterning using scanning electron microscopy (**Figure 3.1**). The nanopatterning was accurate on both the more compliant polymer with a Young's modulus of 6.7 MPa (NOA76; **Figure 3.1B**) and the stiffer material with a modulus of 2.4 GPa (NOA86; **Figure 3.1C**). We isolated vSMCs from WT and S1KO mice and cultured them on the different surfaces for 48 hours. We performed a quantitative analysis of the alignment and morphology of the cells on nanopatterned and nonpatterned surfaces of both moduli. Under standard culture conditions, S1KO and WT vSMCs aligned similarly to the nanogrooves (**Figure 3.2A, B**). WT and S1KO vSMCs also elongated similarly to nanogrooves, as indicated by the elliptical form factor (EFF**; Figure 3.2C**). Treatment with TNF-α increased the elongation of the cells and caused them to align with the nanopatterning (**Figure 3.3**). Syndecan-1 knockout vSMCs had reduced elongation in all of the substrates (**Figure 3.3B, C**). In addition, knockout of SDC1 reduced the alignment of the cells on both the 6.7 MPa and 2.4 GPa modulus materials (**Figure. 3.3D**). To test the effect of Rock inhibition and Yap/Taz inhibition on alignment and elongation, we cultured the cells in the presence of

Y27632 and Verteporfin. Inhibition of Yap/Taz and Rock did not significantly affect orientation of the vSMCs in response to the nanogrooves (**Figure 3.4A**). In addition, Yap/Taz inhibition significantly reduced elongation for both genotypes (**Figure 3.4C, D**).

3.3.2. Loss of syndecan-1 increases nuclear localization of Yap/Taz in response to nanopatterned substrates.

The Hippo signaling pathway and its intermediates Yap and Taz have been linked to mechanosensing in many cell types.(Dupont et al., 2011) Immunostaining on vSMCs grown on the patterned and nonpatterned substrates demonstrated that S1KO vSMCs had increased nuclear localization of Yap/Taz on all of the substrates. In addition, on the 2.4 GPa substrates nanopatterning led to increased nuclear localization of Yap/Taz (**Figure 3.5**). Cytoplasmic Yap/Taz was similar between genotypes on equivalent substrates, both soft and stiff. Overall, the nuclear/cytoplasmic ratio of Yap/Taz increased in response to nanopatterning on 2.4 GPa substrates and this increase was significantly enhanced with SDC1 knockout. Treatment with Verteporfin (Hippo pathway inhibitor) or Latrunculin A (disruptor of actin cytoskeletal organization) eliminated differences in Yap/Taz localization between WT and S1KO vSMCs (**Figure 3.5E**).

3.3.3. Syndecan-1 knockout increases nuclear Smad2/3 in response to nanopatterning.

TGF-β signaling pathway is known to be mechanically responsive(Baker et al., 2008; Maeda et al., 2011) and nanotopography has been shown to alter Smad-mediated signaling in mesenchymal stem cells.(Kato et al., 2014) We grew WT and S1KO vSMCs on nanopatterned substrates and measured the phosphorylation and localization of Smad2/3, a mediator of vSMC function and downstream target of TGF-β signaling.(Ruiz-Ortega, Rodriguez-Vita, Sanchez-Lopez, Carvajal, & Egido, 2007) Knockout of SDC1 increased the nuclear localization of Smad2/3 and led to an increase in total Smad2/3 in the cell (**Figure 3.6A-B**)**.** Loss of SDC1 increased the nuclear localization of Smad2/3 on 2.4 GPa substrates. Knockout of SDC1 also increased the cytoplasmic localization of Smad2/3 on 6.7 MPa nanopatterned substrates. S1KO vSMCs also had a significantly greater cytoplasmic Smad2/3 response to nanopatterning on 6.7 MPa substrates in comparison to WT. However, there was virtually no nuclear Smad2/3 response to nanopatterning on substrates of either stiffness. Phospho-Smad2/3 was significantly increased in the cytoplasm by loss of SDC1 for 2.4 GPa nonpatterned substrates. We treated the cells with inhibitors found that inhibition of Yap/Taz with Verteporfin reduced p-Smad2/3 in the nucleus in the S1KO cells grown on nanopatterned surfaces (2.4 GPa stiffness). Flow cytometric analysis showed increased Smad2/3 and p-Smad2/3 in S1KO vSMCs compared to WT in response to nanopatterning and on the 2.4 GPa substrate (**Figure 3.9C**). Yap/Taz inhibition significantly affected p-Smad2/3 nuclear localization. Smad2/3 localization was altered by disruption of actin polymerization (**Figure 3.8B**)

3.3.4. Syndecan-1 knockout alters distribution and levels of focal adhesion associated proteins.

Integrin-linked kinase (ILK) is an integrin β1 adaptor protein that is essential for the formation of focal adhesions and has been implicated in cell matrix interactions(Sakai et al., 2003) as well as the regulation of vSMC function and response to injury.(Ho et al., 2008) Rac1 is a Rho GTPase involved in the regulation of cytoskeletal rearrangement(Bustelo, Sauzeau, & Berenjeno, 2007) and is a key molecule in vSMC migration, proliferation and the formation of intimal hyperplasia.(Autieri, Kelemen, & Wendt, 2003; Yu et al., 2015; Zhu et al., 2010) In development, ILK regulates the formation of the vascular wall through a Rho/Rock1 mediated mechanism.(Kogata, Tribe, Fassler, Way, & Adams, 2009) For WT vSMCs grown on stiff substrates, there was an increase in ILK for cells grown on the nanopatterned substrates (**Figure 3.7**). In addition, there was a marked reduction in ILK for the S1KO cells on the stiffer substrates in comparison to WT cells. Elevated ILK levels in S1KO vSMCs compared to WT vSMCs in response to nanopatterning were also observed in analysis with flow cytometry (**Figure 3.9B**). There was increased Rac1 in S1KO vSMCs that were grown on stiff, nanopatterned substrates (**Figure 3.7**). For both ILK and Rac1, there were no significant differences between the groups for cells grown on less stiff substrates.

3.3.5. Syndecan-1 knockout increases Rho-associated protein kinase-1 (Rock1) and phospho-myosin light chain (p-MLC).

Focal adhesions are important in mechanosensing of the ECM and applied physical forces. The activation of Rho signaling leads to contraction and an increase in cellular tension. To examine the effect of SDC1 knockout on the Rho signaling pathway, we examined Rock1 immunofluorescence intensity and localization. Rock1 activation leads to an increase in phosphorylation of myosin light chain. Loss of SDC1 increased Rock1 by

almost two-fold, particularly on stiff and nanopatterned substrates (**Figure 3.10**). On 6.7 MPa substrates, Rock1 levels were very similar between genotypes. In response to nanopatterning, Rock1 was significantly increased in S1KO vSMCs compared to WT, approximately a 60% increase in S1KO compared to 12% in WT cells. In addition, myosin light chain (p-MLC) was in S1KO cells in comparison to WT cells on stiff substrates. Consistent with the immunostaining results, flow cytometric analysis also found increased Rock1 levels in S1KO vSMCs compared to WT cells in response to nanopatterning (**Figure 3.9A**).

3.3.6. Syndecan-1 knockout increases vascular smooth muscle cell stiffness and alters the response to contractile stimuli.

As we observed a significant increase in Rock1, p-MLC and Rac-1 as well as increases in Yap/Taz and p-Smad2/3 in S1KO cells, we hypothesized that S1KO led to a cell state with greater cytoskeletal tension and stiffness. We grew the vSMCs on collagen-coated alginate substrates that had varying compliance. After culturing the cells on the substrates, we released them from the plate with trypsin and measured their stiffness using micropipette aspiration. This analysis revealed a significant increase in the Young's modulus of S1KO cells in comparison to WT cells on substrates of very soft (0.5 kPa) or relatively stiff (64 kPa) compliance (**Figure 3.11**). In addition, we further tested the mechanics of the cells using particle-tracking microrheology under control conditions, a contraction stimulus with KCl and treatment with a Rock inhibitor (Y27632). In WT vSMCs, we found that the elastic modulus increased under contraction and decreased after subsequent Rock inhibitor treatment (**Figure 3.12C, D**). Under baseline conditions, S1KO

cells had increased elastic modulus consistent with increased contractile state. In addition, the modulus of the S1KO cells decreased in response to both KCl and Y27632 treatment. In WT cells, the viscous modulus increased with KCl treatment and decreased with Rock inhibition but this was not observed in the S1KO cells (**Figure 3.12C, D**).

3.4 DISCUSSION

Nanotopographical features on engineered materials provide a means for controlling cell function and can provide a powerful means to create *in vitro* tissue equivalent culture systems or improve the response to implanted materials. Nanotopology is known to regulate the function of many cells types including stem cells,(Ahn et al., 2014; Carson et al., 2016) cardiomyocytes(D. H. Kim, Kshitiz, et al., 2012; Mengsteab et al., 2016) and endothelial cells.(Liliensiek et al., 2010) The effects of nanotopographical features on vSMCs have been used to preferentially align cells in the creation of vascular conduits.(Barreto-Ortiz et al., 2013; Zorlutuna et al., 2009) While there is strong evidence for the concept that nanotopographical feature can strongly regulate cell function, the mechanisms of how cells sense and respond to these feature remains largely unexplained. In this work, we demonstrate that loss of the cell surface proteoglycan SDC1 can alter the response of vSMCs to nanotopography, leading to alterations in cell alignment in an inflammatory context, altering mechanosensing through Yap/Taz and Rho-mediated signaling and altering vSMC cell mechanics.

Our group has shown that nanotopography can increase expression of markers of mature vSMC phenotype including calponin, αSMA and desmin.(Chaterji, Kim, et al., 2014) In addition, nanogrooves similar to those used in this study, increased Rock1 and RhoA in comparison to nonpatterned surfaces.(Chaterji, Kim, et al., 2014) In this study, nanopatterning induced a large increase in nuclear localization of Yap/Taz on stiff substrates. The Hippo pathway is well known to be mechanoresponsive to underlying cues from the substrate such as matrix stiffness and attachment area.(Dupont et al., 2011)

Similarly, there was an increase in nuclear p-Smad2/3 in the vSMCs with nanopatterning on stiff materials. Yap/Taz binds to Smad transcription factors to regulate their function.(Varelas et al., 2010) Thus, the presence of nanogrooves provides increased activation of these pathways, effectively causing cell to sense the material as if it had increased stiffness or larger contact area.(Dupont et al., 2011) As our previous work has shown that nanopatterning increases many of the proteins involved in vSMC contraction (eg. calponin and αSMA)(Chaterji, Kim, et al., 2014) and Rac1 in this study, this supports an increase in contractile forces in the cell and increased cytoskeletal tension. Cytoskeletal tension is key in regulating the nuclear localization of Yap/Taz(Dupont et al., 2011) and thus provides a potential mechanism for the alterations in Yap/Taz localization observed with nanopatterning. In our study, changes in Yap/Taz localization were blocked by disruption of the actin cytoskeleton, further supporting cytoskeletal tension as a potential mechanism.

Knockout of SDC1 caused a number of profound changes in the response of vSMC to nanopatterned surfaces. Our group has shown in prior studies that loss of SDC1 in vSMCs leads to increased proliferation, loss of mature vSMC markers including calponin and αSMA, and an increase in phosphorylation and amount of focal adhesion related-molecules paxillin and Src.(Chaterji, Lam, et al., 2014) In this study, one of the most striking findings was the large increase in Rock1 with SDC1 knockout. Coupled with our findings here of increased Rac1 with SDC1 knockout, we suspected that loss of SDC1 led to an increased contractile state of the cell, even in spite of the loss of αSMA and calponin

observed in our previous study.(Chaterji, Lam, et al., 2014) We tested whether the SDC1 knockout vSMCs had increased tension and/or stiffness in their cytoskeleton by measuring the mechanics of the cells in both a detached state with micropipette aspiration and using particle-tracking microrheology in an attached state. In the detached state without the tension of the cytoskeleton from attachment, the SDC1 vSMCs were about two-fold stiffer on stiff or very soft substrates, implying that these SDC1 knockout cells had an inherently greater stiffness. When attached, the SDC1 knockout cells were over four-fold stiffer, implying that the cells became even stiffer than WT cells after attachment and cytoskeletal engagement. With KCl treatment to induce contraction, the WT cells became stiffer and more viscous but, paradoxically, the SDC1 cells became less stiff and had roughly similar viscosity. A Rock inhibitor reduced the cell stiffness in both the WT and S1KO cells to similar levels, demonstrating that Rock1 elevation leads to increase in contraction in S1KO cells. While Rock inhibition altered the biomechanics of the cells it did not alter the signaling responses for Yap/Taz and p-Smad2/3. This suggests that the elevation in Rock1 observed in the study are downstream to signaling through these pathways. Our study also suggests that this contraction causes increases in focal adhesion proteins and is consistent with an increase in nuclear Yap/Taz and p-Smad2/3, observed in our immunostaining experiments. Studies in other cell types have also linked SDC1 to focal adhesion assembly and cytoskeletal remodeling. In lung cancer cells, SDC1 was found to regulate focal adhesion disassembly by activating Rap1.(Ibrahim et al., 2012) In addition, SDC1 has been found to regulate integrin αVβ3 and αVβ5,(Beauvais, Burbach, & Rapraeger, 2004; Beauvais, Ell, McWhorter, & Rapraeger, 2009; McQuade, Beauvais, Burbach, &

Rapraeger, 2006) as well as several other integrins including α2β1(Vuoriluoto et al., 2008) and β4 integrin.(Ogawa, Tsubota, Hashimoto, Kariya, & Miyazaki, 2007) Moreover, in tumor cells, SDC1 knockdown reduced adhesion induced RhoA activation and activate Rac1.(Ishikawa & Kramer, 2010) Our results are consistent with these findings that imply increased adhesion with SDC1 loss and support that Rock1 may mediate increased cytoskeletal tension in the context of greater adhesion strength.

Taken together, our studies have shown that nanotopography can alter signaling through the TGF-β and Hippo pathways through regulating the generation of cytoskeletal tension with the cells. In addition, SDC1 knockout creates a contractile state within the vSMCs leading to increased cell stiffness, changes in the response to contractile stimuli and regulating signaling through Yap/Taz and Smad2/3. Thus, nanotopology and SDC1 knockout appear to have synergistic effects on the activation of the Yap/Taz and Rock-1 mediated pathways. These findings add to our understanding of the mechanisms of mechanosensing in vSMCs and provide guidance for the creation of novel biomaterials that can regulate vascular cell function.

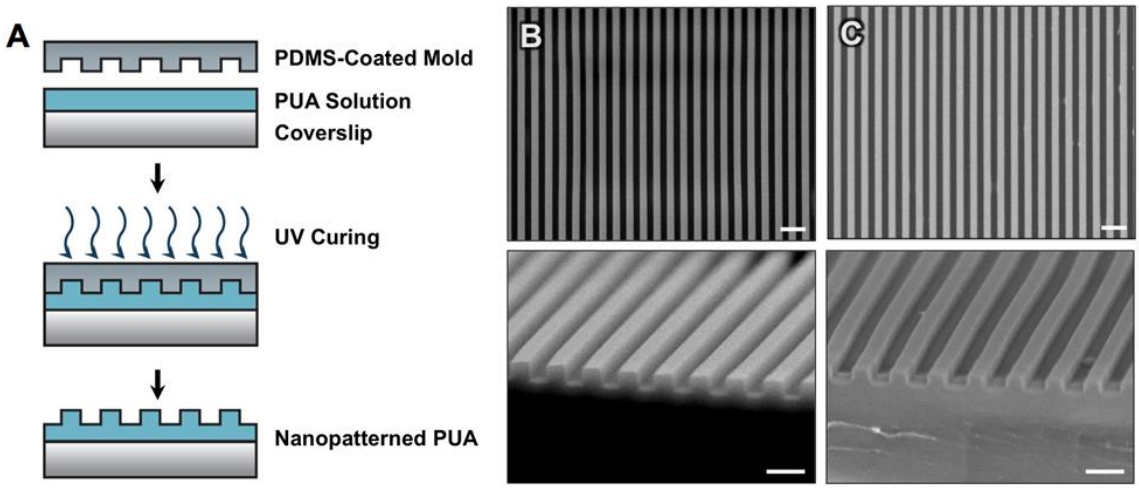

Figure 3.1. Fabrication of anisotropically nanofabricated substrates. (A) Diagram of UV-assisted capillary force lithography (CFL) used to fabricate substrates with nanogrooves. A mold coated with PDMS was placed on top of a coverslip with a polyurethane acrylate (PUA) layer. Capillary force drives the imprinting of the nanopatterned into the polymer layer, which is then polymerized with UV light. (B) Scanning electron microscopy (SEM) images of the surface with nanogrooves on a substrate with 6.7 MPa Young's modulus. (C) SEM images of nanopatterned substrates a Young's modulus of 2.4 GPa. Bar = 1 μm (top images). Bar = 2 μm (bottom images).

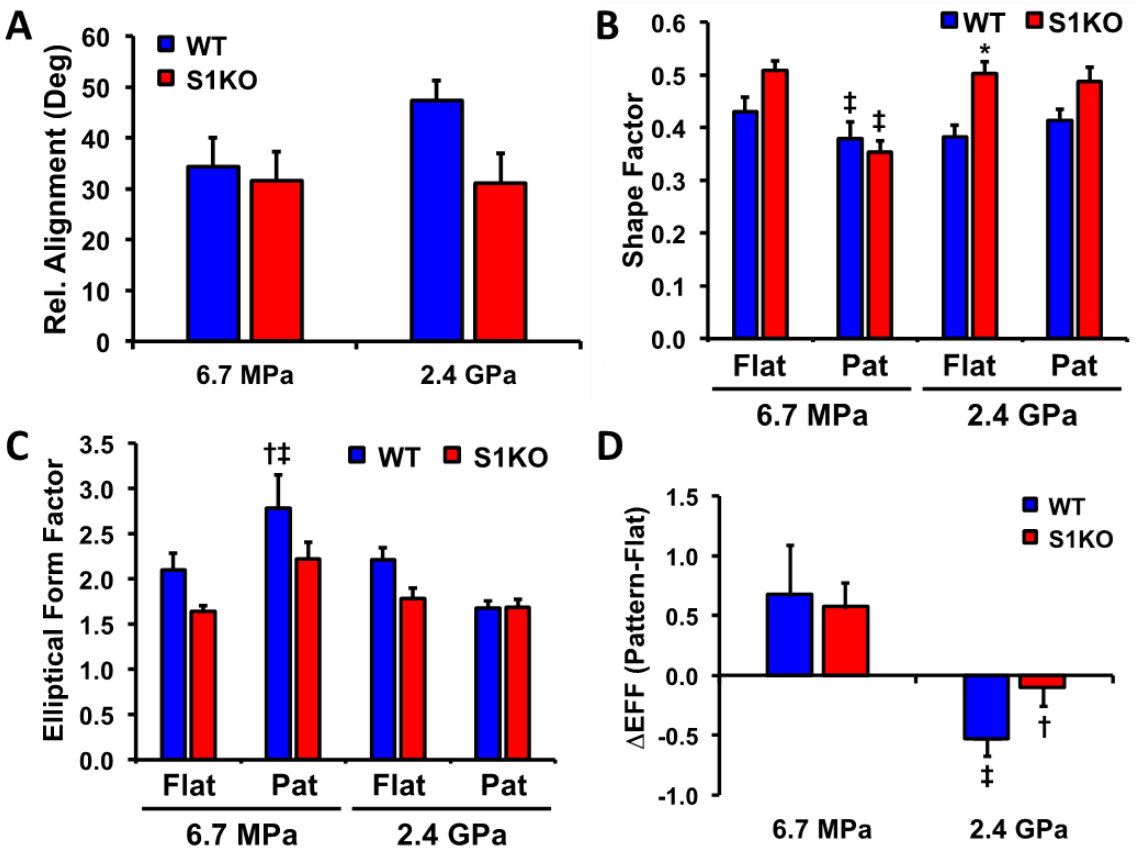

Figure 3.2. Alignment of vascular smooth muscle cells cultured on nanopatterned substrates under standard culture conditions. Wild type (WT) and syndecan-1 knockout (S1KO) vascular smooth muscle cells were grown on the engineered substrates for 48 hours. (A) Quantification of the alignment of the cells with the patterned nanogrooves. (B) Shape factor for cells grown on flat and nanopatterned substrates. (C) Elliptical Form Factor (EFF), a measure of cell elongation, for the cells grown on the various substrates. (D) Change in the EFF (ΔEFF) comparing between cells grown on the patterned and nonpatterned surfaces. $^{*}p<0.05$ versus WT group on the same substrate. $^{\dagger}p<0.05$ versus WT cells grown on a nonpatterned substrate. $^{\ddagger}p<0.05$ versus S1KO cells grown on a nonpatterned substrate.

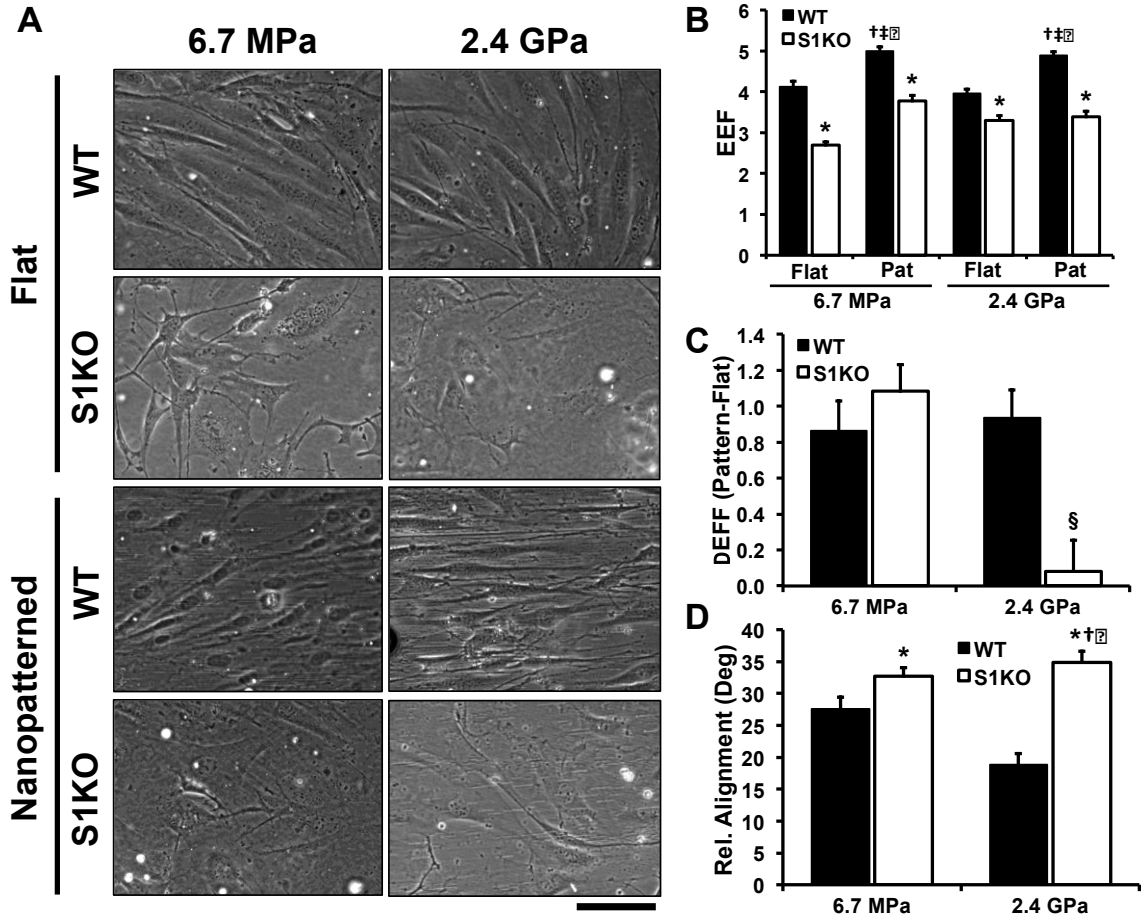

Figure 3.3. Syndecan-1 knockout reduces vascular smooth muscle cell (vSMC) alignment to nanogrooves under TNF-α treatment. (A) Representative phase contrast images of wild type (WT) and syndecan-1 knockout (S1KO) vSMC morphology and orientation on patterned and nonpatterned surfaces. Cells were grown on the substrata for 48 hours under treatment with 20 ng/ml TNF-α. Bar = 25 μm. (B) Elliptical form factor (EFF), a measure of cell elongation, for the cells grown on the various substrates. (C) Change in the EFF (ΔEFF) comparing between cells grown on the patterned and nonpatterned surfaces. (D) Alignment of the cells with the patterned nanogroove. The angle given is the angle between the grooves and the major axis of the cell (lower angle is more aligned). $^{*}p<0.05$ versus WT group on the same substrate. $^{\dagger}p<0.05$ versus WT cells grown on a nonpatterned substrate. $^{\ddagger}p<0.05$ S1KO cells grown on a nonpatterned substrate. $^{\S}p<0.05$ versus all other groups.

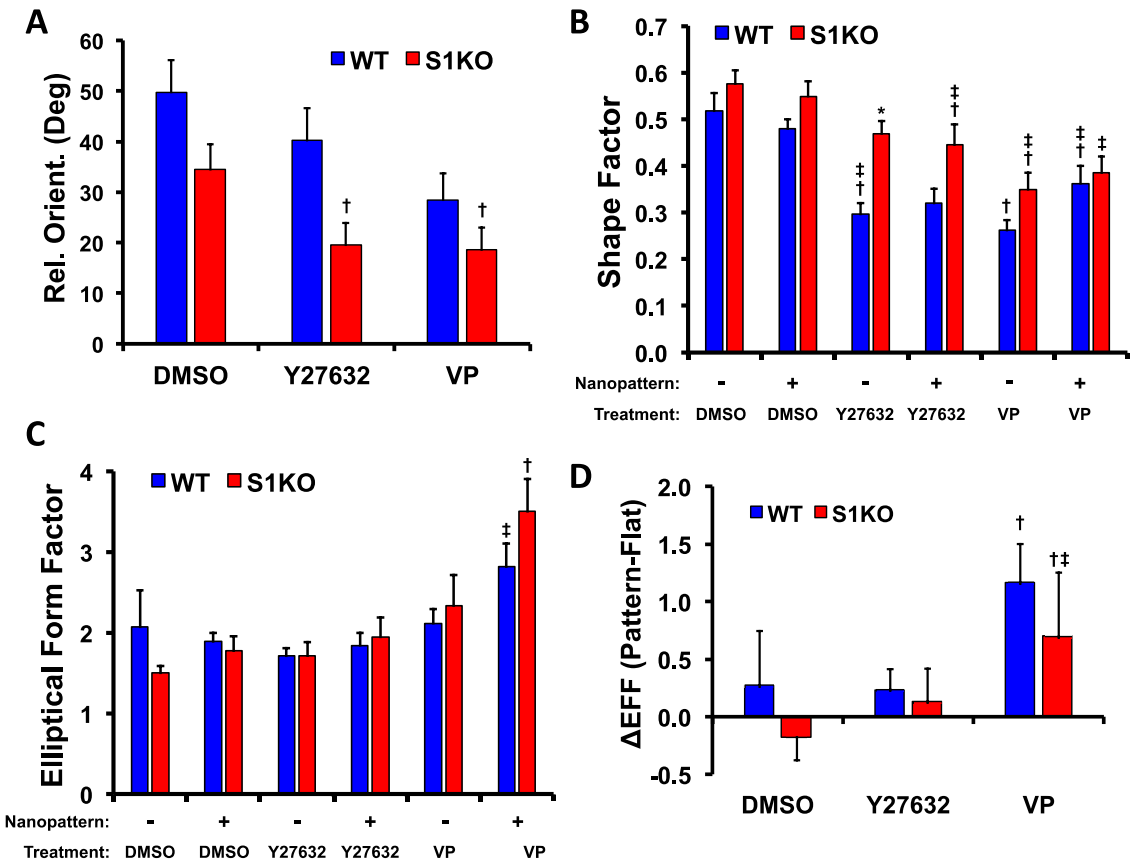

Figure 3.4. Alignment of vascular smooth muscle cells cultured on nanopatterned substrates in response to drug treatment. Wild type (WT) and syndecan-1 knockout (S1KO) vascular smooth muscle cells were grown on 2.4 GPa nanopatterned substrates for 12 hours and treated with 1% DMSO, 10 µM Y27632 or 10 µM Verteporfin (VP) for 48 hours. (A) Alignment of the cells with the patterned nanogrooves. †p<0.05 versus DMSO-treated WT cells. (B) Shape factor (C) Elliptical Form Factor (EFF), a measure of cell elongation, for the cells grown on the various substrates. (D) Change in the EFF (ΔEFF) comparing between cells grown on the patterned and nonpatterned surfaces. *p<0.05 versus WT group of the same treatment and on the same substrate. †p<0.05 versus DMSO-treated WT cells on nonpatterned substrate. ‡p<0.05 versus S1KO cells grown on a nonpatterned substrate.

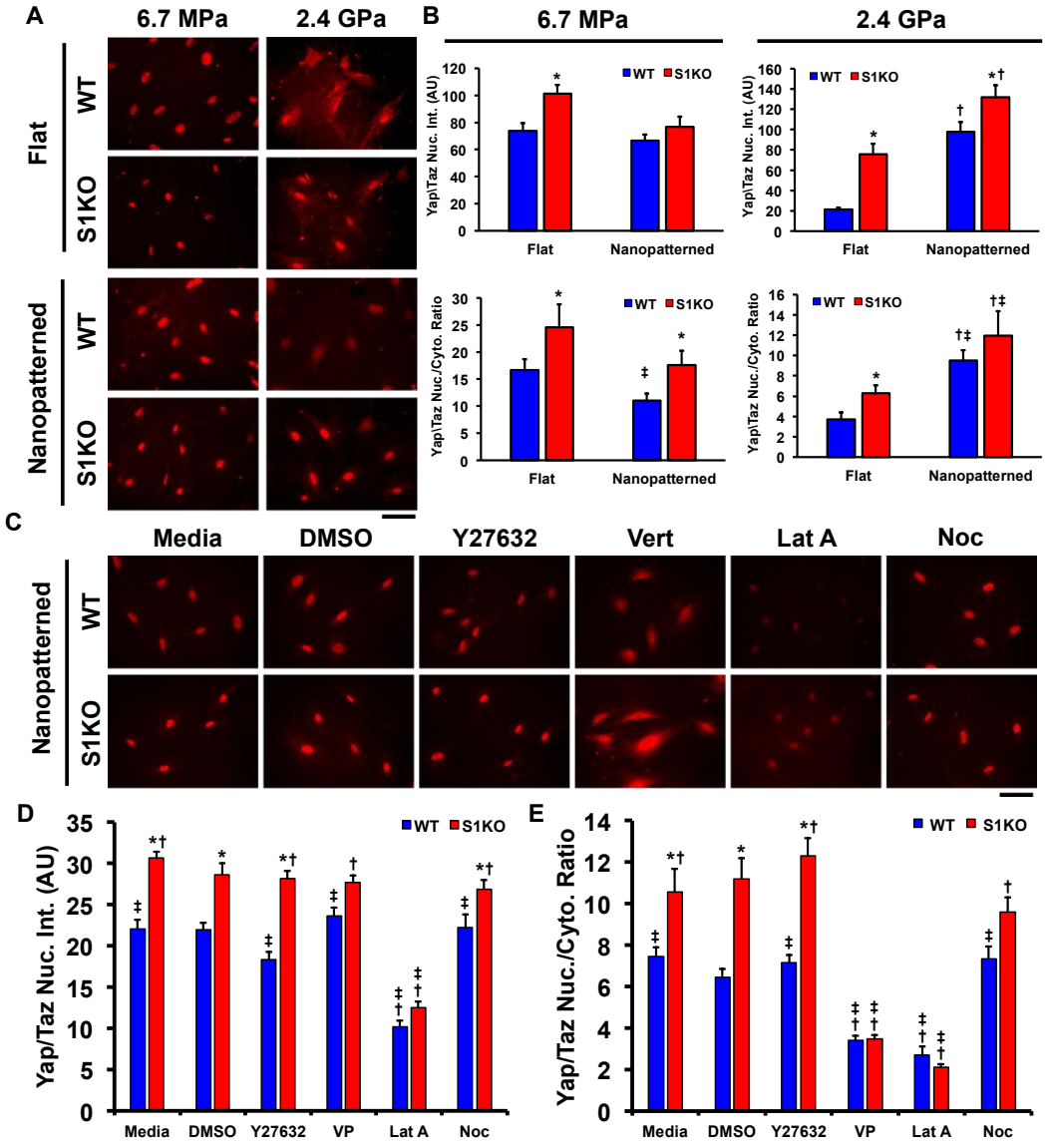
A
6.7 MPa
2.4 GPa
Flat
Nanopatterned
WT
S1KO
B
6.7 MPa
2.4 GPa
WT S1KO
Yap\Taz Nuc. Int. (AU)
Yap\Taz Nuc./Cyto. Ratio
Flat
Nanopatterned
C
Media
DMSO
Y27632
Vert
Lat A
Noc
D
Yap/Taz Nuc. Int. (AU)
Media
DMSO
Y27632
VP
Lat A
Noc
E
Yap/Taz Nuc./Cyto. Ratio

Figure 3.5.

Figure 3.5. Yap/Taz nuclear localization is altered by nanopatterning and knockout of syndecan-1. Wild type (WT) and syndecan-1 knockout (S1KO) vascular smooth muscle cells (vSMCs) were grown on engineered substrates for 48 hours and then immunostained. (A) Images of immunostaining for Yap/Taz. Bar = 200 μm. (B) Quantification of nuclear localization of Yap/Taz in response to the materials. $^{*}p<0.05$ versus WT group on the same substrate. $^{\dagger}p<0.05$ versus same genotype grown on a nonpatterned substrate. $^{\ddagger}p<0.05$ between cells with a different genotype grown on a different substrate. (C) WT and S1KO vSMCs were grown 2.4 GPa nanopatterned substrates for 24 hours, treated with media only, 0.1% DMSO, 10 μM Y27632, 10 μM Verteporfin (Vert), 1 μM Latrunculin A (Lat A) or 10 μM Nocodazole (Noc) for 2 hours and immunostained. Images of immunostaining for Yap/Taz. Bar = 200 μm. (D) Quantification of nuclear localization of Yap/Taz in response to the materials and treatments. $^{*}p<0.05$ versus WT group of same treatment. $^{\dagger}p<0.05$ versus DMSO-treated WT group. $^{\ddagger}p<0.05$ versus DMSO-treated S1KO group.

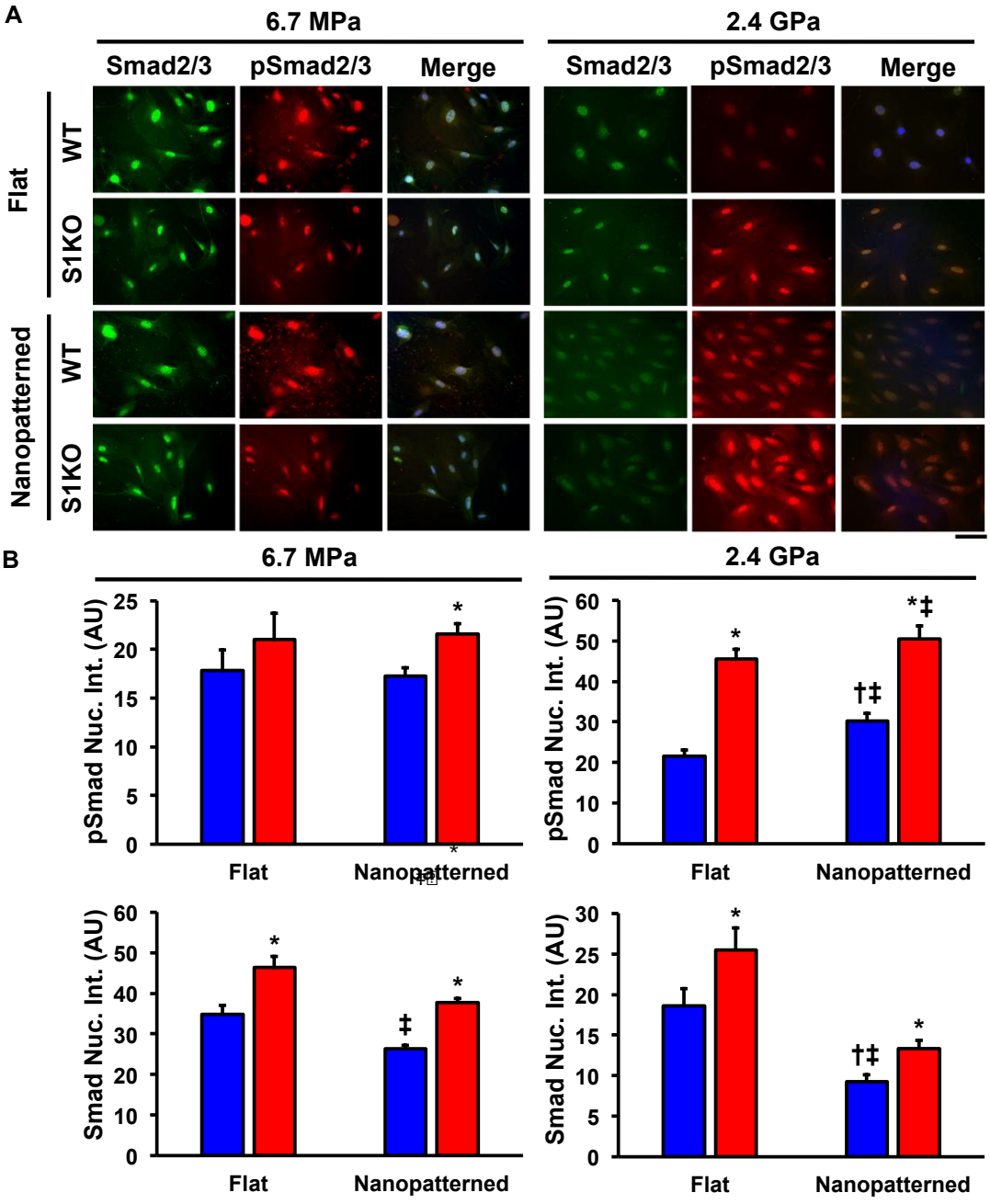
A
6.7 MPa
2.4 GPa
Smad2/3
pSmad2/3
Merge
Flat
WT
S1KO
Nanopatterned
WT
S1KO
B
6.7 MPa
2.4 GPa
pSmad Nuc. Int. (AU)
Smad Nuc. Int. (AU)
Flat
Nanopatterned

Figure 3.6.

Figure 3.6. Syndecan-1 knockout and nanopatterning increase nuclear Smad2/3 signaling. Wild type (WT) and syndecan-1 knockout (S1KO) vascular smooth muscle cells (vSMCs) were grown on engineered substrates for 48 hours and then immunostained for phospho-Smad2/3 (Ser465/467; p-Smad2/3) and Smad2/3. (A) Representative images of the immunostaining for Smad2/3 in WT and S1KO. Bar = 200 μm. (B) Quantification of nuclear localization of p-Smad2/3 and Smad2/3 in the vSMCs grown on engineered substrates. $^{*}p<0.05$ versus WT group on the same substrate. $^{\dagger}p<0.05$ versus WT cells grown on a nonpatterned substrate. $^{\ddagger}p<0.05$ S1KO cells grown on a nonpatterned substrate.

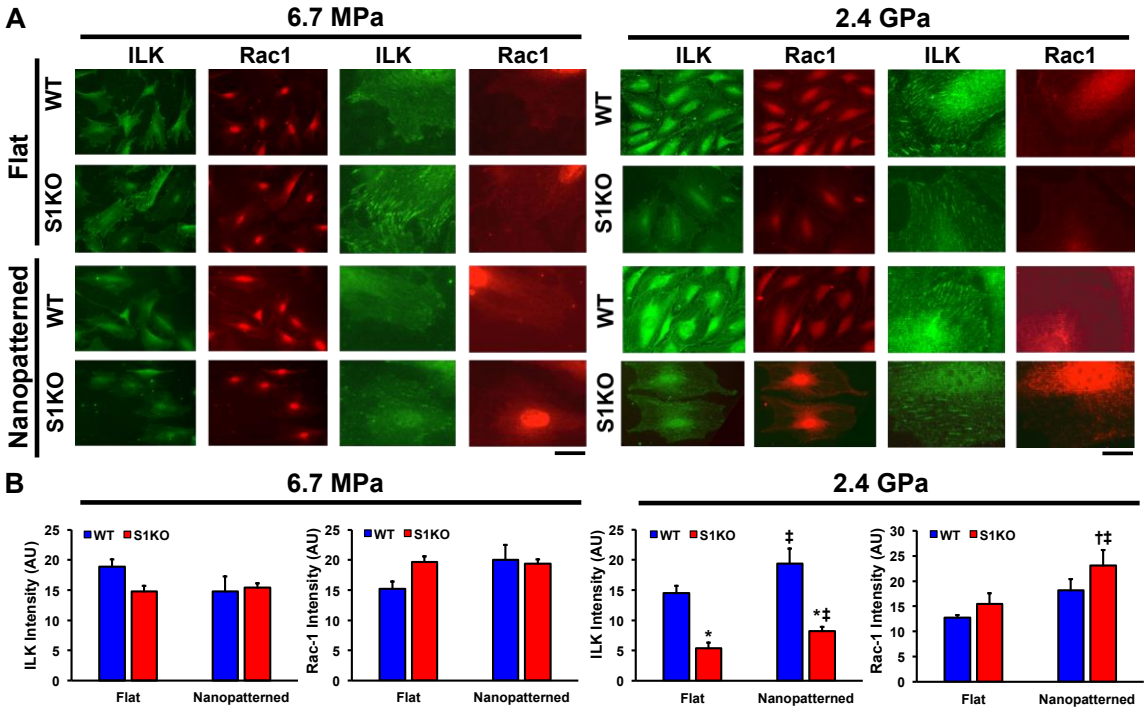

Figure 3.7. Syndecan-1 knockout and increased substrate stiffness decrease ILK signaling. Wild type (WT) and syndecan-1 knockout (S1KO) vascular smooth muscle cells (vSMCs) were grown on engineered substrates for 48 hours and then immunostained for ILK and Rac1. (A) Representative images of the immunostaining for ILK and Rac1. Bar = 200 µm. (B) Quantification of cellular localization of Rac1 and ILK for 6.7 MPa and 2.4 GPa substrates. Mean nuclear intensity, mean cytoplasmic intensity and ratio of mean nuclear intensity to mean cytoplasmic intensity. $^{*}p<0.05$ versus WT group on the same substrate. $^{\dagger}p<0.05$ versus WT cells grown on a nonpatterned substrate. $^{\ddagger}p<0.05$ versus S1KO cells grown on a nonpatterned substrate.

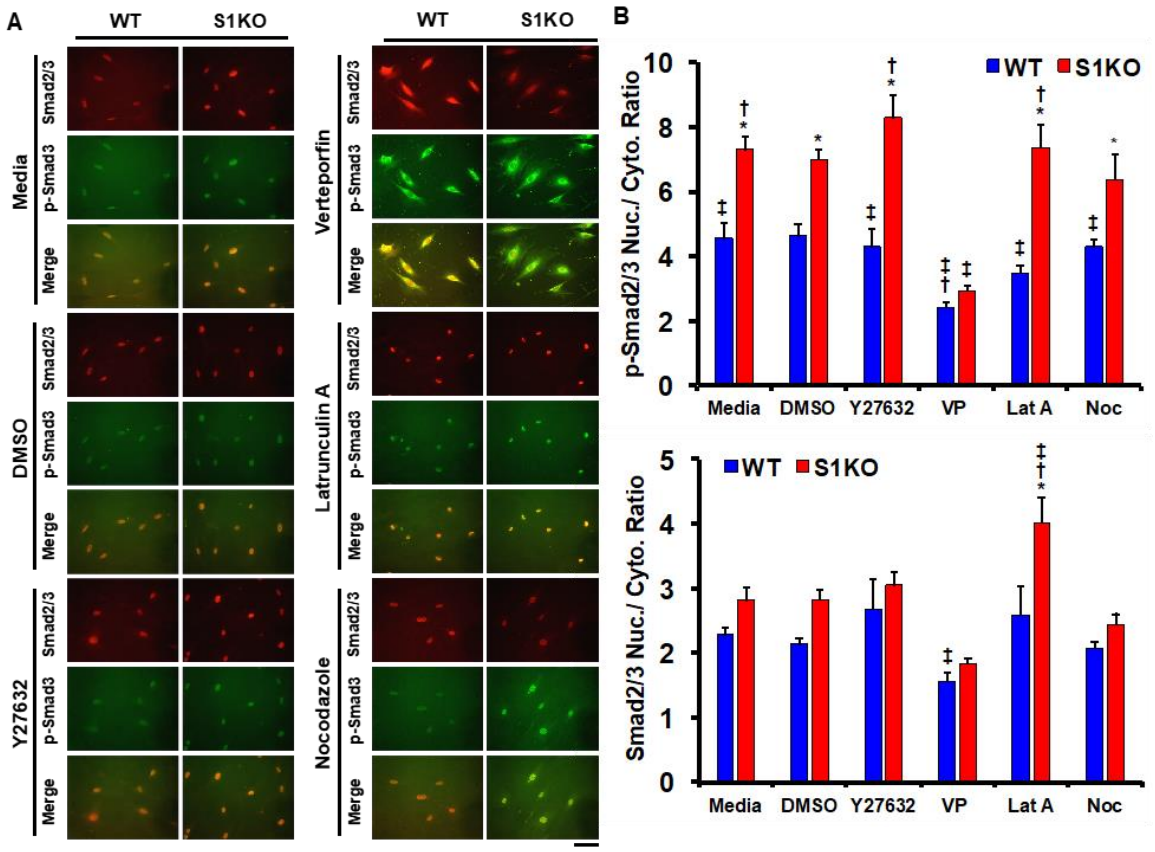

Figure 3.8. p-Smad2/3 localization to the nucleus is altered by Yap/Taz inhibition. WT and S1KO vSMCs were grown 2.4 GPa nanopatterned substrates for 24 hours, treated with media only, 0.1% DMSO, 10 μM Y27632, 10 μM Verteporfin (Vert), 1 μM Latrunculin A (Lat A) or 10 μM Nocodazole (Noc) for 2 hours and immunostained for Smad2/3 and phospho-Smad3 (Ser423/425; pSmad3). (A) Images of immunostaining for Smad2/3 and pSmad3. Bar = 200 μm. (D) Quantification of nuclear localization of Smad2/3 and pSmad3 in response to the materials and treatments. $^{*}p<0.05$ versus WT group of same treatment. $^{\dagger}p<0.05$ versus DMSO-treated WT group. $^{\ddagger}p<0.05$ versus DMSO-treated S1KO group.

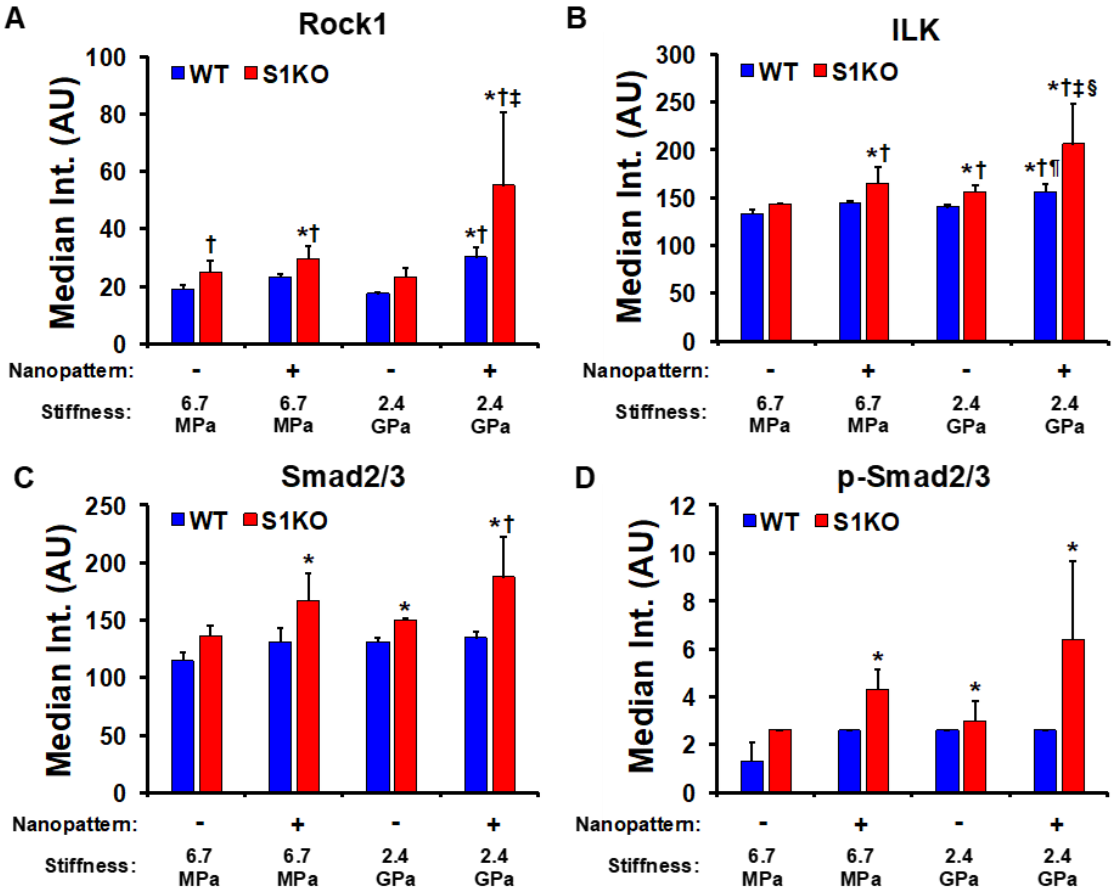

Figure 3.9. Loss of Syndecan-1 increases Rock1, ILK, Smad2/3 and p-Smad2/3 protein levels. Wild type (WT) and syndecan-1 knockout (S1KO) vascular smooth muscle cells (vSMCs) were grown on engineered substrates for 48 hours, stained with fluorochrome-conjugated antibodies. Median intensity of staining for (A) Rock1, (B) ILK, (C) Smad2/3 and (D) p-Smad2/3. $^{*}p<0.05$ versus WT group grown on nonpatterned 6.7 MPa substrate. $^{\dagger}p<0.05$ versus WT group grown on nonpatterned 2.4 GPa substrate. $^{\ddagger}p<0.05$ versus WT group grown on nanopatterned 6.7 MPa substrate. $^{\S}p<0.05$ versus S1KO group grown on nanopatterned 2.4 GPa substrate. $^{\P}p<0.05$ versus WT group grown on nanopatterned 2.4 GPa substrate.

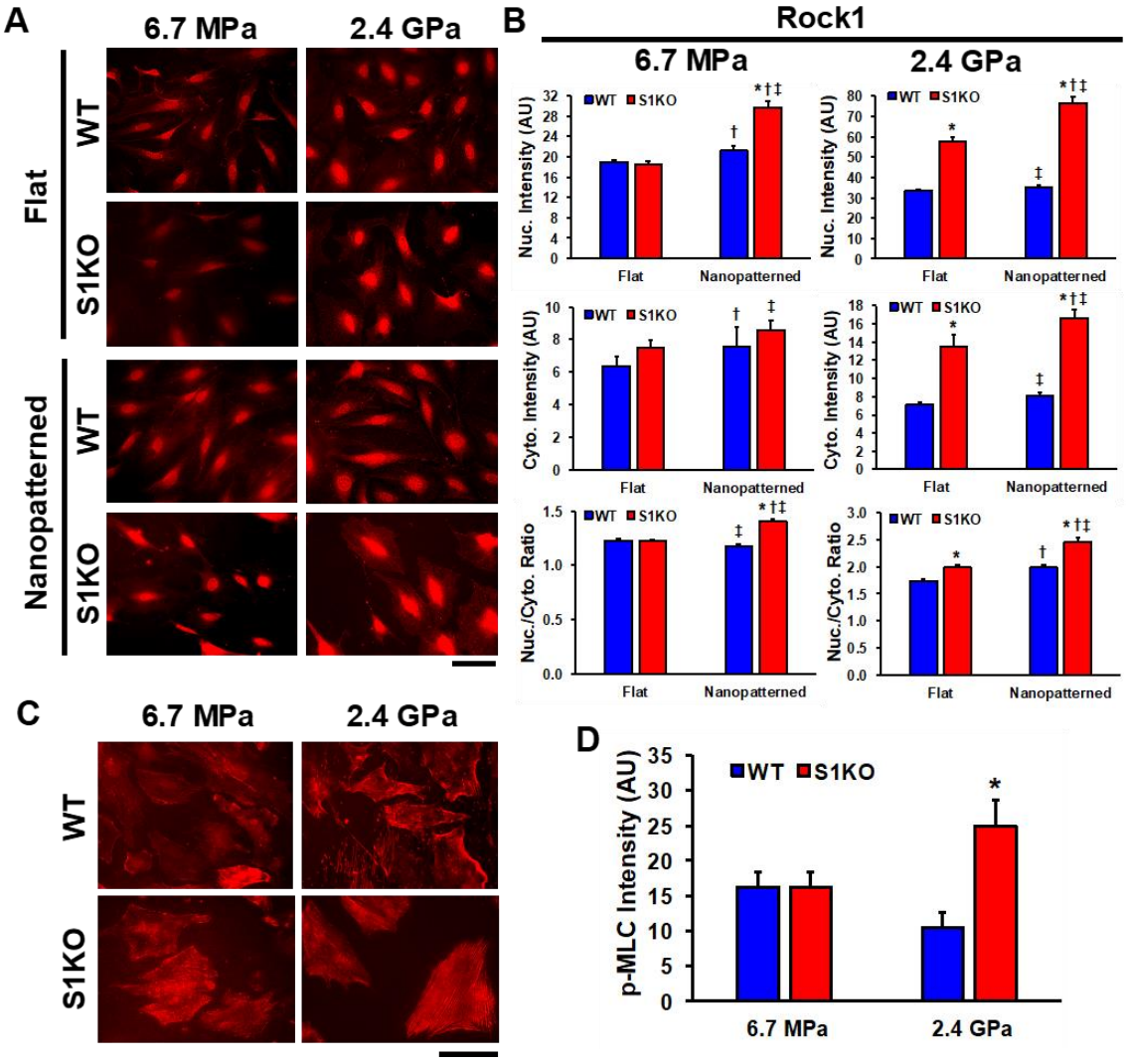

Figure 3.10. Loss of Syndecan-1 increases Rock 1 and p-MLC signaling on nanopatterned substrates and substrata of increased stiffness. Wild type (WT) and syndecan-1 knockout (S1KO) vascular smooth muscle cells (vSMCs) were grown on engineered substrates for 48 hours and then immunostained. (A) Representative images of the immunostaining for Rock1 and p-MLC. Bar = 200 μm. (B) Quantification of nuclear and cytoplasmic Rock1 localization. (C) Representative images of the immunostaining for p-MLC. Bar = 200 μm. (D) Quantification of p-MLC localization. $^{*}p<0.05$ versus WT group on the same substrate. $^{\dagger}p<0.05$ versus WT cells grown on a nonpatterned substrate. $^{\ddagger}p<0.05$ versus S1KO cells on flat surfaces.

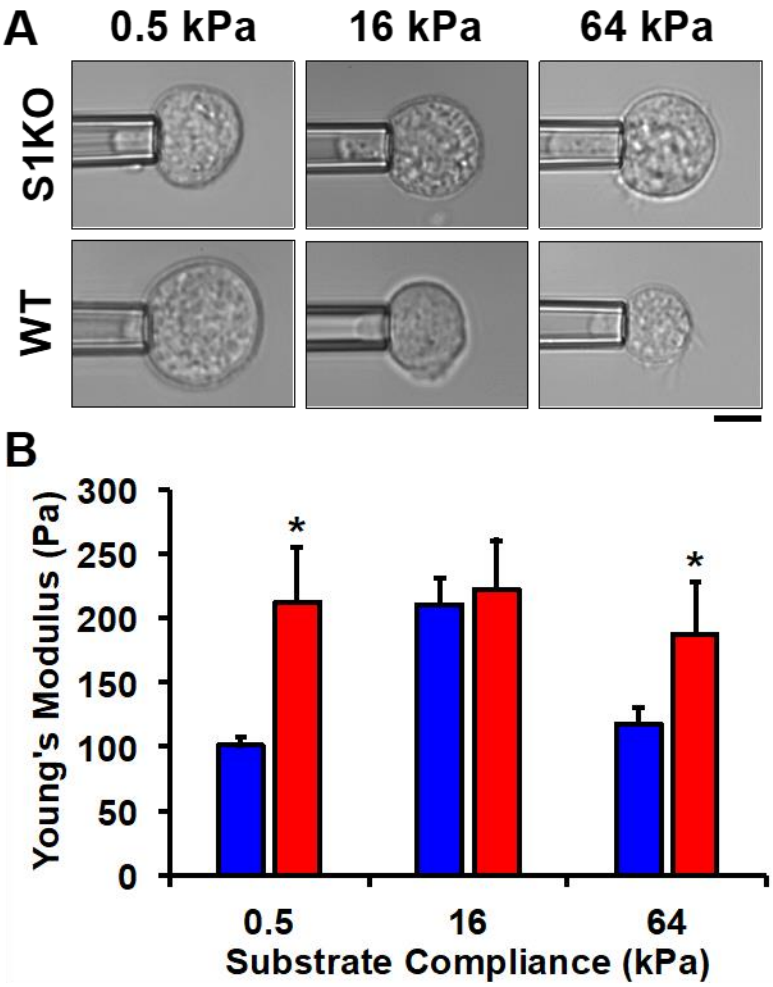

Figure 3.11. Knockout of syndecan-1 increases the stiffness of vascular smooth muscle cells measured by micropipette aspiration. (A) Micropipette aspiration of cells tested at a suction pressure of 400 Pa. Bar = 10 µm. (B) Young's Moduli of vascular smooth muscle cells grown on 0.5, 16 and 64 kPa substrates prior to testing. $^{*}p<0.05$ versus WT cells on the same substrate.

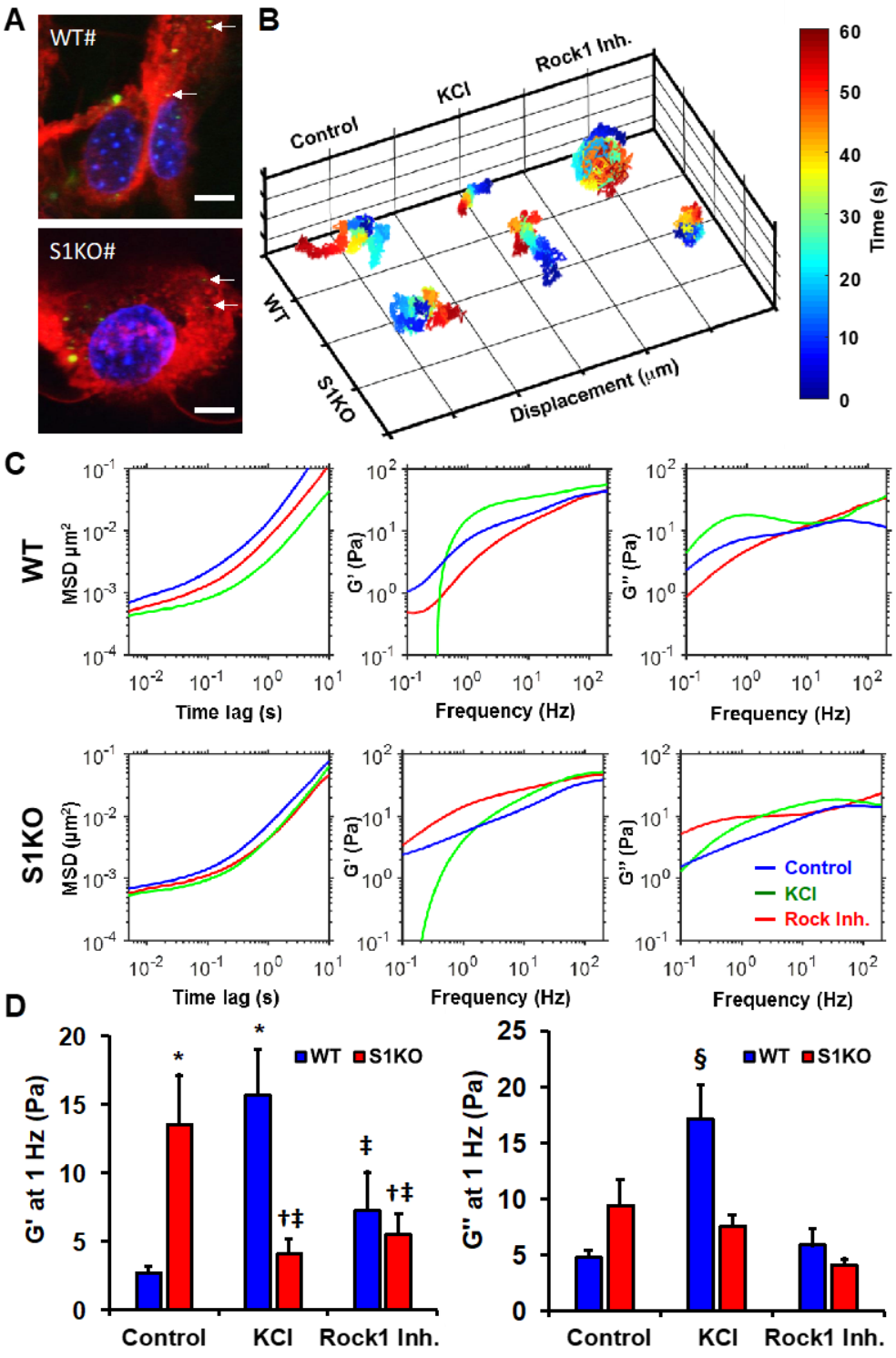
A
WT#
S1KO#
B
Control
KCl
Rock1 Inh.
WT
S1KO
Displacement (μm)
Time (s)
C
WT
S1KO
MSD μm²
MSD (μm²)
Time lag (s)
G' (Pa)
G'' (Pa)
Frequency (Hz)
Control
KCl
Rock Inh.
D
G' at 1 Hz (Pa)
G'' at 1 Hz (Pa)
WT
S1KO
Control
KCl
Rock1 Inh.

Figure 3.12.

Figure 3.12. Syndecan-1 knockout vascular smooth muscle cells have increased stiffness under baseline conditions and have altered response to contractile stimuli. (A) Live cell imaging of WT and S1KO vSMCs with fluorescent nanoparticles. Bar = 10 μm. (B) Representative 3D trajectories of ballistically injected fluorescent nanoparticles in WT and S1KO vSMCs with stimulation by KCl, followed by Rock inhibition. (C) Particle-tracking microrheology analysis in cytoplasm for WT and S1KO vSMCs. The averaged mean-squared displacement (MSD) curves were calculated from trajectories and the averaged frequency-dependent elastic modulus (G') and viscous modulus (G") of the cytoplasm can be approximately computed from the MSD curves. The time step of the 3D particle tracking was 5 ms, and the prescribed tracking duration was set as 60 s. (D) Averaged elastic and viscous moduli for WT and S1KO vSMCs that were sequentially treated with a contractile stimulus (KCl) and then a Rock inhibitor (Y27632). All moduli were evaluated at a frequency of 1 Hz. $^{*}p<0.05$ versus WT group on the same substrate. $^{\dagger}p<0.05$ versus WT cells grown on a nonpatterned substrate. $^{\ddagger}p<0.05$ versus S1KO cells on flat surfaces. $^{\S}p<0.05$ versus all other groups

Chapter 4. Development of a Syndecan-1 FRET Tension Sensor

4.1 INTRODUCTION

While several putative shear-stress mechanosensors have been identified, much is still unknown about shear stress mechanotransduction, especially at the surface of the cell. As a component of the flow-interfacing glycocalyx, SDC1 is an appealing candidate flow sensor. In previous work, our group found that knockout of SDC-1 reduced the shear-stress-induced phosphorylation of Akt and spatial distribution of paxillin phosphorylation in endothelial cells. Knockout of SDC-1 also reduced the shear-stress-induced activation of RhoA.(Voyvodic et al., 2014) Our recent work found that loss of SDC1 resulted increased cellular stiffness, reduced alignment in response to nanogrooves and alterations in signaling pathways affected by substrate stiffness.(Le et al., 2018) These findings indicate a mechanosensory role for SDC1.

Much has been hypothesized about the interactions of the external mechanical environment of cells with the glycocalyx, but very little is known about the transfer of forces to the glycocalyx components such as SDC1. Less still is known about what subdomains of SDC1 are involved in the propagation of tension across the protein. To probe how tension forms on SDC1, we created a syndecan-1 tension sensor (SDC1-TS) containing the TSMod tension sensing module in the ectodomain of SDC1, after amino acid 22 (**Figure 4.1A-B, D**). Flanking the TSMod (a 44-amino acid flagelliform elastic linker) are mTFP (donor) and Venus A206K (acceptor).(Grashoff et al., 2010a) Additionally, we generated three variants of the SDC1-TS to investigate the importance of SDC1's ectodomain (TSΔEcto), GAG chains (TSΔGAG) and cytoplasmic domain (TSΔCyto) in tension propagation (**Figure 4.1B, D**), as well as donor- and acceptor-only controls (**Figure 4.1C**). We then applied the SDC1-TS and its variants to engineered

substrates examine how tension on SDC1 is modulated by substrate stiffness and nanotopography.

Collectively, these tension sensors enabled us to elucidate a number of previously unknown features of SDC1. We found that the GAG chains, which bind the ectodomain directly, contribute to SDC1 tension at the substrate-level (cell-substrate interface). At the surface level of the cell, the core ectodomain contributes to SDC1 tension. The cytoplasmic domain of SDC1 participates in off-loading tension via SDC1's direct association with the cytoskeleton. In response to substrate compliance, SDC1 tension increases with increasing substrate stiffness. Finally, SDC1 tension is altered by the presence of nanogrooves.

4.2 MATERIALS AND METHODS

4.2.1. Creation of the SDC1-TS expression construct

The recombinant lentiviral plasmid containing human *SDC1* was purchased from Genecopoeia (cat# EX-A0087-Lv105). The tension sensing module was cloned from a vector Addgene (cat# 26021) (Grashoff et al., 2010b). The ORF of the tension sensing module (bases 947 to 2494) was cloned into the *SDC1* vector after base 965 (5'ACG GCT GTA 3') (**Appendix B**) by Geneocopoeia's cloning service.

4.2.2. Generation of the SDC1 tension sensor mutants

The TSΔEcto vector was created via PCR using the primers indicated in **Table 4.1** from the SDC1-TS vector template. These primers were used to introduce NheI sites for the ligation of the PCR product. The resulting vector excludes bases 363 through 949 (amino acids 22 through 217) of the human *Sdc1* gene, leaving only 11 amino acids at the N-terminus of the ectodomain of SDC1. The TSΔGAG vector was created via site-directed mutagenesis of serines 37, 45, 47, 206 and 216 of the human *SDC1* gene to alanine (Langford, Stanley, Cao, & Sanderson, 1998). The TSΔCyto vector was created via site-directed mutagenesis of amino acid 278 (ATG, methionine) of the human *SDC1* gene to a stop codon (TGA), removing amino acids 279 through 310, similar to a previous approach. (Miettinen, Edwards, & Jalkanen, 1994). Both site-directed mutagenesis services were performed by Genscript. The Sdc1M (donor-only) and Sdc1V (acceptor-only) constructs were created via PCR from the SDC1-TS vector template (**Table 4.1**).

Table 4.1. Primers used to generate ectodomain mutant of SDC1 tension sensor and bleed-through control vectors

Expression Construct	Primers
TSΔEcto	*Forward* GCATGCTAGCGGAGAATACGGCTGTAATG *Reverse* GCATGCTAGCAGGGCCGGCTGCAGGCTCA
Sdc1M (donor-only)	Forward AGTCGCTAGCGGTCCAGGTGGTGCTATG *Reverse* AGTCGCTAGCTACAGCCGTATTCTCCCCCGA
Sdc1V (acceptor-only)	*Forward* AGTCGCTAGCGTGGCCGTGGAGCCTGAC *Reverse* AGTCGCTAGCTTATGGCCCCTTGTACAGCTC

4.2.3. Molecular biology techniques

PCR was performed with 10 ng of the construct vector, 33 ul of nuclease-free water, 10 µl of 5x Fusion GC Buffer (New England Biolabs), 1 ul of 10 mM dNTPs (New England Biolabs), 2.5 ul of 10 µM forward primer and 2.5 ul of 10 µM reverse primer. Following PCR, the reactions were digested with 1 µl of 20,000 units/ml DpnI (New England Biolabs) at 37°C for 30 min. The reactions were PCR purified (Qiagen) and eluted into 30 µl of nuclease-free water. The PCR product was digested with 1 µl of 20,000 units/ml NheI (New England Biolabs) at 37C for 30 min. Gel electrophoresis was performed at 75V using an 8% agarose gel. Bands of the desired molecular weight were cut from the gels using a razor and gel extraction (Qiagen) was performed. 14 µl of the product was used for the ligation

reaction with 2 µl of T4 ligase and 3 µl of nuclease-free water. T4 ligase (New England Biolabs) in the ligation reactions were deactivated by water bath incubation at 65°C for 10 min. 5 µl of the ligation product was transformed into Stbl3 *E. coli* competent cell line (Invitrogen, cat #C7373-03). 250ul of the culture was plated onto an LB agar plate containing 100 µg/ml ampicillin. The following day, isolated colonies were picked and cultured in LB broth for 16 hours.

4.2.4. Cell culture

Human umbilical vein endothelial cells (HUVECs) from a single donor (Lonza, #C-11200) were cultured in MCDB-131 culture medium (Gibco) with 7.5% fetal bovine serum (FBS), endothelial cell growth supplement (R&D Systems), L-glutamine and antibiotics. 293Ta cells (LT008; Genecopoeia, Inc.) were cultured in DMEM culture medium (Gibco) supplemented with 10% FBS, L-glutamine and antibiotics. 293Ta packaging cells (ATCC) were cultured in DMEM culture medium (Gibco) supplemented with 10% heat-inactivated FBS, L-glutamine and antibiotics. All cells were incubated at 37°C with 5% CO2. Unless otherwise noted, cells were seeded onto glass-bottom dishes (MatTek). The glass-bottom dishes were coated with a solution of 11% (w/v) type I rat tail collagen (Corning) overnight at 4°C.

4.2.5. Lentiviral transduction

A lentiviral packaging kit (LT001; Genecopoeia, Inc.) was used to produce lentivirus. Packaging plasmids for the SDC1-TS, TSΔEcto, TSΔGAG or TSΔCyto sensors and donor-only or acceptor-only were co-transfected with the manufacturer's lentiviral

expression clone into HEK 293Ta packaging cells. Prior to viral infection, HUVECs were cultured in MCDB-131 culture medium 5% heat-inactivated FBS, L-glutamine and antibiotics. Pseudovirus containing the lentiviral expression constructs was harvested and transduced into HUVECs in complete HUVEC culture medium containing 8 μg/ml polybrene. One day after transduction, the media was changed to complete HUVEC culture medium with 2 μg/ml puromycin. Fresh media with puromycin was added daily for five days to create the stable cell line.

4.2.6. Immunostaining and confocal microscopy

Endothelial cells expressing SDC1-TS, TSΔEcto, TSΔGAG, TSΔCyto, mTFP only, Venus only and non-transduced HUVECs at passage 8 were trypsinized and seeded at 5,000 cells/cm^2 onto collagen-coated glass coverslips of 25 mm in diameter. Cells were cultured for 48 hours and washed with PBS at 37°C and fixed with 4% paraformaldehyde for 10 min. Cells were then washed three times with PBS and permeabilized with 0.2% Triton X-100 for 5 min. The cells were blocked with 1% BSA in PBS for 40 minutes and stained with anti-syndecan-1 (12765; Santa Cruz Biotechnology, Inc.) and anti-GFP rabbit (ab6556; Abcam, Inc.) primary antibodies diluted in PBS with 1% BSA overnight at 4°C. The cells were then rinsed with PBS for 10 minutes three times. Secondary antibodies conjugated to fluorophores were added at 1:1000 dilution in 1% BSA in PBS containing 1 μg/ml of DAPI for nuclear staining. After 75 minutes of incubation at room temperature, the cells were rinsed extensively with repeated PBS washes. The coverslips were mounted onto glass slides with anti-fade mounting media (Vector Laboratories, Inc.). Fixed cells

were imaged using a Fluoview FV10i confocal microscope (Olympus) at 60x magnification with oil immersion.

4.2.7. Western blot

Cells were washed twice with cold PBS and lysed with RIPA buffer supplemented with 5 mM EDTA and protease and phosphatase inhibitor cocktail. Lysates were sonicated for 1 min, followed by centrifugation at 14,000 x g for 15 min. The supernatant was collected, and proteins were separated by Bis-Tris gradient (4-12%) gel and transferred onto nitrocellulose membranes. Membranes were blocked in 5% blocker-PBST and incubated with anti-Syndecan-1 antibody (2357; Santa Cruz Biotechnology, Inc.) at room temperature for 2 hours. Immuno-complexes were detected by applying enhanced chemiluminescent substrate (34096; ThermoFisher) to the membranes for 1 minute and immediately imaged using the GBox Chemi XX6 Imager.

4.2.8. Drug treatment

Cells were treated for 20 min with 1 μM latrunculin A in a final DMSO dilution of 1:1000.

4.2.9. Substrates

Glass coverslips. Unless otherwise noted, glass-coverslip-bottom 35 mm petri dishes were used for FRET imaging. Coverslips were coated with a solution of 11% (w/v) type I collagen overnight to facilitate cell attachment.

Substrates of varying compliance. Hydrogels (elastic moduli of 0.2 kPa and 25 kPa) bound to glass coverslips and pre-coated with type I collagen by the manufacturer were utilized. 24-48 hours after seeding, the coverslips were gently rinsed with warm PBS and Tyrode's solution and inverted onto a glass-coverslip with additional Tyrode's solution for sensitized emission imaging.

Micropatterns. Micropatterned glass coverslip chips (CYTOOchip, Cytoo) containing crossbows and Y shapes accommodating 700, 1100 and 1600 μm^2 of cell area (large, medium and small, respectively) were coated with 20 μg/ml type I rat tail collagen according to the manufacturer's instructions and seeded with 20,000 cells/ml and 4 ml/chip. Between 1.5 and 4 hours after seeding, micropatterned coverslips were transferred to a proprietary chip holder and gently rinsed with warm PBS.

Nanopatterned materials. Nanopatterned substrates were fabricated from a polyurethane acrylate (PUA) precursor, as described previously.(D. H. Kim et al., 2009) Briefly, an adhesion promoter (Minuta Tech) was applied to the glass coverslips by spin coating at 2000 rpm for 20 seconds and the coverslips were then baked at 65°C for 20 min. A PUA-based polymer of commercially characterized stiffness (6.7 MPa or 2.4 GPa) was then spin coated onto the glass substrate and a PDMS mold with nanogrooves having an 800:800 nm groove:gap ratio with a 400 nm groove depth was placed on top of the PUA precursor layer. For nonpatterned surfaces, a mold with no features was placed on the polymer layer. Through capillary action, the polymer fills the mold and a nanopatterned surface is obtained. The patterns were UV cured using a wavelength of 365 nm for 60

seconds. The substrates were then placed into well plates and plasma coated to facilitate protein adsorption. The substrates were then coated with a solution of 11% (w/v) type I collagen overnight to facilitate cell attachment.

4.2.10. Sensitized emission FRET evaluation

Cell culture media was replaced with warm PBS, followed by warm HEPES-buffered Tyrode's solution (Alfa Aesar). Sensitized emission imaging was performed using a Zeiss 710 confocal microscope at 40x magnification with immersion oil on a stage heated to 37°C. An HFT 458/514 beam splitter was used. For sensitized emission analysis, three images were obtained. For the donor (mTFP1) channel image, cells were excited with a 458 nm laser and emission was collected between 470-499 nm. For the acceptor (Venus) channel image, excitation was performed with a 514 nm laser and emission was collected between 530-600 nm. The FRET channel image was obtained using excitation of the donor and acceptor emission. Z-stacks were obtained in 0.50 μm steps. For drug treatment experiments, sensitized emission imaging was performed prior to drug treatment for baseline FRET measurements. Imaging was performed 20 min following drug treatment on the same cell.

4.2.11. FRET analysis and image processing

Donor, acceptor and FRET images were loaded into the FRET Analyzer and Colocalization Analyzer plugin for Fiji (Hachet-Haas et al., 2006). Bleed-through correction was performed using the SDC1M (donor-only) and SDC1V (acceptor-only) cell lines cultured on the various substrates utilized. For each slice in a z-stack, apparent FRET

from non-colocalized mTFP and Venus were removed within the plugin. For cells cultured on the nanopatterned substrate, which produces autofluorescence, background-subtraction for each channel and z-position was performed before FRET-indexed images were generated. The default "Fire" lookup table (LUT) assigned by the plugin was changed to a modified "Jet" LUT. Z-stacks, z-projections, side views and 3D projections were created using Fiji software. Surface- and substrate-level z-slices were determined by evaluation of side views. Z-projections were generated by average intensity. Masks were created in Photoshop (Adobe) using Venus channel images to distinguish zero-FRET from regions where the sensor was not present.

4.2.12. FRET index quantification from images

Substrate-level and surface-level slices were identified from orthogonal views of z-stacks, and average z-projections were generated. For the quantification of FRET index, cells were subdivided lengthwise, and the first and last third of the cell was traced, avoiding the nucleus. The mean FRET index was obtained from these traced regions. For cells grown on substrates of varying stiffness, FRET index was measured instead from side views (in triplicate) due to deformation of 0.2 kPa substrates by the cells. For profile scans of cells grown on crossbow micropatterns and nanopatterned substrates, a 10-pixel tall region spanning the cell was drawn perpendicular to the micropattern or the direction of the nanopattern. For treatment experiments and shear stress experiments, relative FRET index was calculated by normalizing to baseline FRET index measurements of the same cell.

4.2.13. Statistical analysis

All results are shown as mean ± standard error of the mean. Comparisons between only two groups were performed using a Mann-Whitney test. Differences were considered significant at $p<0.05$. Multiple comparisons between groups were analyzed by a two-way ANOVA, followed by Dunnett's post-hoc test. A 2-tailed probability value <0.05 was considered statistically significant.

4.3 RESULTS

4.3.1. Localization of the SDC1 tension sensor

To validate whether the SDC1-TS localized properly within the cell, we immunostained non-transduced HUVECs and HUVECs expressing the SDC1-TS, TSΔEcto, TSΔGAG and TSΔCyto for Venus and SDC1. Although staining for SDC1 labels both native SDC1 and the tension sensors, it confirmed that the TS, TSΔEcto and TSΔGAG localize within the cell as expected. However, the TSΔCyto accumulates around and depresses the nucleus **(Figure 4.2)**.

4.3.2. Western blot

Western blot analysis confirmed the expected sizes for the SDC1-TS and mutant versions of the TS (**Figures 4.3-4.4).**

4.3.3. The SDC1 tension sensor is under higher tension than the ectodomain mutant sensor.

We cultured cells expressing the tension sensors, evaluated FRET using sensitized emission, imaging through the entire height of the cells (**Figure 4.5A, C**). This enabled the separation of surface-depth FRET, as well as substrate-depth FRET. At the surface level, tension on TSΔEcto was significantly lower than the complete SDC1-TS, as indicated by increased FRET index. At the substrate level, tension on TSΔEcto and TSΔGAG was lower than the complete SDC1-TS. However, tension on TSΔGAG at the surface level was similar to that of SDC1-TS at the surface level (**Figure 4.5B**). Under these baseline conditions, there were no significant differences in FRET index between the surface and substrate levels for any given sensor.

4.3.4. Cytoskeletal disruption reduces SDC1 tension.

As SDC1 is linked directly to the cytoskeleton via its cytoplasmic domain, we considered that cytoskeletal tension could influence SDC1 tension.(Carey, Bendt, & Stahl, 1996) To test whether the tension sensors respond to changes in cytoskeletal tension, we disrupted the cytoskeleton by treatment with 1 μM latrunculin A, observing increases in FRET for the SDC1-TS, TSΔEcto and TSΔGAG (**Figure 4.6A-B**). This increase in FRET was not exhibited by the TSΔCyto sensor.

4.3.5. Substrate compliance modulates SDC1 tension.

Our previous work indicated that SDC1 is important for smooth muscle cell mechanosensation of substrate stiffness. To examine if substrate compliance modulates tension on SDC1, itself, we cultured cells expressing the TS and mutant versions of the tension sensor onto collagen type I-coated hydrogels with elastic moduli of 0.2 or 25 kPa and evaluated FRET (**Figure 4.7A-B**). Cells expressing the SDC1-TS, TSΔEcto and TSΔCyto exhibited significantly higher tension (lower FRET) across the sensors when cultured on the 25 kPa substrate, compared to those cultured on the 0.2 kPa substrate. TSΔGAG exhibited no significant change in tension in response to substrate compliance. Compared to SDC1-TS, higher tension was observed in TSΔGAG on the 0.2 kPa substrate. TSΔCyto exhibited higher tension compared to SDC1-TS on the 25 kPa substrate (**Figure 4.7B**).

4.3.6. SDC1 tension is increased in regions of cellular adhesion.

SDC1 is known to cluster and turnover in focal adhesions.(Altemeier, Schlesinger, Buell, Parks, & Chen, 2012) Our observation that TSΔGAG is under less tension that SDC1-TS at the substrate level, under baseline conditions, led us to ask whether adhesion to the ECM contributes to SDC1 tension. To examine the response of SDC1 tension to regions of cellular adhesion, we utilized micropatterned chips (Cytoo), which spatially control adhesion at the level of a single cell. We cultured cells expressing the SDC1-TS and mutant versions of the sensor onto type I collagen crossbow and Y-shaped micropatterns, which are adhesive but surrounded by a non-adhesive coating (**Figure 4.8A**). We then evaluated FRET at the level of the micropattern (**Figure 4.8B**). Profile scans through FRET index images of cells cultured on the 1100 um^2 (medium) crossbow micropatterns (**Figure 4.9A**) indicated decreased FRET for SDC1-TS over adhesive regions (**Figure 4.9B**). The ratio of adhered-FRET and unadhered FRET for SDC1-TS was decreased in SDC1-TS compared to TSΔEcto on crossbows (**Figure 4.10A**).

4.3.8. SDC1 tension increases in response to nanogrooves.

Our previous work showed that the loss of SDC1 alters the mechanosensation of substrate stiffness and nanotopography. To understand how nanopatterning affects SDC1 tension, we cultured cells expressing the SDC1-TS and mutant versions of the sensor onto type I collagen-coated 2.4 GPa unpatterned (flat) and nanopatterned substrates and evaluated FRET (**Figure 4.11A-C**). FRET profiles of the substrate-level of the cell, perpendicular to the direction of the nanogrooves, revealed increased tension on SDC1-TS in regions of the cell adhered to the peaks of the nanopattern, compared to SDC1-TS on

the flat substrate (**Figure 4.12A**). Overall, nanopatterning increased tension on SDC1 (**Figure 4.13**). TSΔEcto and TSΔGAG on nanopatterned substrates exhibited decreased tension compared to SDC1-TS on the same substrate, while TSΔCyto exhibited increased tension. On flat substrates, only TSΔGAG and TSΔCyto exhibited increased tension compared to TS on the same substrate (**Figure 4.13**).

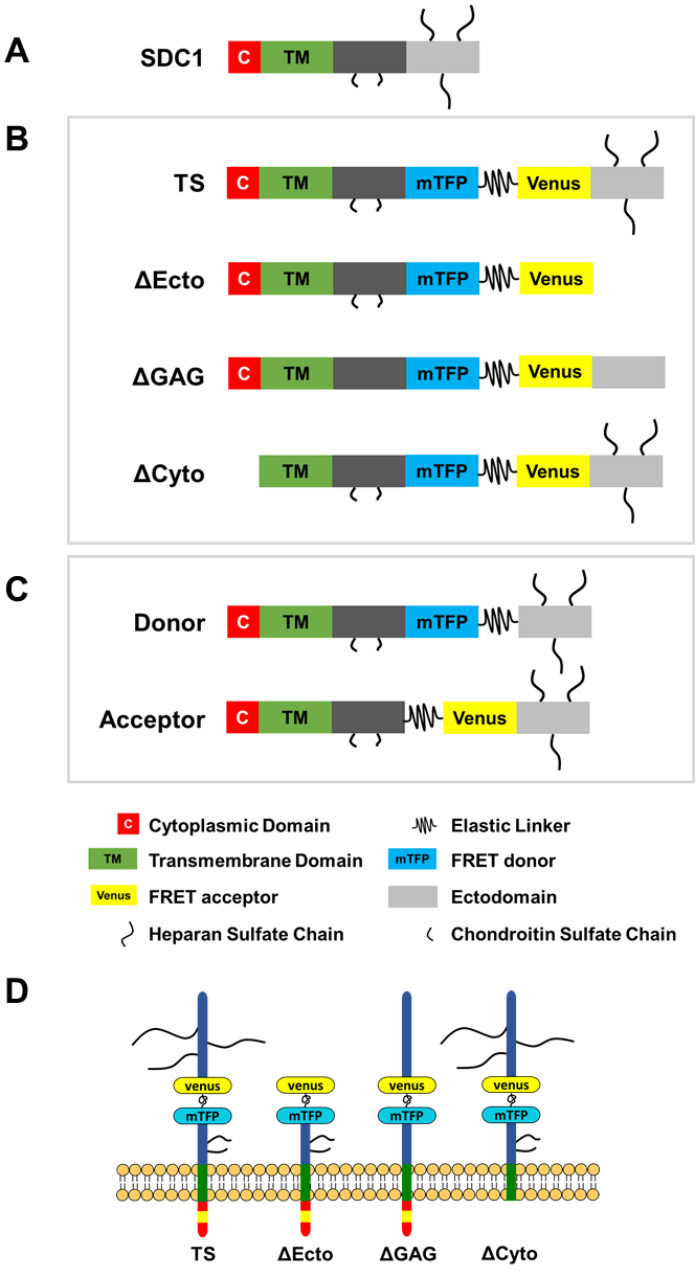

Figure 4.1. Diagram of SDC1 tension sensors. (A) Human SDC1 protein. (B) A FRET construct was inserted into the extracellular domain of SDC1 to create the SDC1 tension sensor (TS). An ectodomain mutant (ΔEcto), glycosaminoglycan attachment site mutant (ΔGAG) and cytoplasmic domain mutant (ΔCyto) were created to investigate SDC1 subdomains in tension propagation. (C) Donor- and acceptor-only controls for bleed-through correction. (D) Alternative diagram of tension sensors.

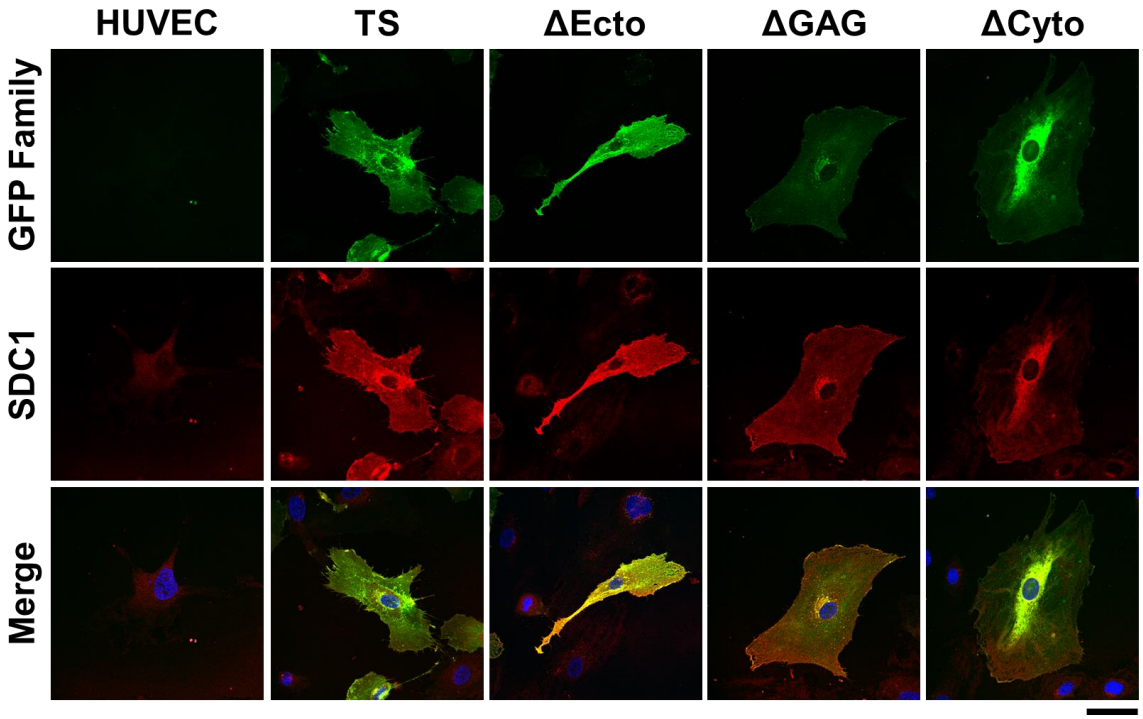

Figure 4.2. Representative immunostaining for GFP family and SDC1. Localization of the tension sensing construct (GFP family) and SDC1 within non-transduced human umbilical vein endothelial cells (HUVECs) and HUVECs expressing the SDC1 tension sensor (TS), ectodomain mutant (ΔEcto), glycosaminoglycan attachment site mutant (ΔGAG) or cytoplasmic domain mutant (ΔCyto). Bar = 50 μm.

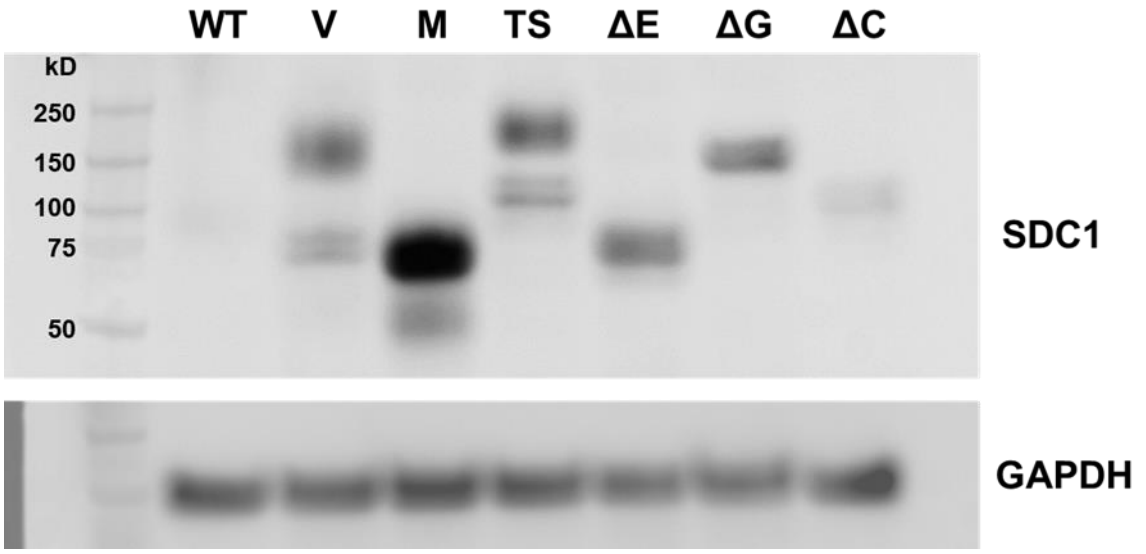

Figure 4.3. Western blot for SDC1. Non-transduced human umbilical vein endothelial cells (HUVECs) (WT), HUVECs expressing acceptor only (V) and donor only (M) bleed-through controls, SDC1 tension sensor (TS), ectodomain mutant (ΔE), glycosaminoglycan chain attachment site mutant (ΔG) and cytoplasmic domain mutant (ΔC).

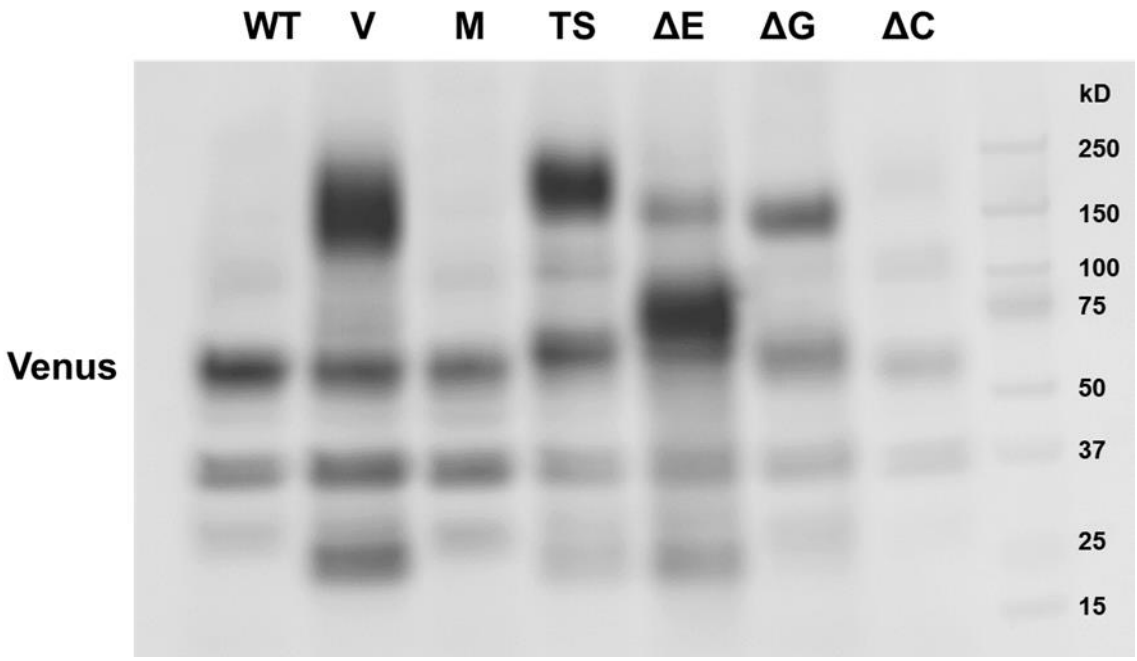

Figure 4.4. Western blot for Venus. Non-transduced HUVECs (WT), HUVECs expressing acceptor only (V) and donor only (M) bleed-through controls, syndecan-1 tension sensor (TS), ectodomain mutant (ΔE), glycosaminoglycan chain attachment site mutant (ΔG) and cytoplasmic domain mutant (ΔC).

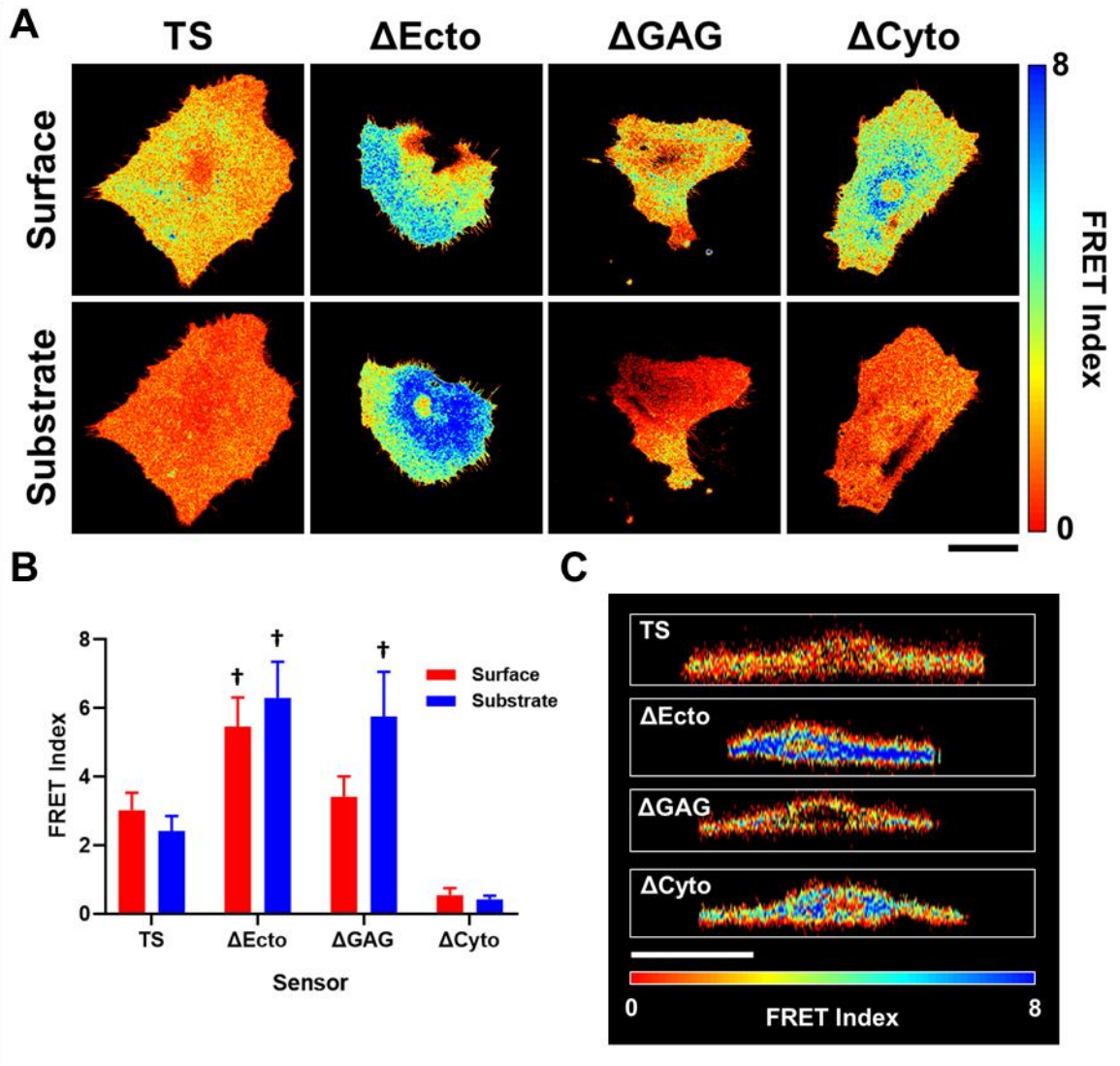

Figure 4.5. Baseline FRET in SDC1 tension sensor and mutant sensors. (A) Representative surface- and substrate-level z-projected FRET index images of cells expressing the SDC1 tension sensor (TS), ectodomain mutant (ΔEcto), glycosaminoglycan chain attachment site mutant (ΔGAG) and cytoplasmic domain mutant (ΔCyto). Bar = 50 μm. (B) Quantification of FRET index at the surface and substrate levels. $^{\dagger}p<0.05$ versus TS at the same cellular level. n = 10-16. (C) Side views. Bar = 50 μm.

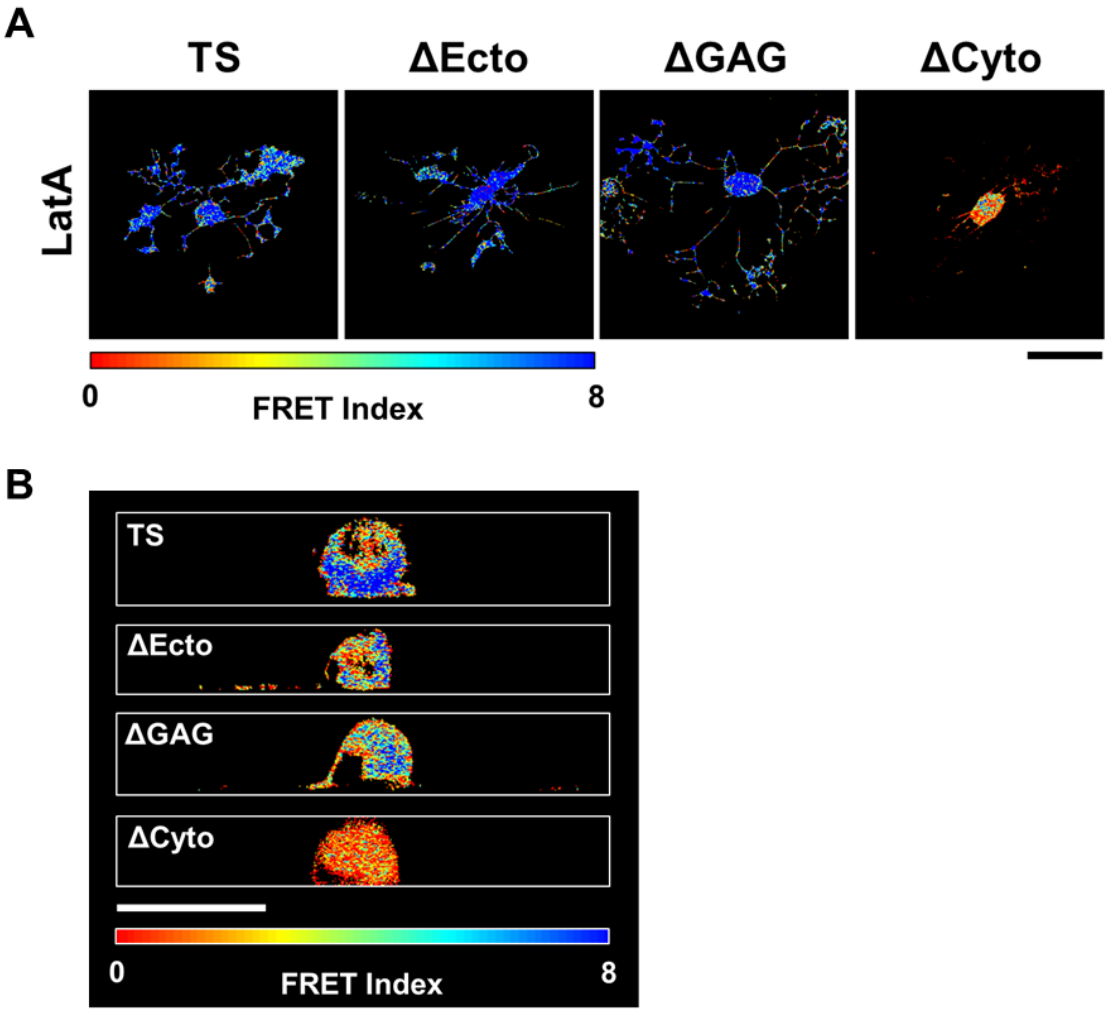

Figure 4.6. Cytoskeletal disruption decreases tension on SDC1 tension sensor. Cells expressing the SDC1 tension sensor (TS), ectodomain mutant (ΔEcto), glycosaminoglycan chain attachment site mutant (ΔGAG) and cytoplasmic domain mutant (ΔCyto) were treated with 1 μM latrunculin A (LatA). (A) Representative FRET index images. (B) Representative side views. Bars = 50 μm.

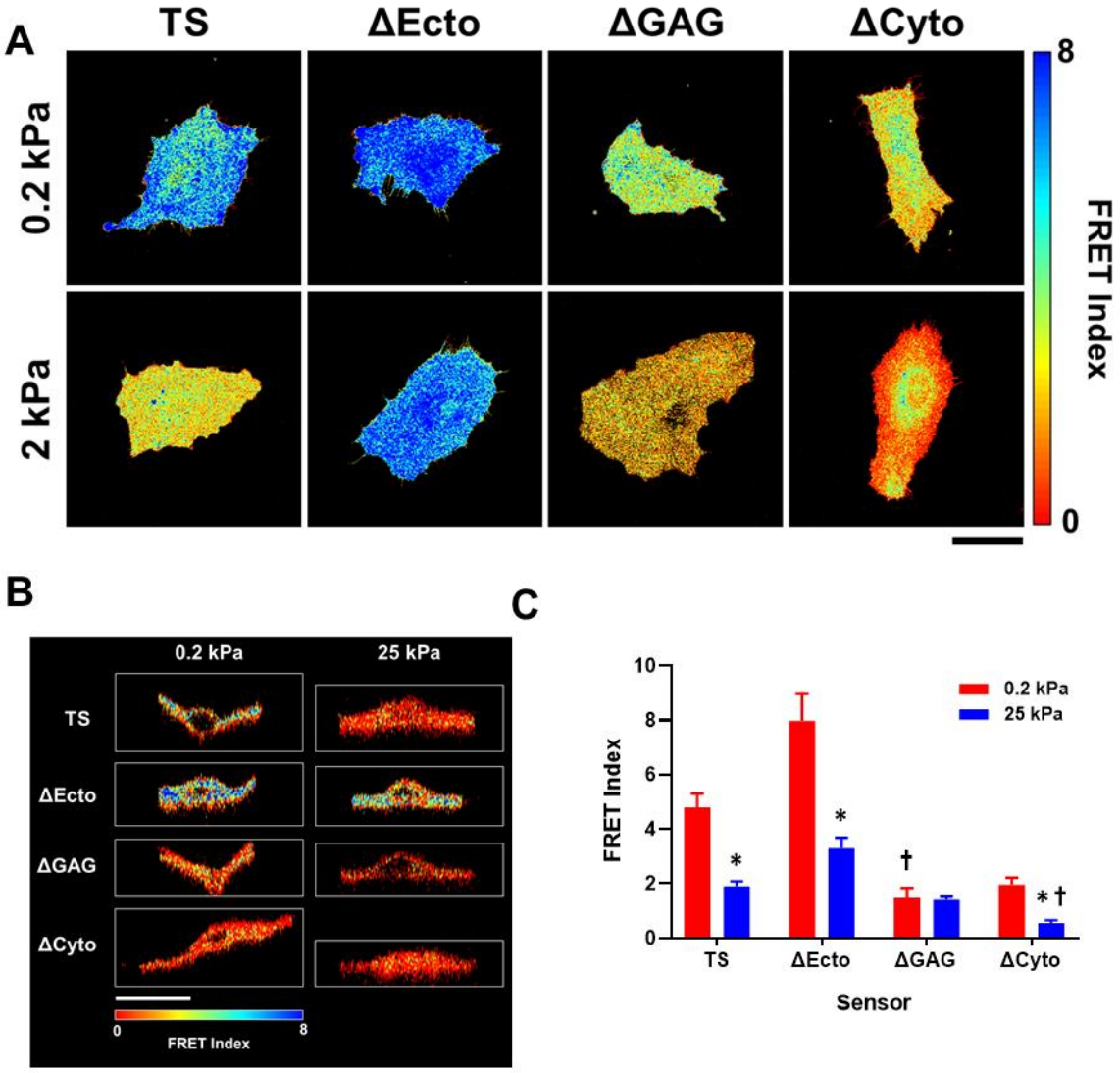

Figure 4.7. Tension on SDC1 tension sensor decreases in response to decreased substrate compliance. Cells expressing the SDC1 tension sensor (TS), ectodomain mutant (ΔEcto), glycosaminoglycan attachment site mutant (ΔGAG) and cytoplasmic domain mutant (ΔCyto) were cultured on 0.2 kPa and 25 kPa hydrogels coated with collagen type I. (A) Representative maximum z-projected FRET index images. (B) Side views. Bars = 50 μm. (B) Quantification of surface- and substrate-level FRET indices. $^{*}p<0.05$ versus cells expressing the same sensor, cultured on 0.2 kPa substrate. $^{\dagger}p<0.05$ versus TS cells cultured on the same substrate. $n = 10$.

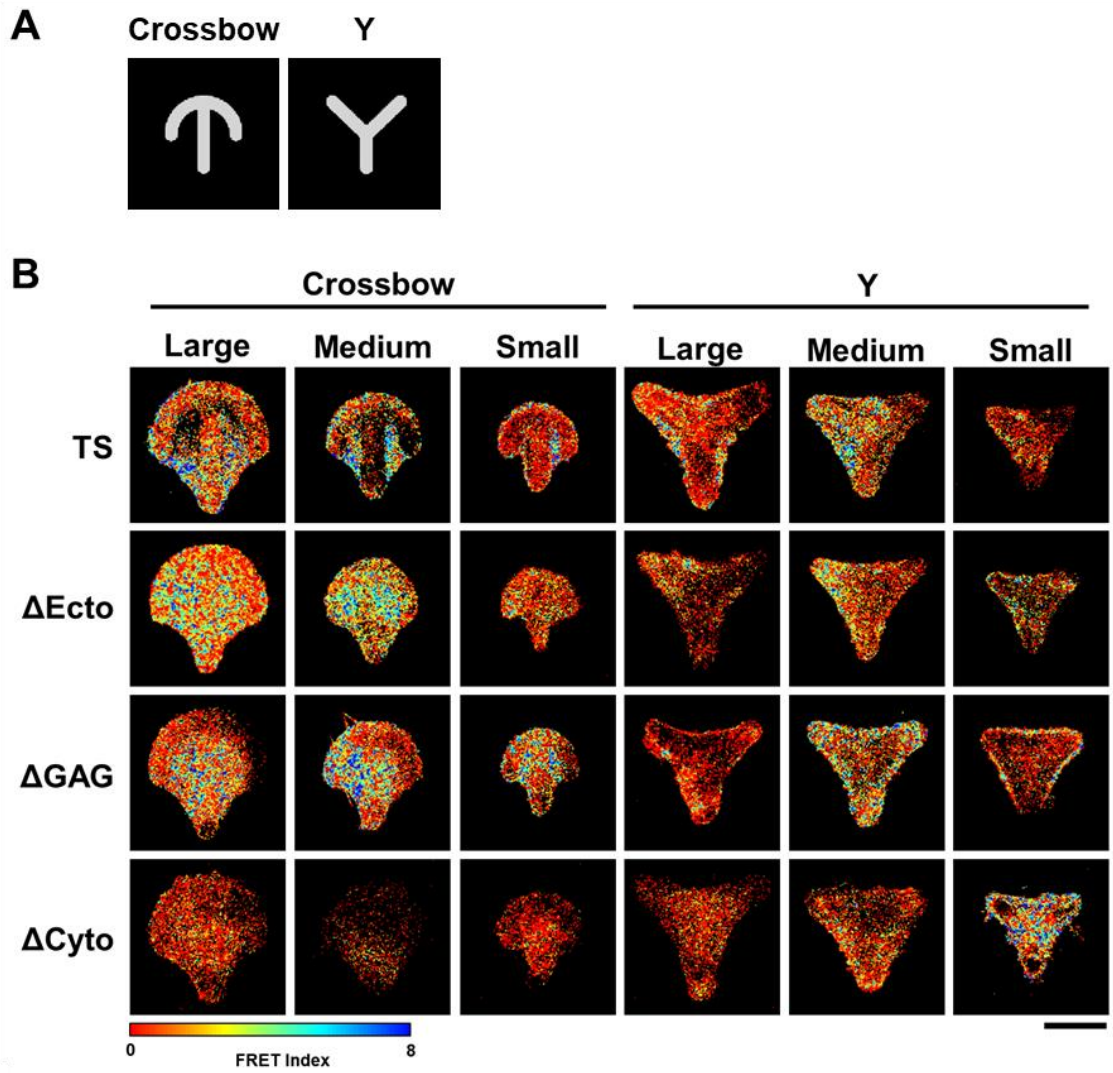

Figure 4.8. Tension on SDC1 is increased in regions of cellular adhesion. Human umbilical vein endothelial cells (HUVECs) expressing the SDC1 tension sensor (TS), ectodomain mutant (ΔEcto), glycosaminoglycan attachment site mutant (ΔGAG) and cytoplasmic domain mutant (ΔCyto) were cultured onto micropatterned substrates and evaluated for FRET. (A) Diagram of crossbow and Y-shaped micropatterns. Black, non-adherent regions. Gray, adherent regions coated with collagen type I. (B) Representative substrate-level FRET index images. Bar = 25 μm.

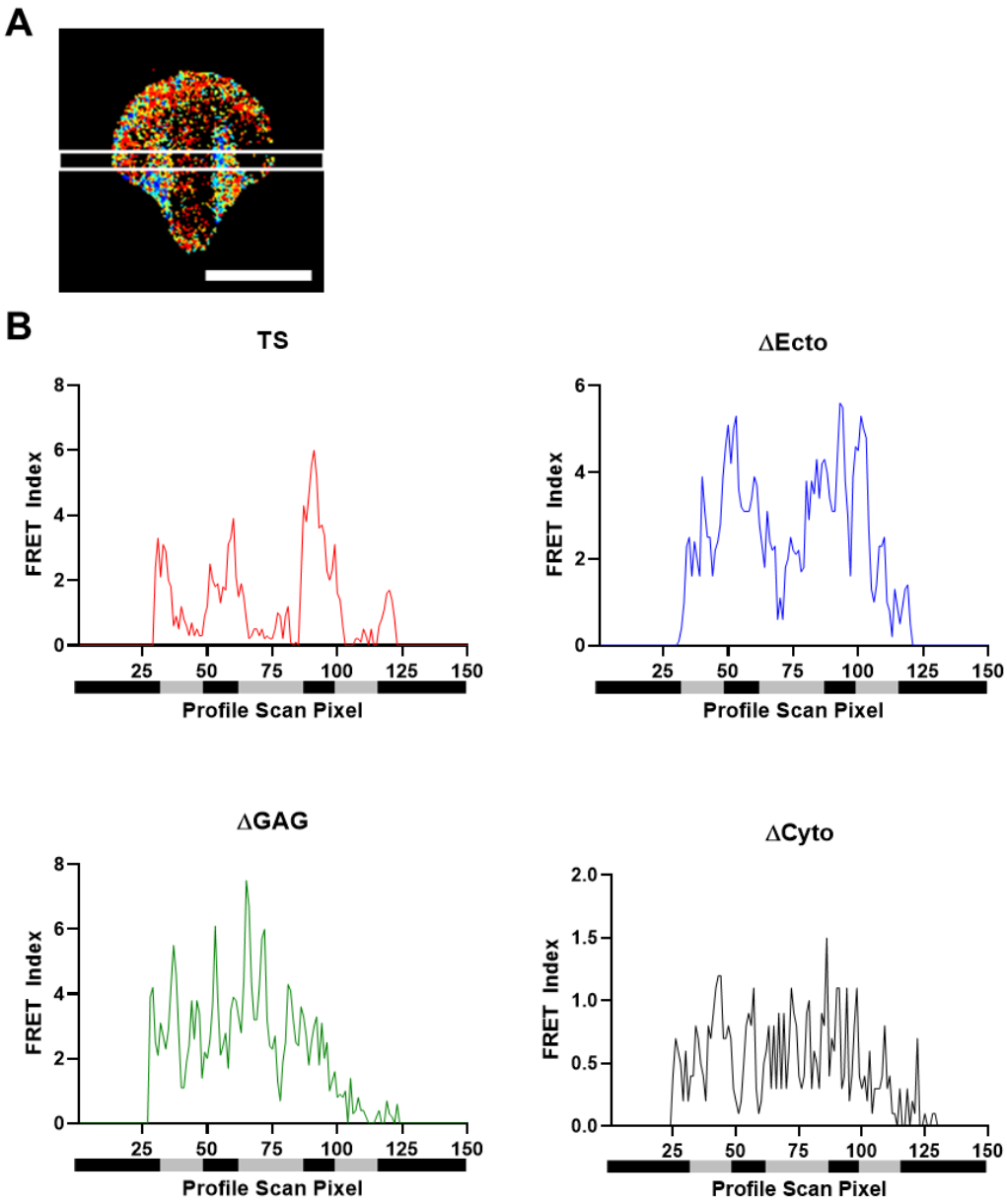

Figure 4.9. Tension sensor FRET profiles in response to micropatterning. Human umbilical vein endothelial cells (HUVECs) expressing the SDC1 tension sensor (TS), ectodomain mutant (ΔEcto), glycosaminoglycan attachment site mutant (ΔGAG) and cytoplasmic domain mutant (ΔCyto) were cultured onto crossbow micropatterns and evaluated for FRET. (A) Example profile scan area for FRET index image of cell adhered to 1100 um^2 crossbow. Bar = 25 μm. (B) Representative substrate-level FRET index profiles. Black, non-adherent regions. Gray, adherent regions.

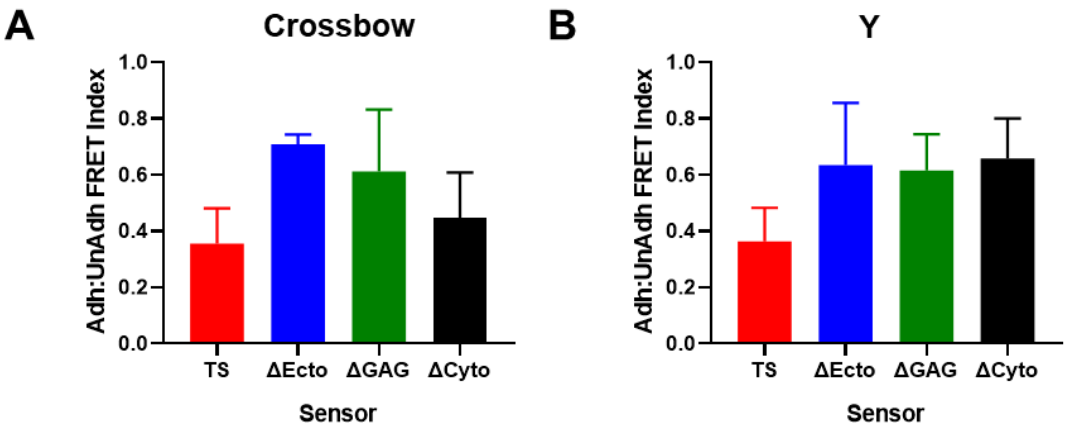

Figure 4.10. Tension on SDC1 is increased in regions of cellular adhesion compared to regions of non-adherence. Human umbilical vein endothelial cells (HUVECs) expressing the SDC1 tension sensor (TS), ectodomain mutant (ΔEcto), glycosaminoglycan attachment site mutant (ΔGAG) and cytoplasmic domain mutant (ΔCyto) were cultured onto crossbow and Y-shaped micropatterns. Quantification of FRET in regions of adhesion, ratioed to FRET in regions of non-adherence for cells cultured on (A) crossbow and (B) Y-shaped micropatterns of all sizes. $n = 3$.

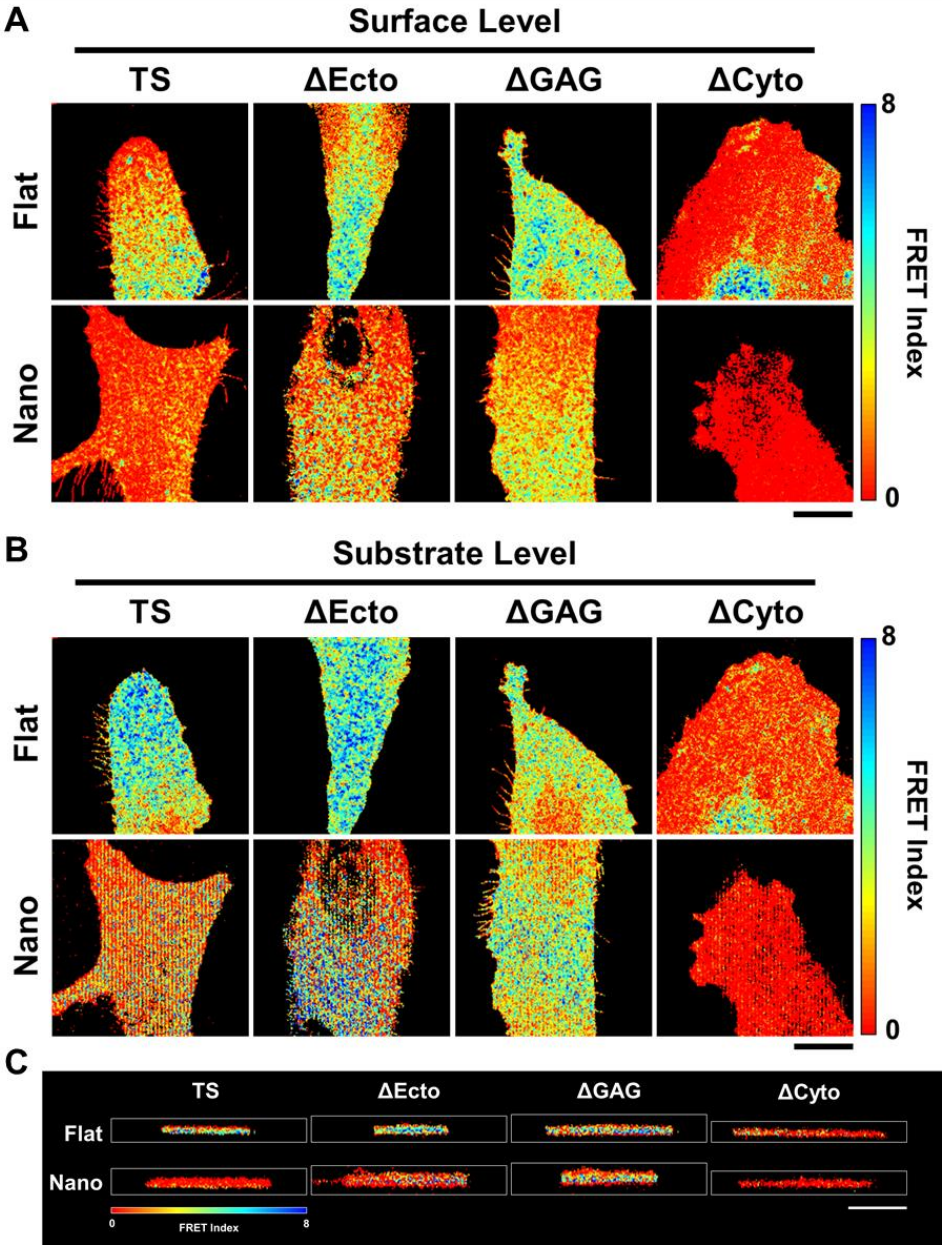

Figure 4.11. Nanogrooves alter tension on SDC1. Human umbilical vein endothelial cells (HUVECs) expressing the SDC1 tension sensor (TS), ectodomain mutant (ΔEcto), glycosaminoglycan mutant (ΔGAG) and cytoplasmic domain mutant (ΔCyto) were cultured onto unpatterned (flat) and nanogrooved (nano) substrates of 2.4 GPa stiffness. Representative (A) substrate and (B) surface-level z-projections of FRET index images. (C) Representative FRET index side views. Bars = 50 μm.

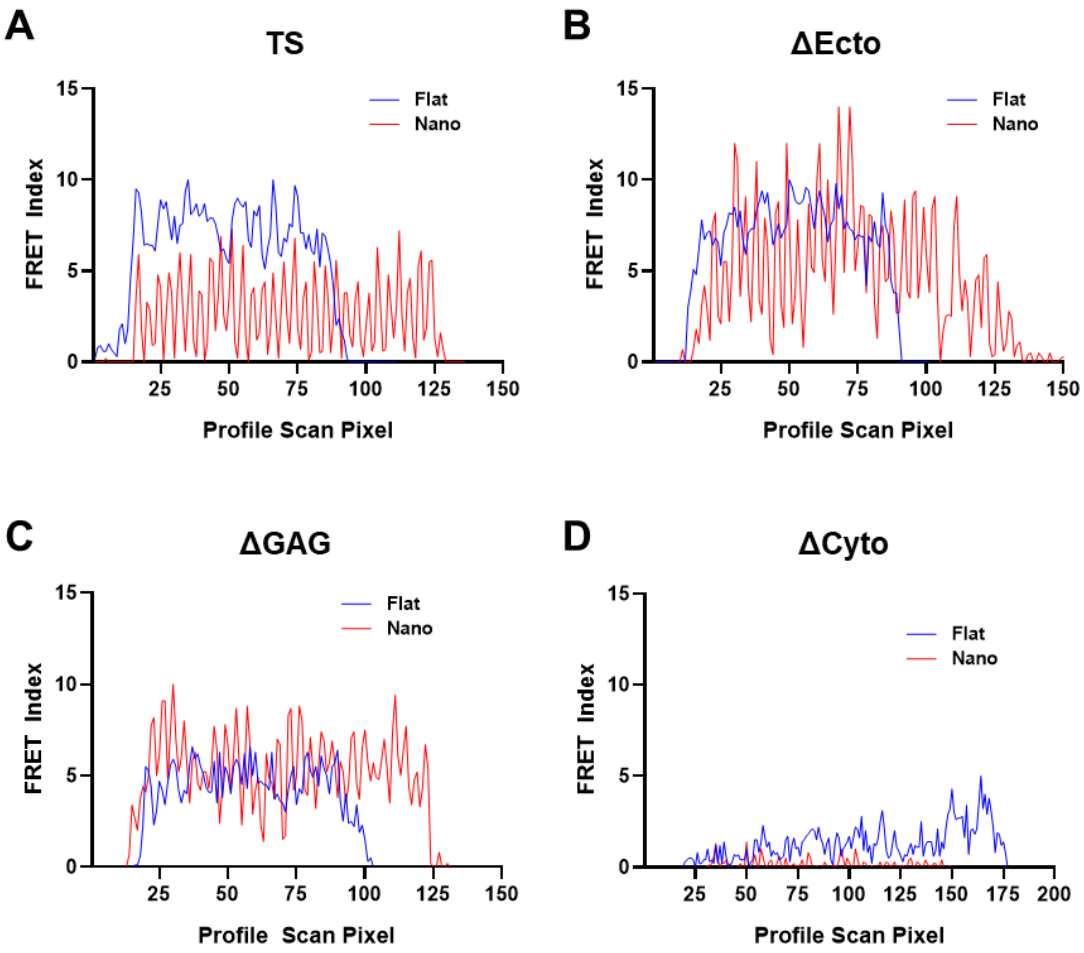

Figure 4.12. Profiles of substrate-level FRET in response to nanogrooves. Human umbilical vein endothelial cells **(**HUVECs) expressing the SDC1 tension sensor (TS), ectodomain mutant (ΔEcto), glycosaminoglycan mutant (ΔGAG) and cytoplasmic domain mutant (ΔCyto) were cultured onto unpatterned (flat) and nanogrooved (nano) substrates of 2.4 GPa stiffness. Representative FRET profiles of substrate-level z-projections, perpendicular to the direction of the nanopattern for cells expressing the (A) TS, (B) ΔEcto, (C) ΔGAG and (D) ΔCyto sensors.

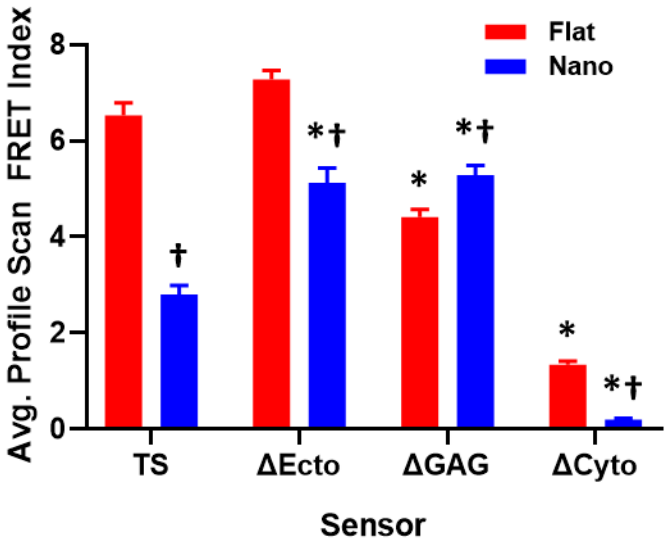

Figure 4.13. SDC1 tension is increased at the substrate level in response to nanogrooves. Human umbilical vein endothelial cells **(**HUVECs) expressing the SDC1 tension sensor (TS), ectodomain mutant (ΔEcto), glycosaminoglycan mutant (ΔGAG) and cytoplasmic domain mutant (ΔCyto) were cultured onto unpatterned (flat) and nanogrooved (nano) substrates of 2.4 GPa stiffness. (A) Quantification of average FRET from FRET profiles at the substrate-level. $^{*}p<0.05$ versus TS on same substrate. $^{\dagger}p<0.05$ versus same sensor on flat substrate. $n = 30$ points.

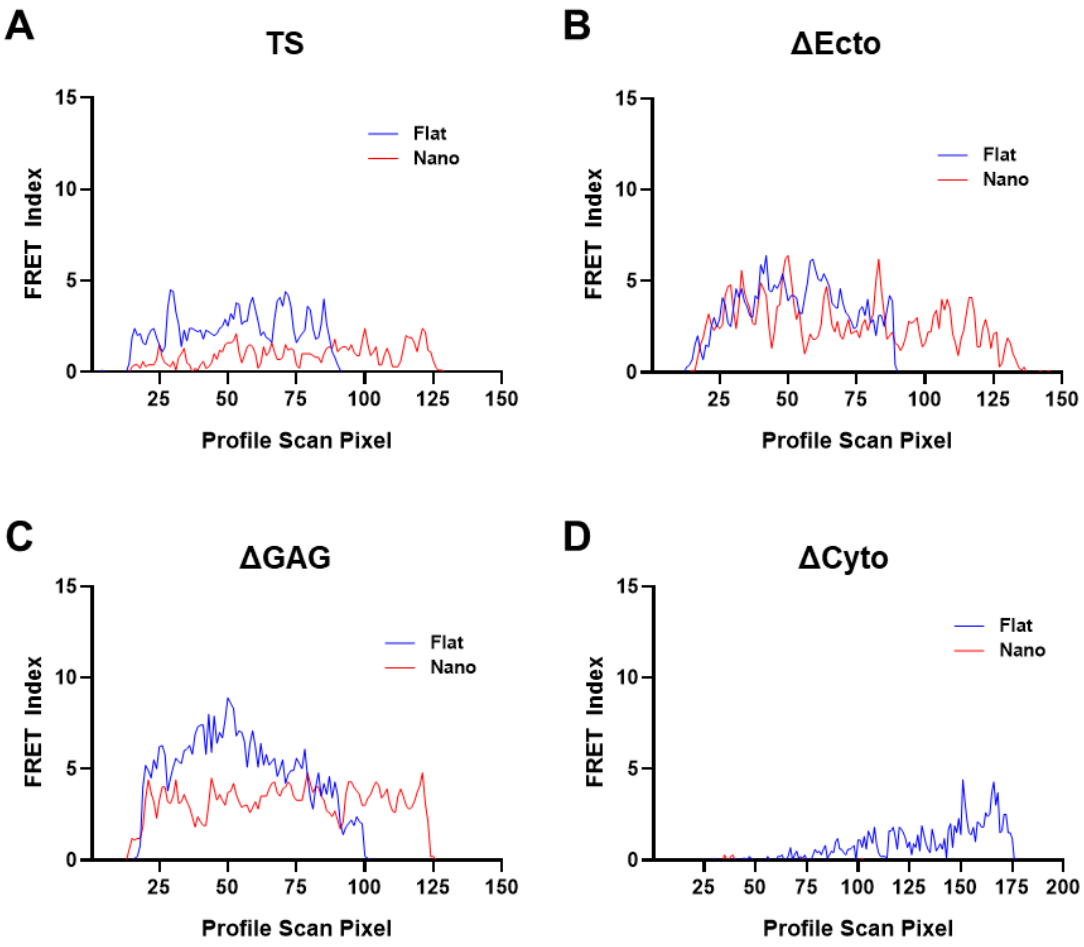

Figure 4.14. Profiles of surface-level FRET in response to nanogrooves. Human umbilical vein endothelial cells **(**HUVECs) expressing the SDC1 tension sensor (TS), ectodomain mutant (ΔEcto), glycosaminoglycan mutant (ΔGAG) and cytoplasmic domain mutant (ΔCyto) were cultured onto unpatterned (flat) and nanogrooved (nano) substrates of 2.4 GPa stiffness. Representative FRET profiles of surface-level z-projections, perpendicular to the direction of the nanopattern for cells expressing the (A) TS, (B) ΔEcto, (C) ΔGAG amd (D) ΔCyto sensors.

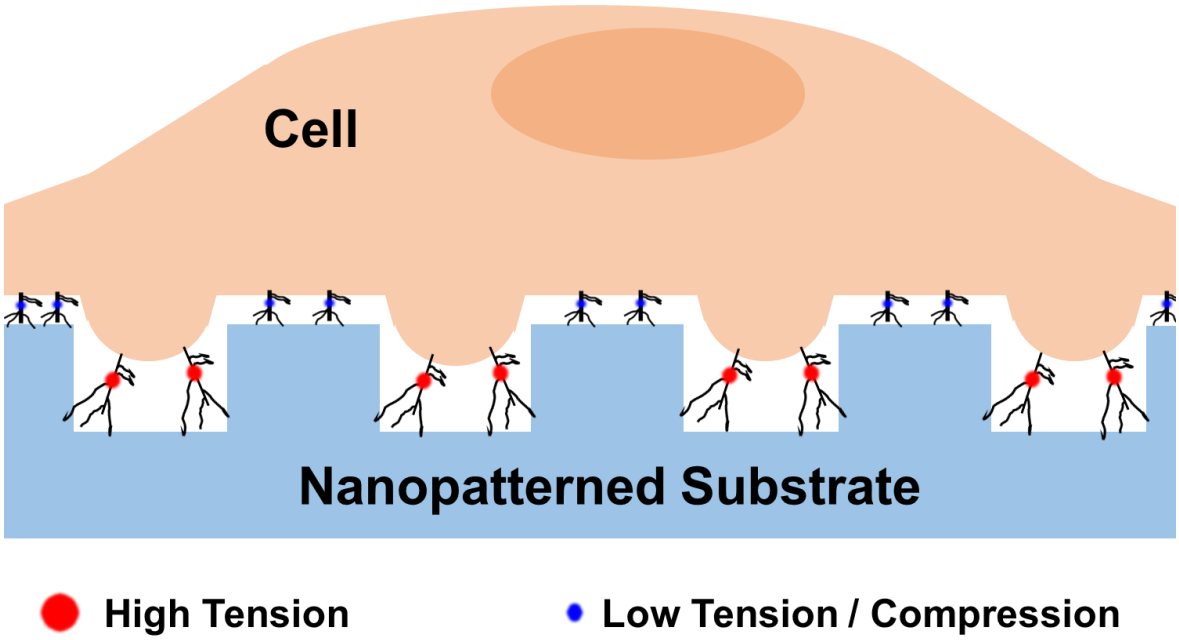

Figure 4.15. Model of SDC1 tension response to 2.4 GPa nanogrooves.

4.4 DISCUSSION

This work provides evidence that tension on SDC1 is modulated by biophysical cues. SDC1 interacts with numerous proteins via its extracellular domain. The vast majority of SDC1's direct protein contacts occur via its extracellular domain, and in particular, the long GAG chains bound to its core ectodomain.

Our finding that SDC1 intension, itself, is responsive to substrate stiffness is consistent with our previous work, which found that SDC1 is involved in the mechanosensation of substrate stiffness.(Le et al., 2018) Previous work from other groups indicated that integrin αVβ3, which is regulated by SDC1, (McQuade et al., 2006) has been implicated as involved in mechanosensation of substrate stiffness.(Jiang, Huang, Cai, Tanase, & Sheetz, 2006) SDC1 is also responsive to the microenvironment of cancer cells (Chute et al., 2018; Su, Blaine, Qiao, & Friedl, 2007) and even modulate tissue stiffness.(Chute, Keely, Alexander, & Friedl, 2013)

Under baseline conditions, decreased tension at the substrate level and similar tension at the surface level for TSΔGAG compared to the complete sensor suggest that the GAG chains are required for SDC1 tension at the substrate level, but are not important for SDC1 tension at the surface level. This is consistent with the known direct binding of the heparan sulfate chains to the extracellular matrix. (Eriksson & Spillmann, 2012; Koda, Rapraeger, & Bernfield, 1985; Mattson et al., 2017; Vuoriluoto et al., 2008) Interestingly, loss of the cytoplasmic domain, and thus direct association with the cytoskeleton, did not abolish tension on SDC1 suggesting that SDC1 does not require a direct linkage to the

cytoskeleton for tension propagation. As SDC1 is linked indirectly to the cytoskeleton by other means(Beauvais et al., 2004; Beauvais & Rapraeger, 2003), exploration of the role of the αV integrins in SDC1 tension propagation is warranted. The reduced FRET observed in TSΔCyto may also be due to changes in localization of the sensor as a result of the loss of the cytoplasmic domain, misfolding of the sensor or decreased expression levels.

Our finding that SDC1-TS located in adhered regions of the cell is under higher tension indicates that the link between the ECM and SDC1 is important for SDC1 tension. When we cultured the cells expressing the tension sensors onto compliant substrates, we observed no significant difference in tension between TSΔGAG adhered to 0.2 kPa and 25 kPa substrates. This is consistent with our baseline FRET observations for TSΔGAG. Taken together, these findings are suggestive of a model in which SDC1 tension increases during adhesion. Interestingly, TSΔEcto was responsive to change in substrate compliance, suggesting that the TSΔEcto sensor is under compression on the 25 kPa substrate.

In Aim 1, we observed based on increases in Yap/Taz and Rock1 that S1KO vSMCs are under more tension when adhered to nanopatterns. Here, the alternating FRET index pattern we observe for SDC1-TS on nanopatterned substrates could be indicative of alternating high and low tension or alternating high tension and compression. We observed that SDC1 tension is higher within nanogrooves and decreased in the regions of the nanopattern peaks (**Figure 4.15**), which is consistent with a model in which the cell is pulling back with more force on nanopatterning. This may be due to the presence of more

adhesion sites per unit area TSΔGAG tension on the flat substrate is similar to TSΔGAG tension on nanopatterned substrates, also consistent with our model.

Chapter 5. Mechanisms of Syndecan-1 Tension Sensing

5.1 Introduction

We recently created and validated a FRET-based SDC1-TS that enabled the visualization of SDC1 tension in response to substrate-mediated cues. In Chapter 4, we found that tension on SDC1 increases upon binding with the substrate and that flexible substrates reduce SDC1 tension. Here, we explored the mechanisms of SDC1 tension, examining the relationships between SDC1 tension, its integrin binding partners, Rho-mediated cytoskeletal tension and focal adhesion formation. We also examined the response of SDC1 tension to fluidic shear stress and endothelial tube formation.

SDC1 is known to bind and regulate integrins αVβ3 and αVβ5. Upon clustering with SDC1 and IGF-1R, this complex affects such processes as cell survival, angiogenesis and metastasis.(Beauvais & Rapraeger, 2003; Rapraeger, 2013) When the interaction of SDC1 with the αV is disrupted with synstatin, a peptide derived from SDC1, cell spreading is reduced.(Beauvais et al., 2009) This suggested to us that the αV might contribute to SDC1 tension. In our original design of the SDC1 tension sensor, we positioned the mTFP-elastic linker-Venus FRET construct in the ectodomain of SDC1, just before the docking site for the αV integrins. Our ectodomain mutant of the SDC1-TS, SDC1-TSΔEcto, lacks the docking site.

5.2 MATERIALS AND METHODS

5.2.1. Cell culture

Human umbilical vein endothelial cells (HUVECs) from a single donor (Lonza, #C-11200) were cultured in MCDB-131 culture medium (Gibco) with 7.5% fetal bovine serum (FBS), endothelial cell growth supplement (R&D Systems), L-glutamine and antibiotics.

5.2.2. Cell lines

HUVECs expressing the SDC1-TS, SDC1-TSΔEcto, SDC1-TSΔGAG, SDC1-TSΔCyto, created in Chapter 4, were used in the studies. HUVECs expressing only mTFP or only Venus were used for bleed-through correction of FRET indexing.

5.2.3. Sensitized emission evaluation of FRET

Cell culture media was replaced with warm PBS, followed by warm HEPES-buffered Tyrode's solution (Alfa Aesar). Sensitized emission imaging was performed using a Zeiss 710 confocal microscope at 40x magnification with immersion oil on a stage heated to 37°C. An HFT 458/514 beam splitter was used. For sensitized emission analysis, three images were obtained. For the donor (mTFP1) channel image, cells were excited with a 458 nm laser and emission was collected between 470-499 nm. For the acceptor (Venus) channel image, excitation was performed with a 514 nm laser and emission was collected between 530-600 nm. The FRET channel image was obtained using excitation of the donor and acceptor emission. Z-stacks were obtained in 0.50 μm steps. For drug treatment experiments, sensitized emission imaging was performed prior to drug treatment for

baseline FRET measurements. Imaging was performed 20 min following drug treatment on the same cell.

5.2.4. FRET analysis and image processing

Donor, acceptor and FRET images were loaded into the FRET Analyzer and Colocalization Analyzer plugin for Fiji (Hachet-Haas et al., 2006). Bleed-through correction was performed using the Sdc1M (donor-only) and Sdc1V (acceptor-only) cell lines cultured on the various substrates utilized. For each slice in a z-stack, apparent FRET from non-colocalized mTFP and Venus were removed within the plugin. For cells cultured on the nanopatterned substrate, which produces autofluorescence, background-subtraction for each channel and z-position was performed before FRET-indexed images were generated. The default "Fire" lookup table (LUT) assigned by the plugin was changed to a modified "Jet" LUT. Z-stacks, z-projections, side views and 3D projections were created using Fiji software. Z-projections were generated by average intensity. Masks were created in Photoshop (Adobe) using Venus channel images to distinguish zero-FRET from regions where the sensor was not present.

5.2.5. FRET index quantification from images

Substrate-level and surface-level slices were identified from orthogonal views of z-stacks, and average z-projections were generated. For the quantification of FRET index, cells were subdivided lengthwise, and the first and last third of the cell was traced, avoiding the nucleus. The mean FRET index was obtained from these traced regions. For shear stress experiments, FRET index was measured from the first (upstream) and last (downstream)

quarter of the cell in the direction of flow from side views, in triplicate. For treatment experiments and shear stress experiments, relative FRET index was calculated by normalizing to baseline FRET index measurements of the same cell.

5.2.6. Drug treatment

Cells were treated for 20 minutes using the drugs shown in **Table 5.1.** The synstatin peptide encompasses amino acids 93-120 of human *SDC1*.(Rapraeger, 2013)

Table 5.1. Drug Treatments

Drug	Conc. (μM)	Vendor
(+)-Blebbistatin*	50	EMD Millipore
(-)-Blebbistatin*	50	EMD Millipore
PF-573,228*	10	Tocris
PP2*	50	Sigma-Aldrich
Y27632*	10	Sigma-Aldrich
Manganese chloride tetrahydrate	0.5	Sigma-Aldrich
Synstatin	1	Genscript
Cilengitide	10	R&D Systems

* denotes 1:1000 DMSO dilution during treatment

5.2.7. Tube formation experiments

Chilled Matrigel (25 μl; Corning) was applied to coverslip glass bottom 35 mm dishes on ice and spread using a cell scraper to create a thin-layer of basement matrix and then incubated for 30 minutes at 37°C, adapted from the method described by Faulkner and others (2014) (Faulkner et al., 2014). Cells were seeded at 2,500 cells/cm^2 onto the Matrigel in DMEM medium with 7.5% fetal bovine serum, L-glutamine, penicillin-streptomycin, 100 ng/ml VEGF and 10 ng/ml FGF-2. Immediately before imaging, the medium was

gently replaced with warm PBS, followed by warm Tyrode's solution. Sensitized emission imaging was performed 4, 6- and 8-hours following seeding.

5.2.8. Application of shear stress

Slides containing six flow channels (μ-slide, IBIDI) were coated with type I rat tail collagen overnight and seeded with HUVECs expressing SDC1-TS. The cell culture medium was aspirated and replaced with Tyrode's solution (Alfa-Aesar) pre-warmed to 37°C. Sixty-ml syringes (BD) with an inner diameter of 26.72 mm and silicone tubing were also filled with pre-warmed Tyrode's solution. Shear stress was applied to the channels using a syringe pump (KD Scientific). Sensitized emission imaging of cells under static conditions was performed with the flow system attached to the channels but without the induction of flow. Following imaging under static conditions, flow was initiated, and sensitized emission imaging was immediately repeated under static (static-static) or flow conditions (static-12 dynes/cm^2). For 12 dynes/cm^2 shear stress, 9.46 ml/min flow was used, distributed across three syringes connected to the inflow via a syringe scaffold. The resulting sets of images for the static-static experiment were designated as: 1) Baseline FRET and 2) Static FRET. The sets of images for the static-flow experiment were designated as: 1) Baseline FRET and 2) Flow FRET.

5.2.9. Quantification of FRET under shear stress

Three orthogonal slices were obtained from the z-stacks, through the nucleus of each cell, in the direction of flow. The length of each cell was sub-divided into fourths, with the first and fourth segments designated as the upstream and downstream lengths of

the cell. The first and fourth segments were further sub-divided into a substrate and surface-level areas, resulting in regions designated as upstream surface-level, upstream substrate-level, downstream surface-level and downstream substrate-level (**Figure 5.14A**). These regions were traced in Fiji software and the mean FRET index were obtained for each.

For each cell in the static-static experiments, Static FRET was divided by Baseline FRET to obtain Rel. Static FRET for that cell. The Rel. Static FRET for that cell was divided by the average Rel. Static FRET for the entire group to obtain Normalized Static FRET. Similarly, for each cell in the static-flow experiments, Flow FRET was divided by Baseline FRET to obtain Rel. Flow FRET for that cell. The Rel. Flow FRET for that cell was divided by the average Rel. Static FRET for the entire static-static group to obtain Normalized Flow FRET.

5.2.10. Statistical analysis

All results are shown as mean ± standard error of the mean. Comparisons between only two groups, for which relative FRET is shown (normalized to baseline FRET), were performed using a Wilcoxon matched-pairs signed rank test. Differences were considered significant at $p<0.05$. Comparisons between only two unpaired groups with relative FRET values, were performed using a Mann-Whitney test. Differences were considered significant at $p<0.05$. Multiple comparisons between groups were analyzed by a Kruskal-Wallis test followed by Dunn's post-hoc test. A 2-tailed probability value <0.05 was considered statistically significant.

5.3 RESULTS

5.3.1. Integrin activation with manganese increases SDC1 mechanical tension.

SDC1 activates and directly interacts with integrins αVβ3 and αVβ5 and inhibition of this interaction has been shown to reduce cell spreading.(Beauvais et al., 2009) For this reason, we wanted to examine whether integrins influence SDC1 tension. To determine the response of the SDC1-TS to integrin activation, we treated cells expressing the TS and mutant versions of the TS with manganese, which induces the activation and clustering of integrins (Cluzel et al., 2005; Mould et al., 2002) (**Figures 5.1-5.2**). We then evaluated the FRET response to manganese treatment, relative to FRET under the baseline untreated conditions. Integrin activation markedly increased tension on the TS at the surface level of the cell. All other sensors demonstrated increased tension at the substrate level. No difference in response to integrin activation was observed between the surface and substrate for any sensor (**Figure 5.3**).

5.3.2. DMSO treatment increases tension on SDC1.

We performed 1:1000 DMSO treatments as a number of the drug treatments in this study are solubilized in DMSO, finding that DMSO, itself, causes increased FRET (**Figure 5.4A, C**). Both the surface and substrate level demonstrated a marked decrease in FRET, compared to pre-treatment FRET (**Figure 5.4B**). For this reason, we began performing an additive correction to post-treatment relative FRET values for those treatments solubilized in DMSO: Y-27632, PF-573,228, PP2 and (-)-Blebbistatin.

5.3.3. Inhibition of rho-associated protein kinase decreases SDC1 mechanical tension at the surface level.

To understand the modulation of SDC1 by Rho-mediated cytoskeletal tension, we treated cells expressing the TS with the rho-associated protein kinase (ROCK) inhibitor Y-27632 (**Figure 5.5A-B**). We observed a slight decrease in SDC1 tension at the surface level of the cell, relative to baseline conditions and with correction for the FRET-decreasing effect of DMSO treatment alone. (**Figure 5.5C**).

5.3.4. Focal adhesion kinase (FAK) inhibition increases surface-level SDC1 tension.

To examine the effect of FAK inhibition on SDC1 tension, we treated cells expressing the SDC1-TS with 10 μM PF-573,228 (**Figure 5.6A, C**).(Golubovskaya et al., 2012) Surface-level SDC1-TS tension increased in response to treatment, relative to baseline conditions and with correction for the FRET-decreasing effect of DMSO treatment alone (**Figure 5.6B**).

5.3.5. Response of SDC1 tension to Src-family kinase inhibition

We observed no significant change in SDC1-TS FRET at either the surface or the substrate level in response to treatment with 50 μM PP2, an inhibitor of Src-family kinases.(Nerlich et al., 2009; Orlandini et al., 2008)

5.3.6. Response of SDC1 tension to myosin ii inhibition

We treated cells expressing the SDC1-TS with the inactive enantiomer (+)-Blebbistatin (Bleb) and the active enantiomer (-)-Blebbistatin (**Figure 5.8A-B, C**).(Chervin-Petinot et al., 2012) After adjustment for the change in FRET due to (+)-Bleb

in DMSO, tension on the SDC1-TS was not significantly affected by myosin ii inhibition (**Figure 5.8B**).

5.3.7. Inhibition of SDC1 interaction with integrins increases SDC1 tension.

To inhibit the interaction of SDC1 with αVβ3 and αVβ5, we treated cells expressing SDC1-TS and TSΔEcto with a peptide derived from the docking site for integrins on SDC1, synstatin (SSTN) (**Figure 5.9A-B, D**).(Rapraeger, 2013) SSTN treatment increased tension on both SDC1-TS and SDC1-TSΔEcto at the surface level and the substrate level, compared to baseline tension. For the SDC1-TS, the relative change in tension in response to SSTN treatment did not significantly differ between the surface level and the substrate level (**Figure 5.9C**).

5.3.8. Inhibition of αv integrins increases substrate-level SDC1 tension.

Cilengitide blocks the activation of the αv integrins. We treated cells expressing the SDC1-TS and TSΔEcto with cilengitide (CLGT), (**Figure 5.10A-B, D**). CLGT treatment significantly increased tension on SDC1 at the substrate level, but did not affect surface-level SDC1 tension. For SDC1-TS, the relative change in tension in response to CLGT was significantly greater at the substrate level than the surface level (**Figure 5.10C**).

5.3.9. Fluidic shear stress alters the distribution of SDC1 tension on endothelial cells.

Vascular endothelial cells are subject to fluidic shear stress, which influences vascular remodeling, and protect against or promote atherosclerosis. Previous work from our group found that the loss of SDC1 alters the shear stress-induced activation of Akt signaling, as well as shear stress-induced intracellular spatial gradients of phosphorylated

paxillin. Additionally, the activation of RhoA in response to shear stress was reduced in S1KO knockout endothelial cells, compared to wild-type cells. These findings are suggestive a role for SDC1 in the mechanosensation of shear stress.(Voyvodic et al., 2014)

To examine how tension across SDC1 responds to shear stress, we seeded HUVECs expressing the TS and mutant versions of the TS on microchannels and subjected them to baseline static conditions, followed by static (static-static) or 12 dynes/cm^2 of shear stress (static-flow) (**Figures 5.11A, 5.12A**) , performing FRET imaging during each condition (**Figures 5.11B-C, 5.12B-C, 5.13**) . During our analysis, we subdivided cells into four regions with respect to the direction of flow: upstream surface level, upstream substrate level, downstream surface level and downstream substrate level (**Figure 5.14A**)**.** In response to flow, TS cells exhibited an increase in tension on the upstream cellular surface and upstream substrate level in response to flow, relative to FRET at baseline static. In those regions, the TSΔGAG also exhibited an increase in tension in response to flow (**Figure 5.14B, C**). At the downstream surface level of the cell, the TSΔCyto sensor exhibited compression in response to flow (**Figure 5.14C**). Interestingly, marked compression was observed at the downstream substrate level of TS cells in response to flow. In this region, TSΔEcto and TSΔGAG exhibited no change in tension in response to flow, and their FRET response under flow differed significantly from SDC1-TS. The cytoplasmic domain mutant of the TS exhibited compression (**Figure 5.1E**).

5.3.10. Tension on SDC1 is altered during endothelial tube formation.

To determine if SDC1 tension is affected by endothelial tube formation, we induced tube formation in HUVECs expressing the SDC1-TS and evaluated FRET over the first eight hours. SDC1 was under high tension throughout this period, but decreased SDC1 tension was observed at the junctions of cells forming tubes (**Figure 5.15**).

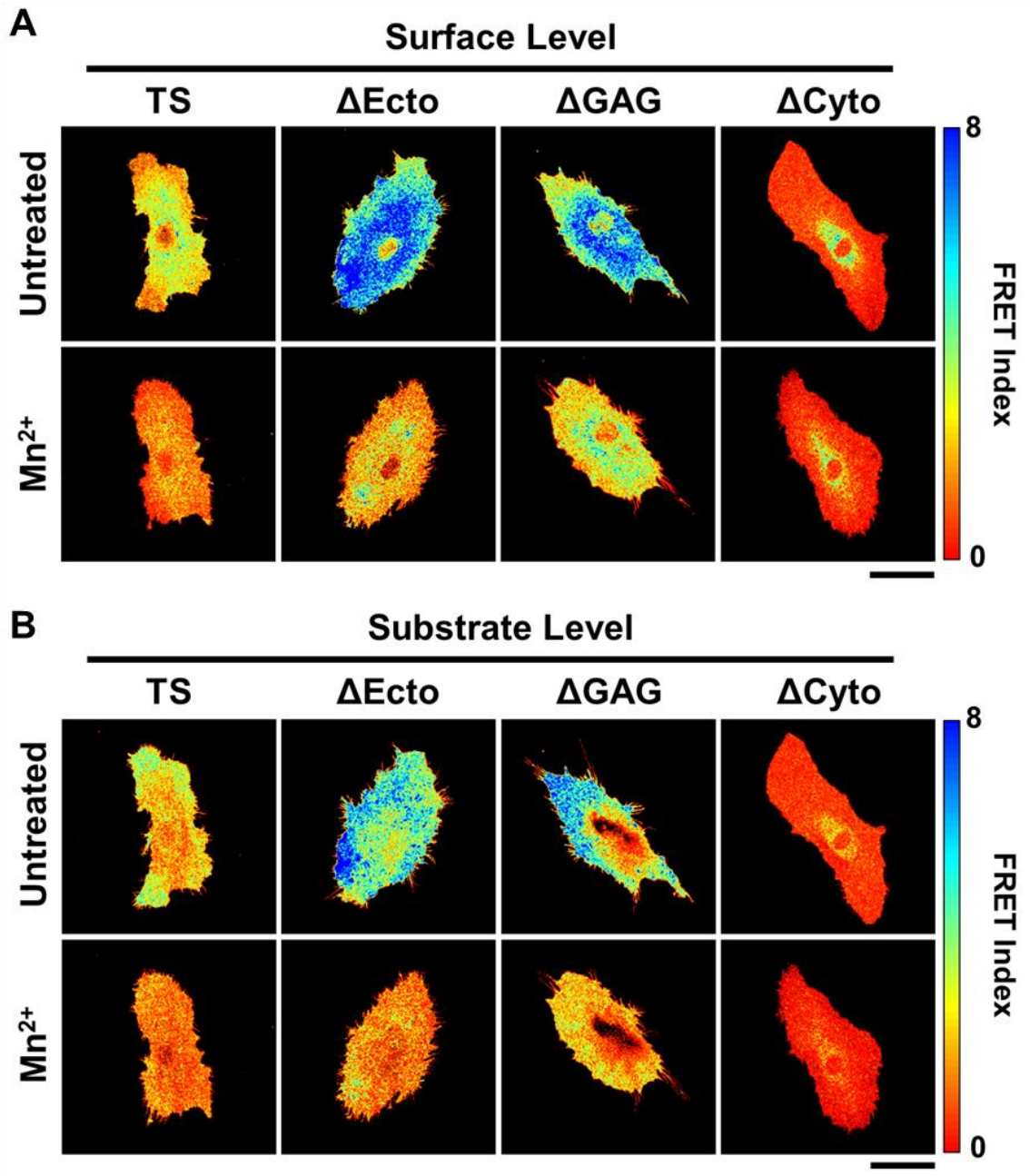

Figure 5.1. FRET response of SDC1 tension sensor to integrin activation using manganese. Human umbilical vein endothelial cells (HUVECs) expressing the SDC1 tension sensor (TS), ectodomain mutant (ΔEcto), glycosaminoglycan mutant (ΔGAG) and cytoplasmic domain mutant (ΔCyto) were evaluated for FRET before and after treatment with 0.5 μM Mn^{2+}. Representative (A) surface- and (B) substrate-level z-projected FRET index images. Bars = 50 μm.

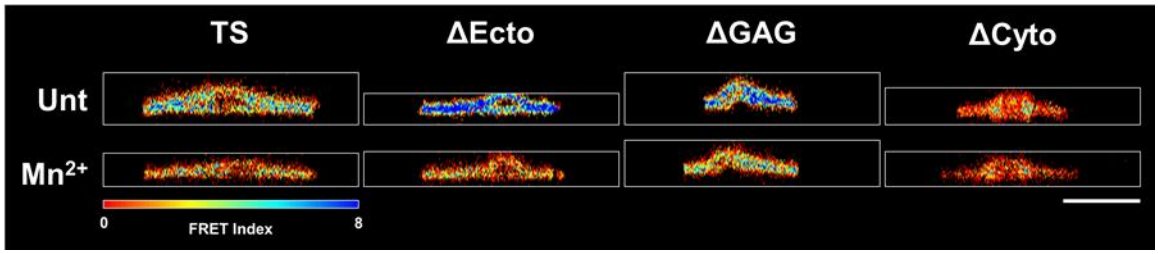

Figure 5.2. FRET response of SDC1 tension sensor to integrin activation using manganese. Human umbilical vein endothelial cells (HUVECs) expressing the SDC1 tension sensor (TS), ectodomain mutant (ΔEcto), glycosaminoglycan mutant (ΔGAG) and cytoplasmic domain mutant (ΔCyto) were evaluated for FRET before and after treatment with 0.5 μM Mn^{2+}. Representative FRET index side views. Bar = 50 μm.

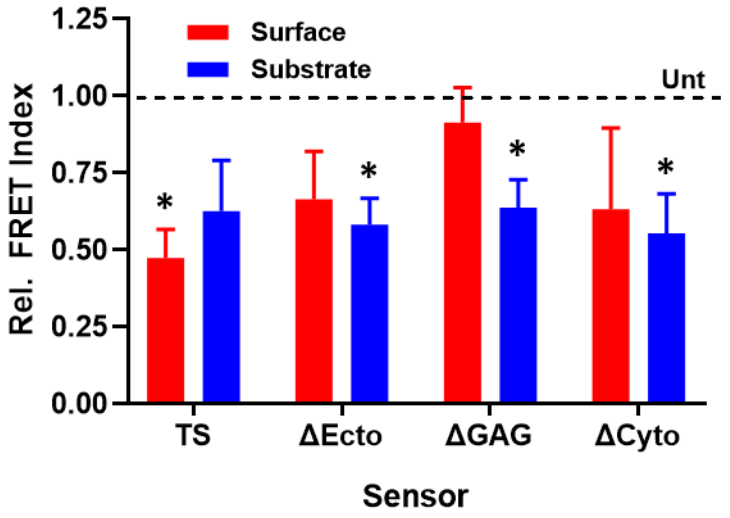

Figure 5.3. Integrin activation using manganese increases tension on SDC1. Human umbilical vein endothelial cells (HUVECs) expressing the SDC1 tension sensor (TS), ectodomain mutant (ΔEcto), glycosaminoglycan mutant (ΔGAG) and cytoplasmic domain mutant (ΔCyto) were evaluated for FRET before and after treatment with 0.5 μM Mn^{2+}. Quantification of surface and substrate-level FRET indices after Mn^{2+} treatment, relative to FRET indices under the untreated condition. $^{*}p<0.05$ versus untreated FRET. $n = 5$.

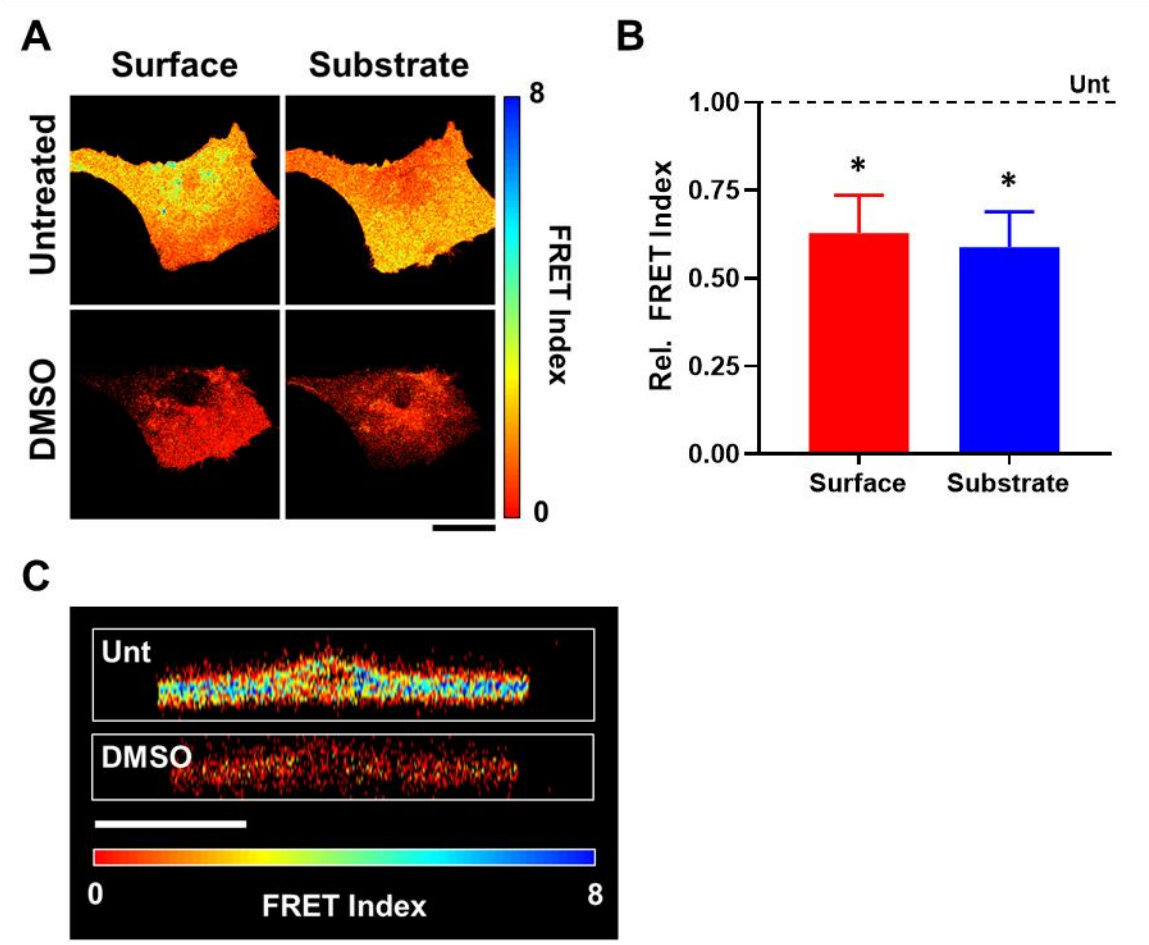

Figure 5.4. DMSO increases tension on SDC1. (A) Representative surface- and substrate-level, z-projected FRET index images of cells expressing the SDC1-TS before and after treatment with 1:1000 DMSO. Bar = 50 μm. (B) Quantification of surface- and substrate-level FRET indices after DMSO treatment, relative to FRET indices under the untreated condition. $^{*}p<0.05$ versus baseline untreated FRET at the same cellular level. $n = 10$. (C) Side views. Bar = 50 μm.

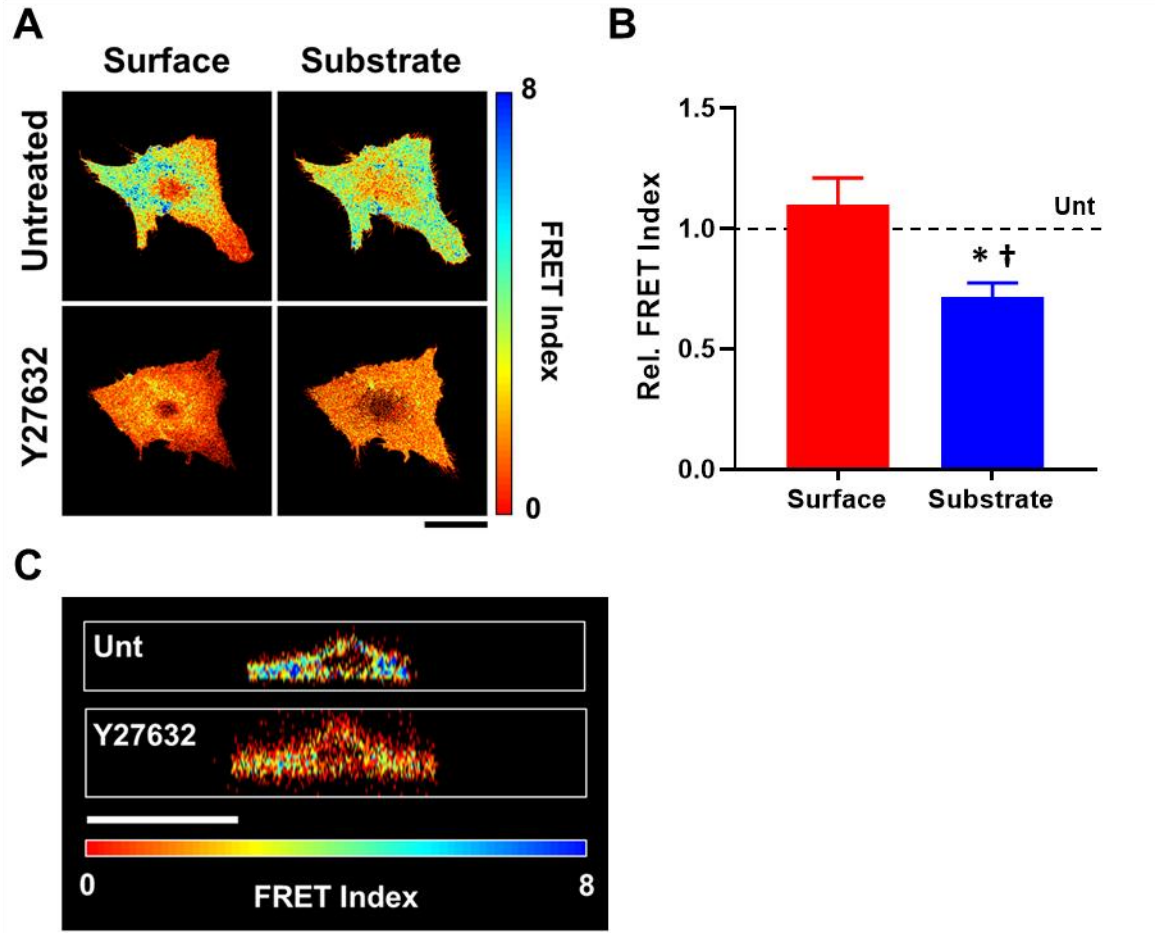

Figure 5.5. Rock inhibition increases SDC1 tension at the substrate level. (A) Representative surface- and substrate-level, z-projected FRET index images of cells expressing the SDC1-TS before and after Rock inhibition with 10 μM Y27632 in DMSO. Bar = 50 μm. (B) Quantification of surface- and substrate-level FRET indices after Y27632 treatment, relative to FRET indices under the untreated condition and normalized by change in FRET indices under DMSO. $^{*}p< 0.05$ versus baseline untreated substrate-level FRET. $^{\dagger}p<0.05$ versus Y27632-treated surface-level FRET. $n = 6$. (C) Side views. Bar = 50 μm.

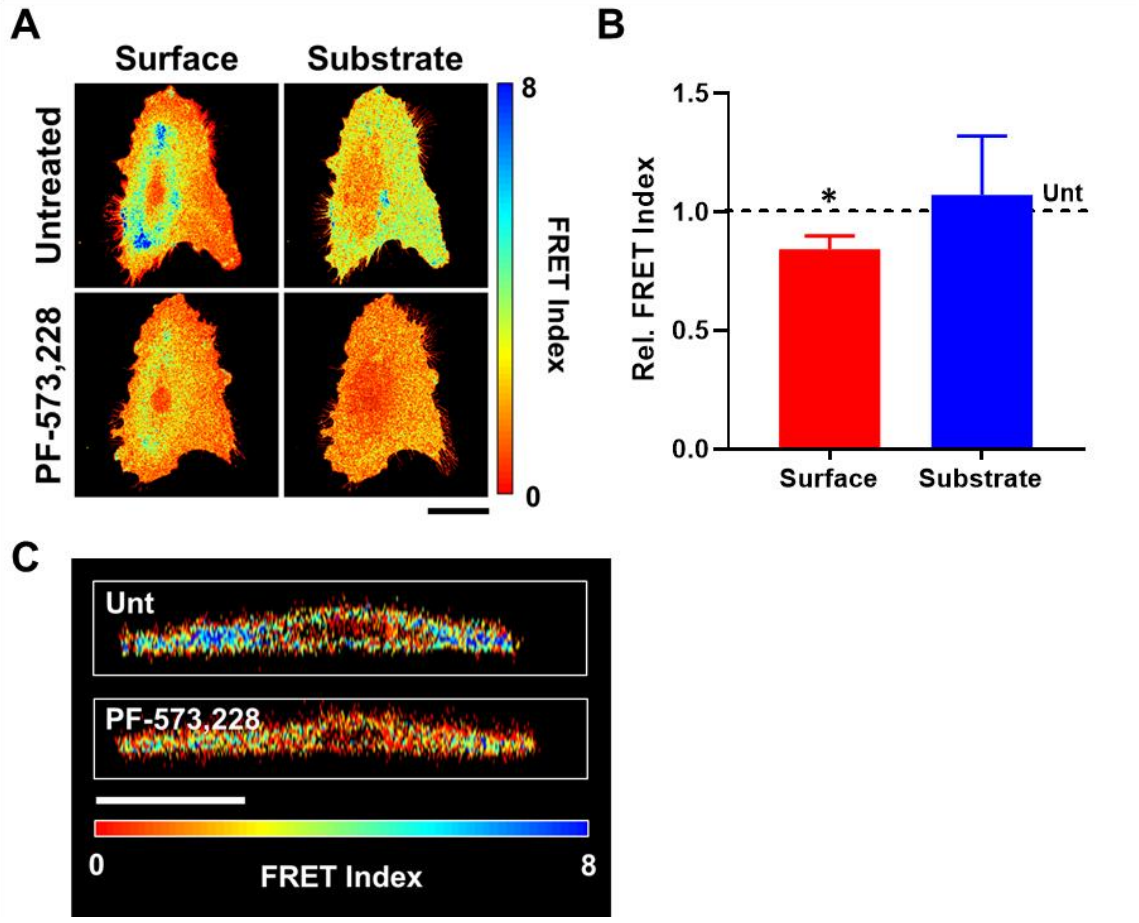

Figure 5.6. FAK inhibition increases surface-level SDC1 tension. (A) Representative surface- and substrate-level, z-projected FRET index images of cells expressing the SDC1-TS before and after treatment with 10 μM PF-573,228 in DMSO. Bar = 50 μm. (B) Quantification of surface- and substrate-level FRET indices after PF-578,228 treatment, relative to FRET indices under the untreated condition and normalized by change in FRET indices under DMSO. $^{*}p<0.05$ versus baseline untreated FRET at substrate level. $n = 6$. (C) Side views. Bar = 50 μm.

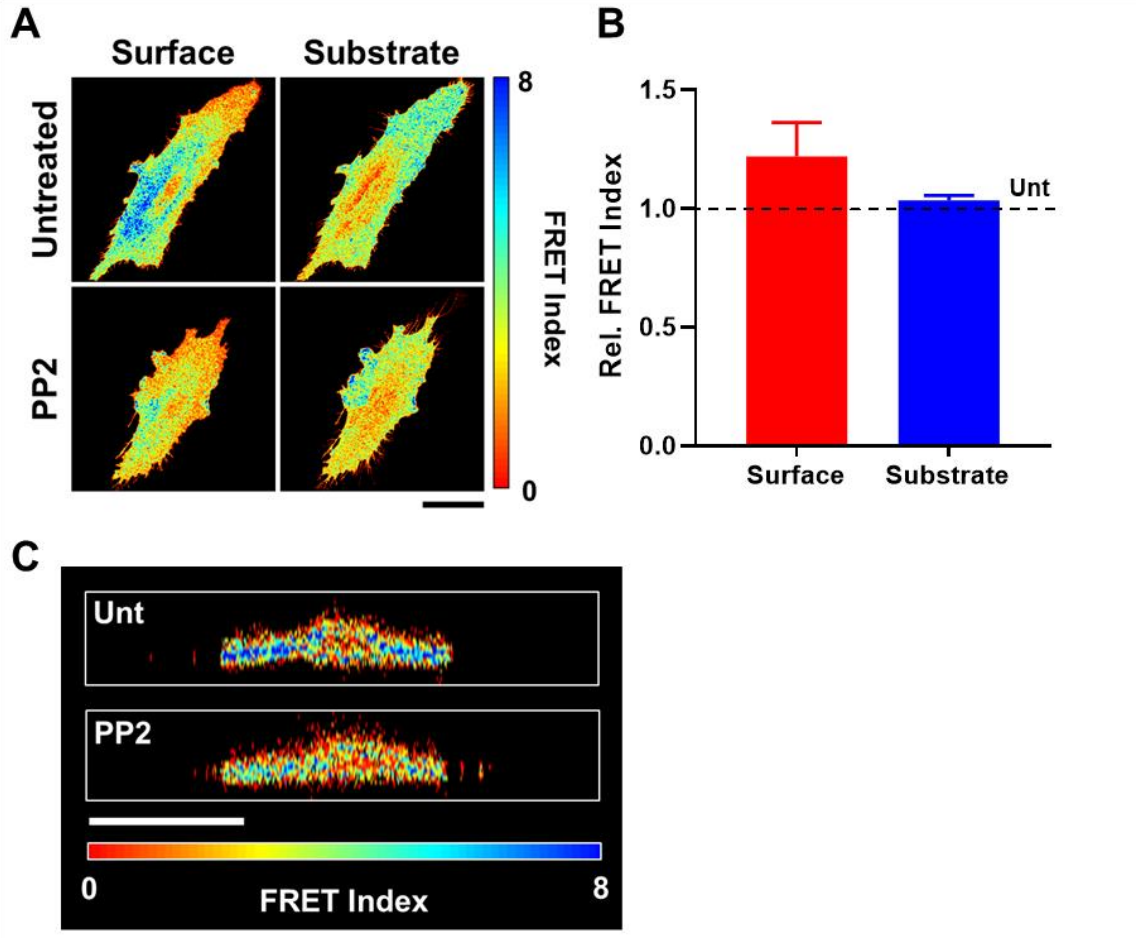

Figure 5.7. Modulation of SDC1 tension by Src inhibition. (A) Representative surface- and substrate-level, z-projected FRET index images of cells expressing the SDC1-TS before and after treatment with 50 μM PP2 in DMSO. Bar = 50 μm (B) Quantification of surface- and substrate-level FRET indices after PP2 treatment, relative to FRET indices under the untreated condition and normalized by change in FRET indices under DMSO. *n* = 8. (C) Side views. Bar = 50 μm.

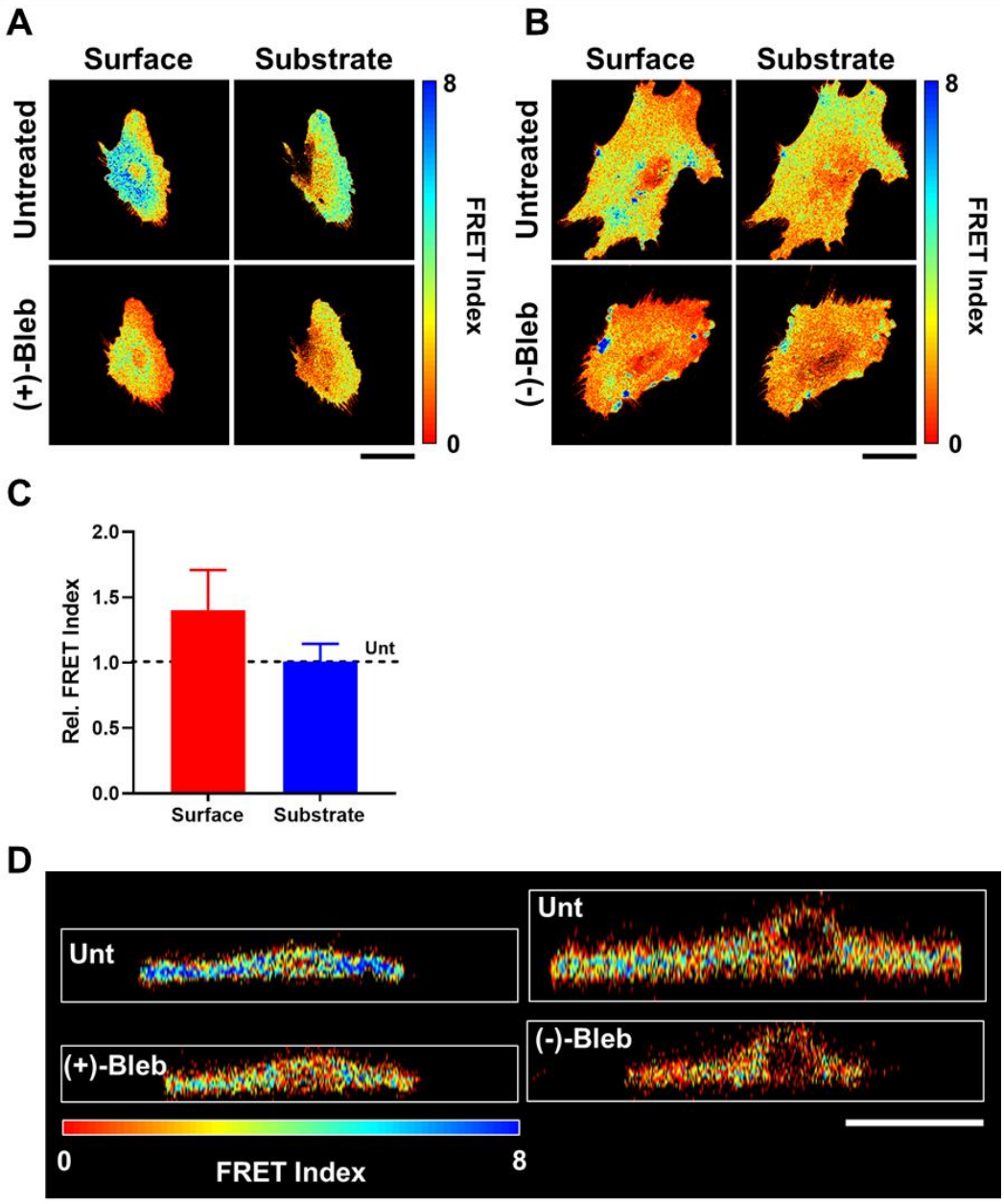

Figure 5.8. Modulation of SDC1 tension by myosin ii inhibition. Representative surface- and substrate-level, z-projected FRET index images of cells expressing the SDC1-TS before and after treatment with 50 μM (A) (inactive) (+)-Blebbistatin (Bleb) or (B) (active) (-)-Bleb in DMSO. Bars = 50 μm (C) Quantification of surface- and substrate-level FRET indices after (-)-Bleb treatment, relative to FRET indices under the untreated condition and adjusted for change in FRET indices under (+)-Bleb in DMSO. *n* = 6. (D) Side views. Bar = 50 μm.

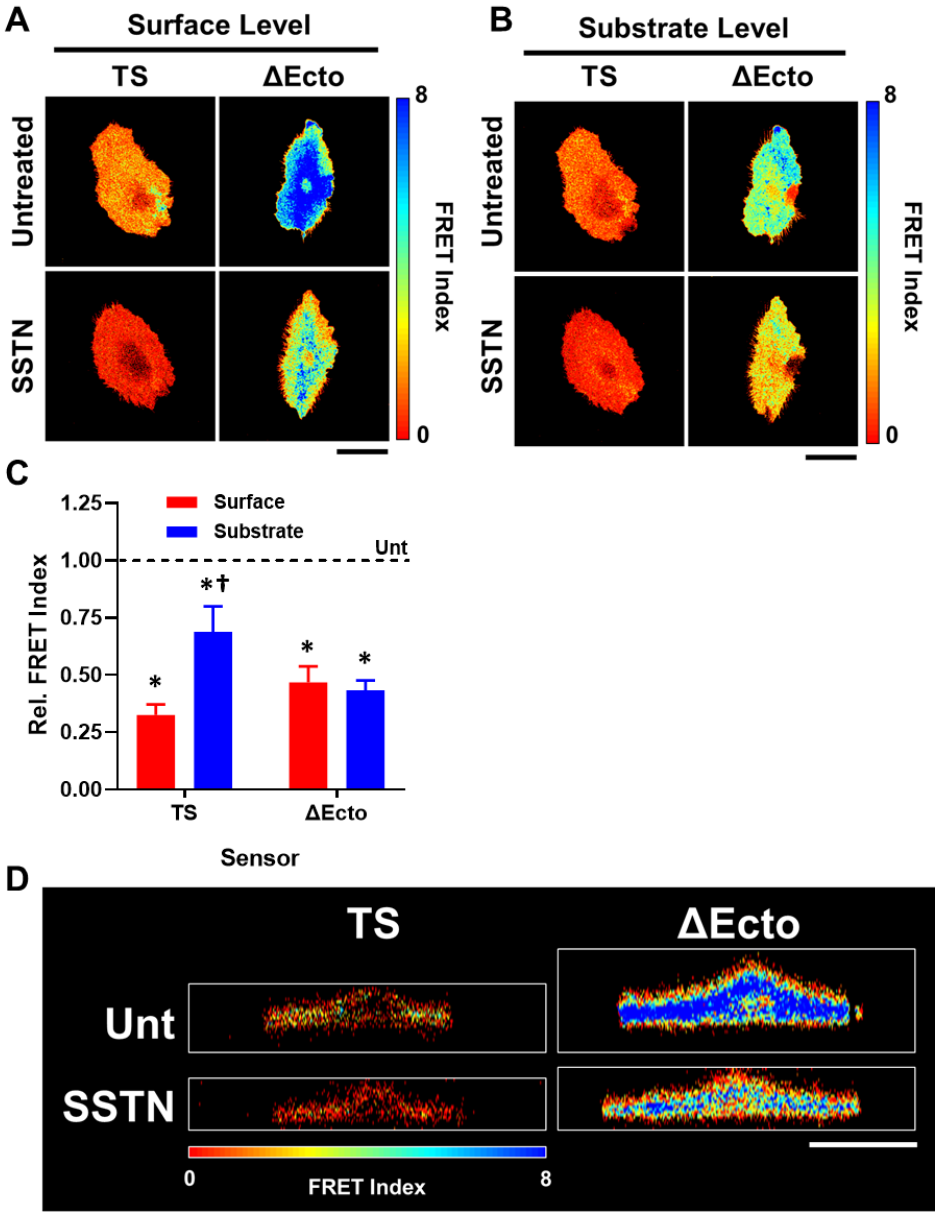

Figure 5.9. Inhibition of SDC1 interaction with integrins increases SDC1 tension. Representative (A) surface- and (B) substrate-level, z-projected FRET index images of cells expressing the SDC1-TS (TS) and ectodomain mutant (ΔEcto) before and after treatment with 1 μM synstatin (SSTN). (C) Quantification of surface- and substrate-level FRET indices after SSTN treatment, relative to FRET indices under the baseline untreated condition. $^{*}p<0.05$ versus baseline untreated FRET. $^{\dagger}p<0.01$ versus SSTN-treated surface-level TS FRET. $n = 6$. (D) Side views. Bars = 50 μm.

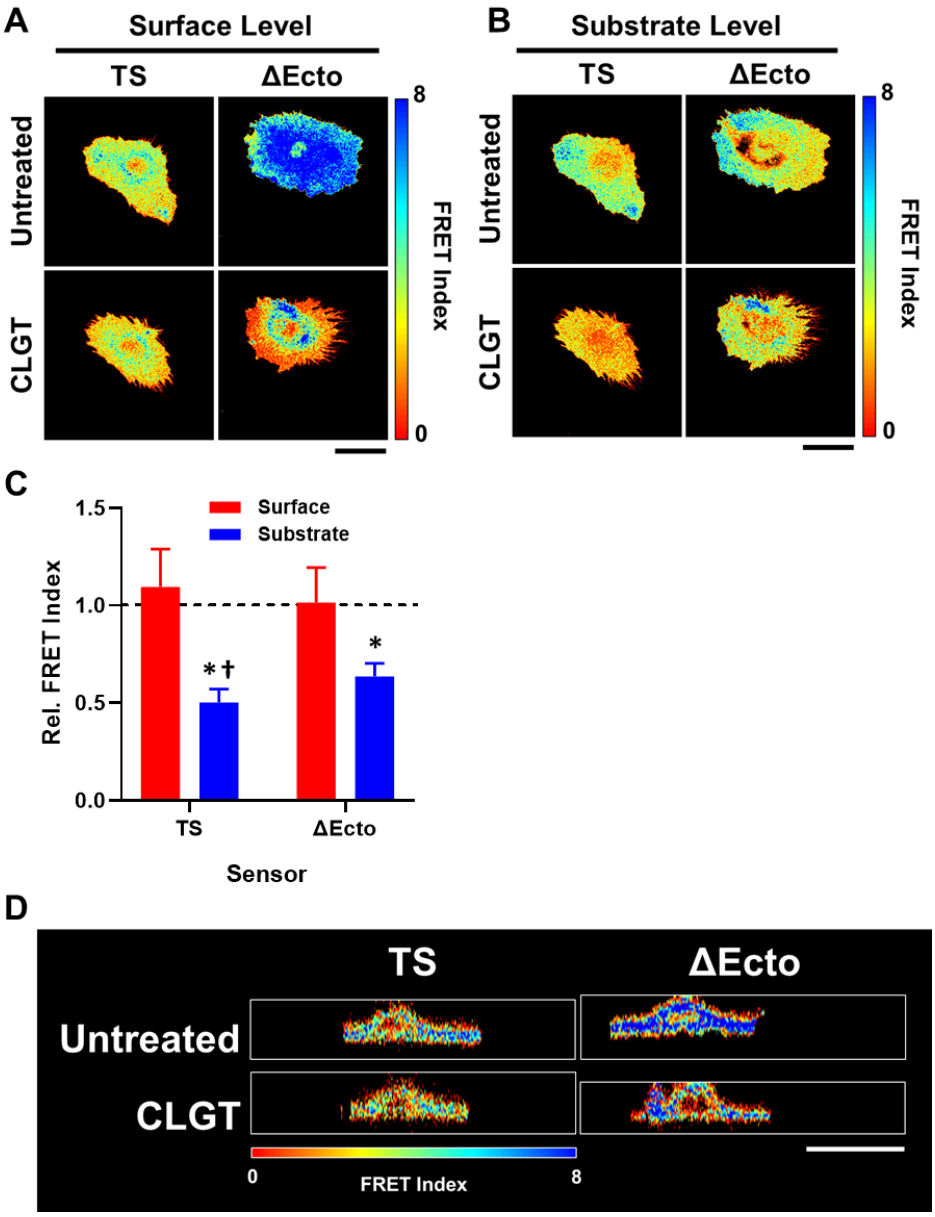

Figure 5.10. Substrate-level SDC1 tension increases in response to the inhibition of αv integrins. Representative (A) surface- and (B) substrate-level, z-projected FRET index images of cells expressing the SDC1-TS (TS) and ectodomain mutant (ΔEcto) before and after treatment with 10 μM cilengitide (CLGT). Bars = 50 μm. (C) Quantification of surface- and substrate-level FRET indices after CLGT treatment, relative to FRET indices under the baseline untreated condition. *$p<0.05$ versus baseline untreated FRET. $^{\dagger}p<0.05$ versus TS surface-level CLGT-treated FRET. $n = 8$. (D) Side views. Bar = 50 μm.

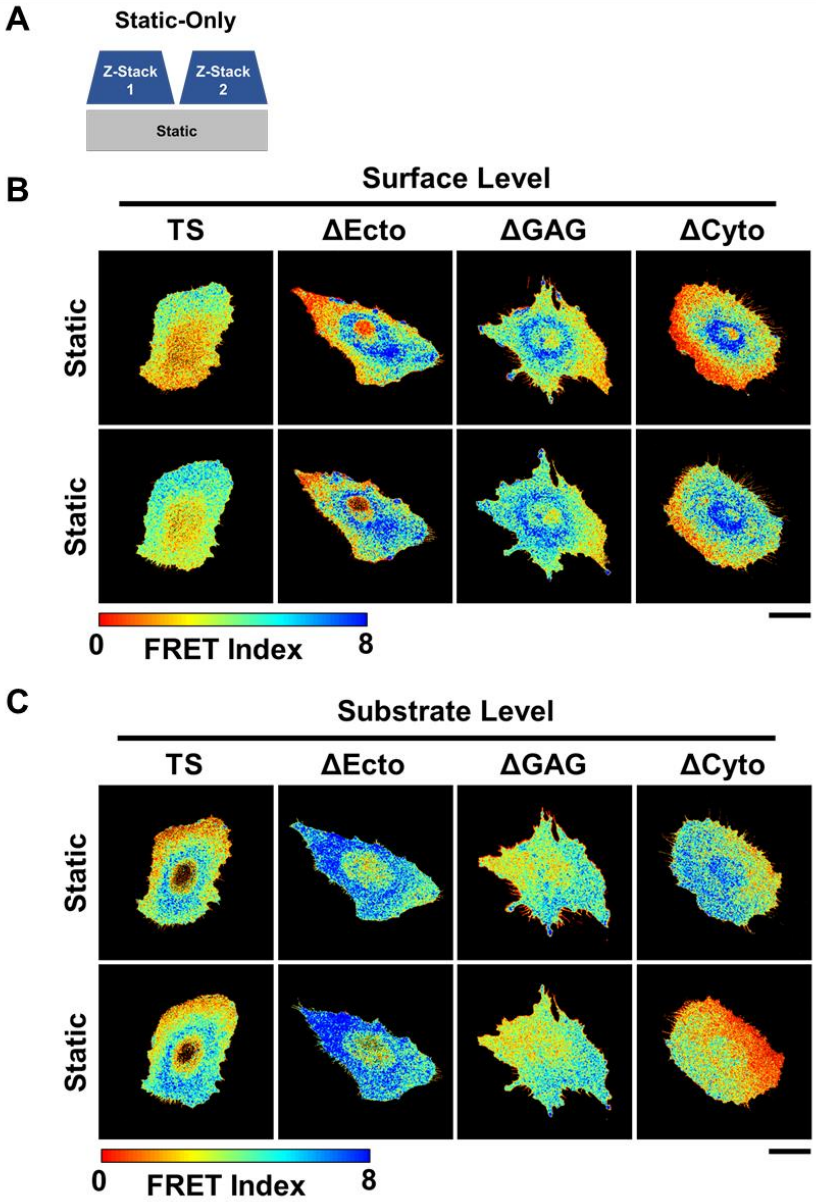

Figure 5.11. Response of SDC1 tension sensors to static-static conditions. Cells expressing the SDC1-TS (TS), ectodomain mutant (ΔEcto), glycosaminoglycan mutant (ΔGAG) and cytoplasmic domain mutant (ΔCyto) sensors were cultured in type I collagen-coated microchannel slides and evaluated for FRET under static-static conditions. (A) Diagram of experiment. Representative (B) surface- and (C) substrate-level, z-projected FRET index images of cells expressing the sensors under an initial static condition, followed by a second static condition. Bars = 50 μm.

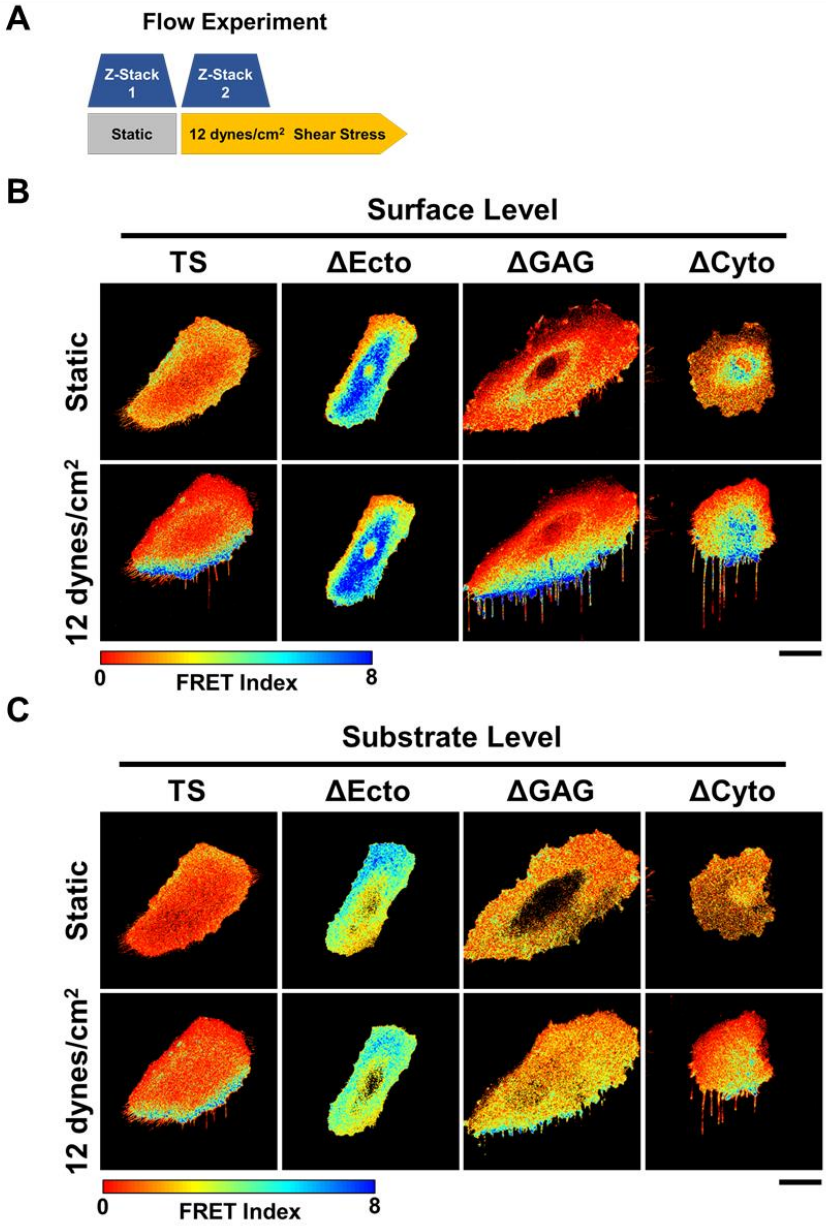

Figure 5.12. Response of SDC1 tension sensors to shear stress. Cells expressing the SDC1-TS (TS), ectodomain mutant (ΔEcto), glycosaminoglycan mutant (ΔGAG) and cytoplasmic domain mutant (ΔCyto) sensors were cultured in microchannel slides coated with collagen type I and evaluated for FRET under static conditions, followed by 12 dynes/cm^2 shear stress. (A) Diagram of experiment. Representative (B) surface- and (C) substrate-level, z-projected FRET index images of cells expressing the sensors under an initial static condition, followed by flow. Bars = 50 μm.

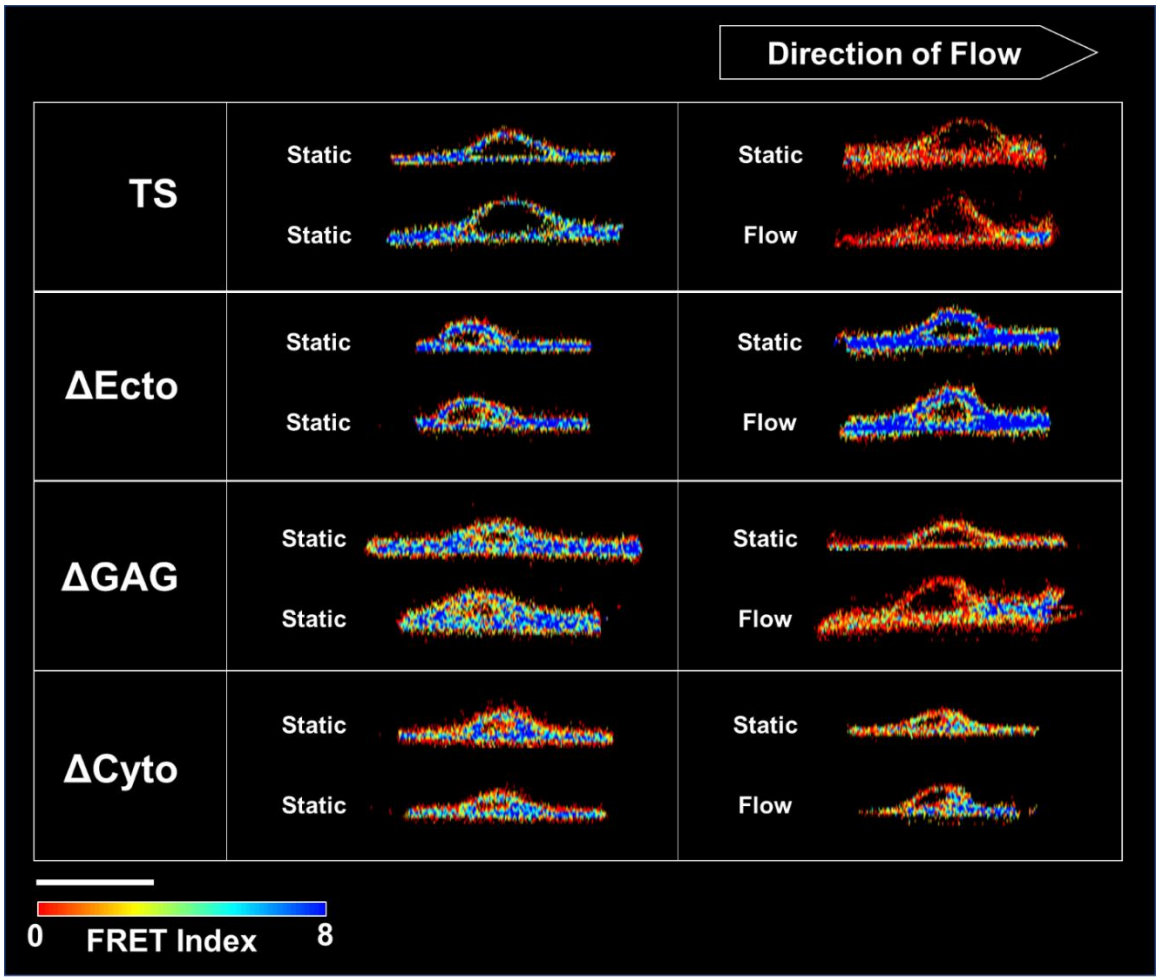

Figure 5.13. Side views of response of SDC1 tension sensors to static-static and static-flow conditions. Representative FRET side views of cells expressing the SDC1-TS (TS), ectodomain mutant (ΔEcto), glycosaminoglycan mutant (ΔGAG) and cytoplasmic domain mutant (ΔCyto) sensors under static-static and static, followed by 12 dynes/cm^2 shear stress.

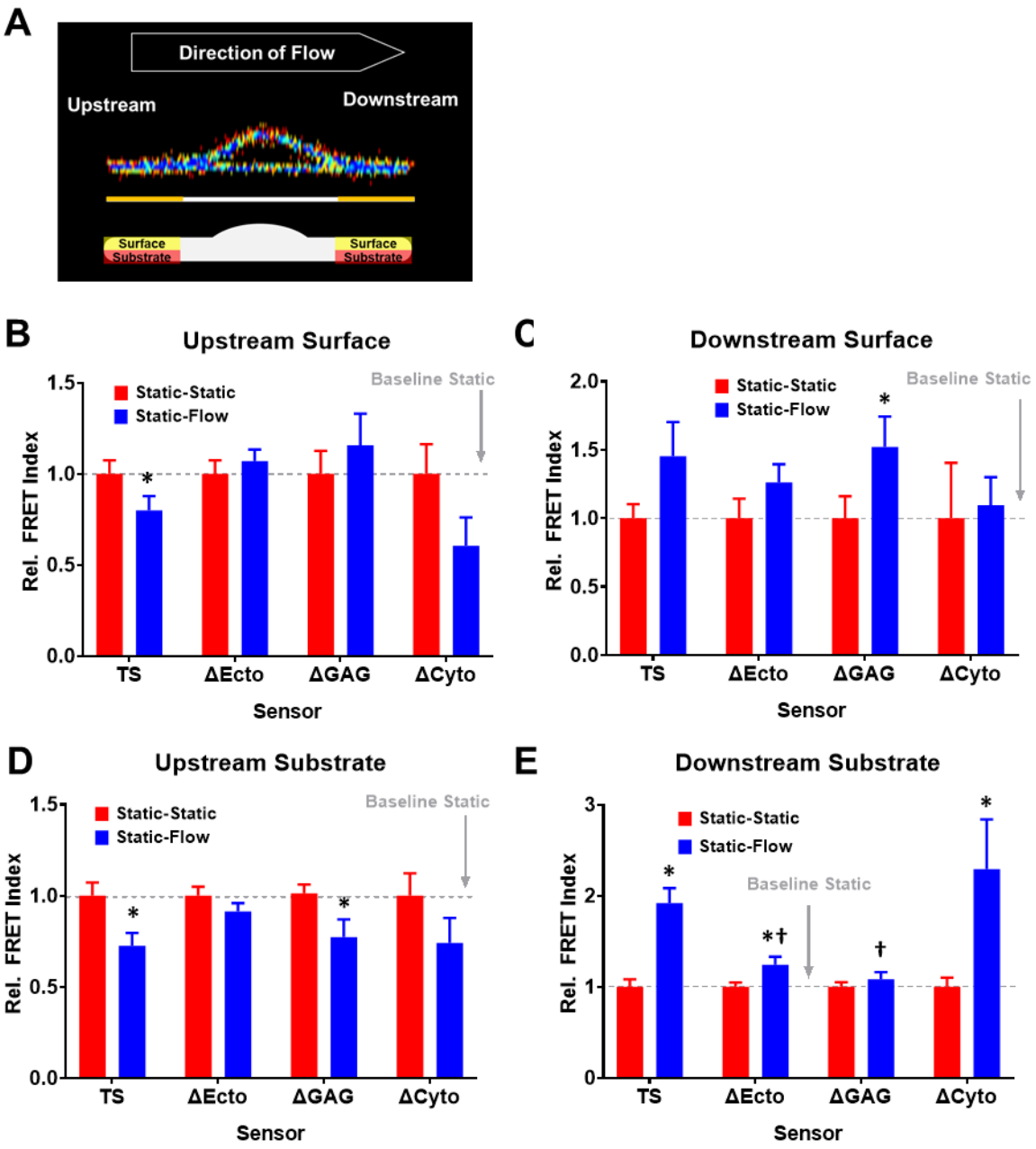

Figure 5.14. SDC1 compresses at the substrate level, downstream of the direction of flow. (A) Diagram of subdivisions of FRET index images with respect to the direction of flow. Quantification of FRET index at the (B) upstream surface, (C) downstream surface, (D) upstream surface and (E) downstream surface of the cell under static-static and static-flow conditions, relative to FRET under the initial static condition. $^{*}p<0.05$ versus baseline static condition. $^{\dagger}p<0.05$ versus TS FRET at upstream substrate under flow. $n = 15$.

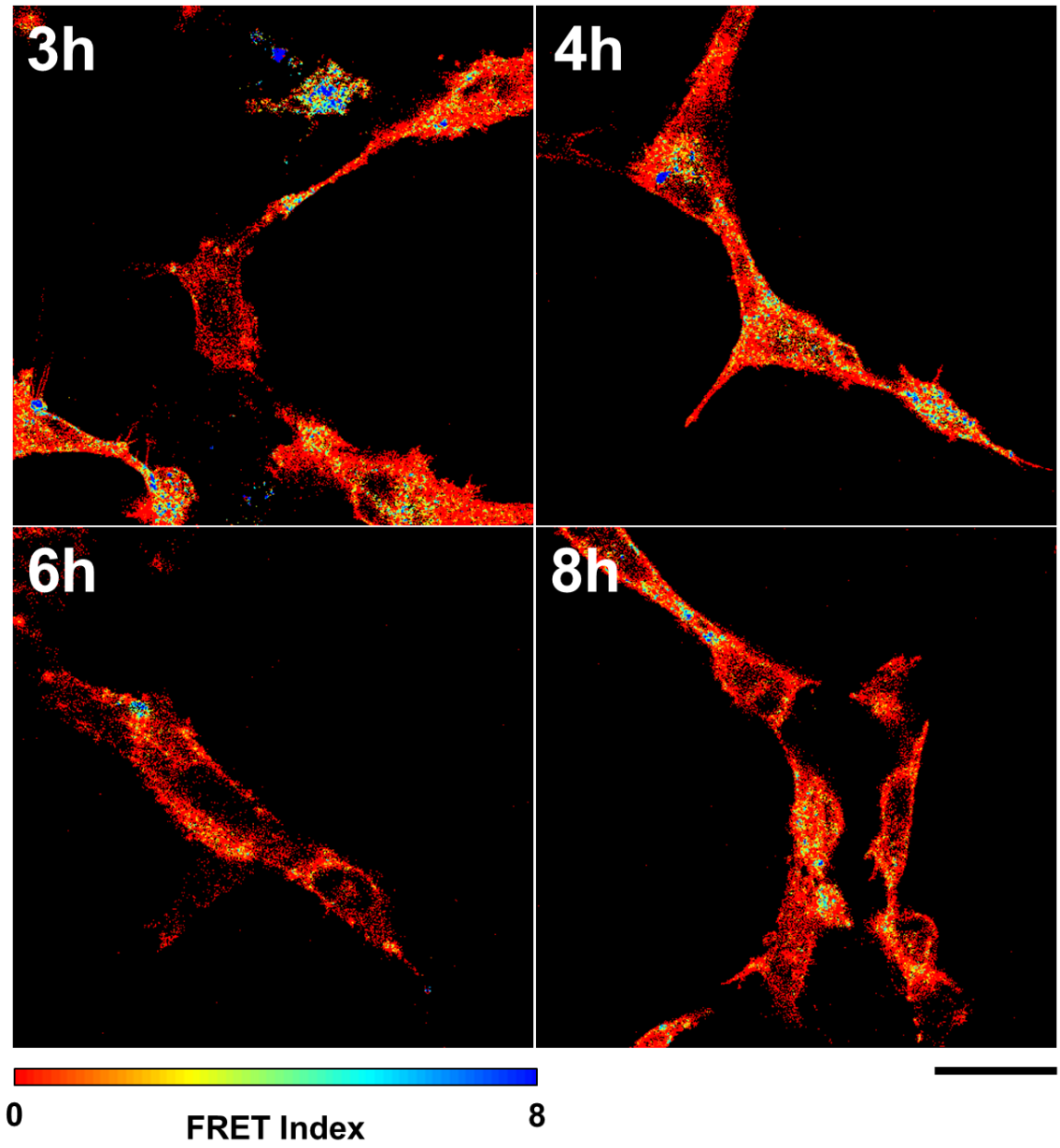

Figure 5.15. SDC1 tension during endothelial tube formation. Representative FRET index images of HUVECs expressing the SDC1-TS over the first 8 hours of tube formation.

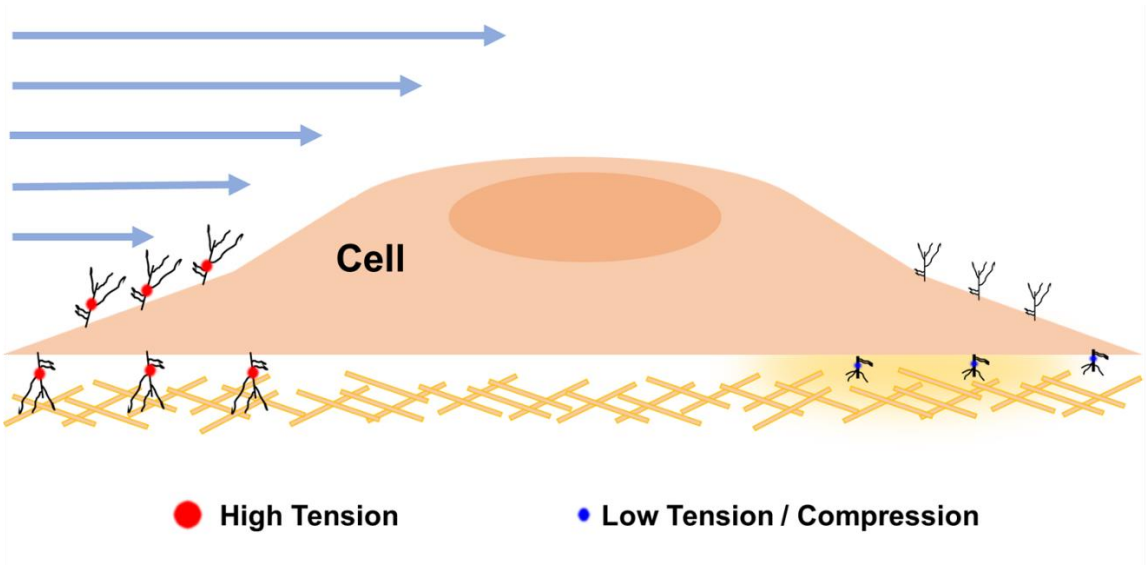

Figure 5.16. Model of SDC1 tension response to 12 dynes/cm^2 shear stress.

5.4 DISCUSSION

Here, we demonstrate that integrin binding with SDC1 contributes to SDC1 tension and that fluidic shear stress induces a spatial gradient of SDC1 tension in response to flow. Removal of the glycocalyx has been shown to reduce glycocalyx reduces the shear-stress-mediated response of endothelial cells. Because enzymatic removal of heparan sulfate is known to also affect the response of endothelial cells to shear-stress, heparan sulfate-containing transmembrane proteins are appealing candidates. Indeed, knockout of SDC1 leads to reduced Akt phosphorylation in response to shear-stress.(Voyvodic et al., 2014)

SDC1 is a co-receptor to several integrins, and many of the shear-stress-mediated responses, including Akt phosphorylation, have been observed by previous groups are downstream of integrin. In our recent work, we demonstrate first that SDC1, itself, is under tension, and that components of its extracellular domain are involved in this force propagation. Additionally, the inhibition of players involved in cytoskeletal tension, such as ROCK, increases SDC1 tension. Decoupling of SDC1 from the αv integrins increases SDC1 tension, while inactivation of αv integrins also increases SDC1 tension at the substrate level, implying that the αV integrins contribute to SDC1 tension during binding of the ECM.

SDC1 is required for the activation of integrins αVβ3 and αVβ5(Beauvais et al., 2009) but has also been shown to require integrin αVβ3 to mediate cell spreading(Beauvais et al., 2004) and mediate the alignment of ECM fibers,(Yang & Friedl, 2016) suggesting an interdependence between these proteins in mechanosensation. Our data are suggestive

of a model in which, upon adhering, the cell reaches out with SDC1, binding the ECM. At that moment, SDC1 is tense and stretched. The integrins, however, cannot reach the ECM due to their size relative to SDC1. SDC1 then may bind to the integrin, causing SDC1 to shorten and its tension to decrease. In such a model, mature focal adhesions would spatially exclude SDC1. This model is supported by other work that has indicated that syndecans are absent in mature focal adhesions.(Roper, Williamson, & Bass, 2012)

The presence of DMSO in our cytoskeletal disruption and focal adhesion disruption experiments pose some challenges for the interpretation of FRET following the drug treatments. Additionally, our method of quantification may fail to capture local changes in FRET distribution in response to the treatments. For this reason, we made some qualitative observations of the leading edges of the cells before and after treatment. We observed that at baseline levels, a thin, high-tension edge appears to be present in the leading edge, along with high-tension filopodia and a distinctive FRET pattern within the leading edge that resembled high- and low-tension patches. After treatment with Y27632 and PF-573,228, this pattern appears to change, while treatment with the active isoform of Blebbistatin and PP2 resulted in no change in this FRET pattern, which may suggest that Rock and FAK are involved in SDC1 tension, but myosin ii and the src-family kinases are not.

The hunt for mechanosensors of shear stress has pointed to several potential proteins. Integrin αVβ3 is known to undergo activation, primarily at the endothelial-substrate interface, in response to shear stress.(Chen et al., 2015; Tzima, del Pozo, Shattil, Chien, & Schwartz, 2001) Previous work found that knockdown of SDC1 in bovine aortic

endothelial cells abrogated endothelial cell elongation in the direction of flow, indicating that SDC1 is required for the transmission of flow-mediated force to the cytoskeleton.(Ebong, Lopez-Quintero, Rizzo, Spray, & Tarbell, 2014) Loss of SDC1 has also been observed to abolish several early signaling events occur in endothelial cells within 15 minutes of shear-stress application, including Akt phosphorylation, the establishment of a spatial phosphorylation gradient in paxillin and RhoA activation.(Voyvodic et al., 2014) In this study, tension on the complete Sdc1TS was responsive to the application of shear stress within 15 minutes of the initiation of flow. The lack of tension response in the TSΔEcto sensor in response to shear stress suggests that SDC1s interaction with αv integrins is necessary for its ability to mechanosense, consistent with the activation of integrin αVβ3 in response to shear stress.

Our shear stress experiments suggest that the GAG chains of SDC1 are important for upstream surface-level tension formation in SDC1 in response to flow. Our observation that compression occurs on the SDC1-TS and TSΔCyto but not TSΔEcto and TSΔGAG suggest that GAGs are essential for developing compression at the downstream substrate level. As a cell experiences shear stress, it may be that the cell is being pulled by shear stress on the upstream side, leading to the cell resisting fluidic shear on the downstream side by compressing, and thus causing compression on SDC1 (**Figure 5.16**).

Chapter 6. Conclusions

SDC1's list of functions is ever expanding, and our work provides new evidence for SDC1 in vascular mechanosensing. Building on previous work from our group, we found that SDC1 is involved in sensing nanotopography in engineered materials. SDC1 Nanotopography, itself, can alter signaling through the TGF-β and Hippo pathways through the regulation of cytoskeletal tension. In Chapter 4, we developed and validated a SDC1 tension sensor, which enabled the visualization of changes in tension on SDC1 during mechanosensation. We found that SDC1 tension increases with substrate stiffness and can be altered with nanopatterning. One unexpected finding was that loss of the SDC1 cytoplasmic domain increased SDC1 tension. In Chapter 5, our work indicated that SDC1 tension is influenced by its binding to αV integrins. Additionally, we demonstrated that during shear-stress, endothelial cells exhibit a spatial gradient of SDC1 tension that requires the SDC1 ectodomain. We observed tension on SDC1 on the upstream region of the cell and compression on SDC1 on the downstream region.

Future work is needed to solidify SDC1's mechanosensing story. One obvious future direction would involve incorporating FLIM to our FRET evaluation approach. Utilizing light sheet microscopy would improve temporal resolution and enable the evaluation of FRET in earlier phases of SDC1 tension propagation. Co-immunoprecipitation of proteins bound to SDC1 during SDC1 mechanosensing of compliance substrates and shear-stress would further elucidate SDC1 mechanosensing

mechanisms. Time-lapse FRET imaging of migrating cells expressing the tension sensors would enable the examination of SDC1 tension in the leading versus the lagging end. Another topic that could be explored is the impact of ECM component on SDC1 tension and strength of binding. In this work, we only utilized type I collagen, but SDC1 is known to bind other ECM proteins, such as fibronectin, tropoelastin, laminin, vitronectin, among others.(Stepp et al., 2002)

We applied shear-stress to non-confluent endothelial cells, which yielded interesting insight into the spatial distribution of SDC1 tension across endothelial cells. Ideally, these experiments would have also been performed on a confluent monolayer of endothelial cells to better mimic the intimal layer of arteries *in vitro*. However, our attempts to culture a monolayer with our TS-expressing cell lines were unsuccessful. Even cultured at high confluency, our cells overlapped. Previous work from other groups has shown that lower or higher than normal *SDC1* expression in endothelial cells can induce phenotype and morphological changes leading to similar overlapping. The creation of cell lines that express SDC1—both SDC1TS and wild-type SDC1—at "normal" levels could help to address this problem.

In the future, expression of the SDC1TS in vascular smooth muscle cells would enable the examination of SDC1 tension in the context of smooth muscle cell function. Additionally, the combination of SDC1TS expression and knockdown of *SDC1* in endothelial cells would enable future researchers to examine tension on SDC1TS in the absence of potential effects of wild-type SDC1 on the glycocalyx.

A broad goal of understanding the role of SDC1 in vascular mechanosensing is utilizing those insights to engineer improved vascular grafts. Endothelial or smooth muscle cells expressing the SDC1TS could be seeded into vascular grafts to study SDC1 tension during colonization of the graft and later, during various flow conditions. Additionally, as SDC1 is involved in leukocyte adhesion to endothelial cells, the SDC1TS could be used to understand SDC1 tension during leukocyte attachment and rolling.

Clearly, there are many exciting potential uses for the SDC1TS toward the aim of increasing our understanding of its complex role in mechanosensation.

Appendix A. Sequence of Syndecan-1 Tension Sensor

Human *SDC1* with TSMod tension sensing construct indicated in bold font.(Grashoff et al., 2010a)

```
   1 GGCCGGGAGA CCTGGCGGAG CTGGGGGTGG GGGGCCAGTT TTTGCAACGG CTAAGGAAGG
  61 GCCTGTGGGT TTATTATAAG GCGGAGCTCG GCGGGAGAGG TGCGGGCCGA ATCCGAGCCG
 121 AGCGGAGAGG AATCCGGCAG TAGAGAGCGG ACTCCAGCCG GCGGACCCTG CAGCCCTCGC
 181 CTGGGACAGC GGCGCGCTGG GCAGGCGCCC AAGAGAGCAT CGAGCAGCGG AACCCGCGAA
 241 GCCGGCCCGC AGCCGCGACC CGCGCAGCCT GCCGCTCTCC CGCCGCCGGT CCGGGCAGCA
 301 TGAGGCGCGC GGCGCTCTGG CTCTGGCTGT GCGCGCTGGC GCTGAGCCTG CAGCCGGCCC
 361 TGCCGCAAAT TGTGGCTACT AATTTGCCCC CTGAAGATCA AGATGGCTCT GGGGATGACT
 421 CTGACAACTT CTCCGGCTCA GGTGCAGGTG CTTTGCAAGA TATCACCTTG TCACAGCAGA
 481 CCCCCTCCAC TTGGAAGGAC ACGCAGCTCC TGACGGCTAT TCCCACGTCT CCAGAACCCA
 541 CCGGCCTGGA GGCTACAGCT GCCTCCACCT CCACCCTGCC GGCTGGAGAG GGGCCCAAGG
 601 AGGGAGAGGC TGTAGTCCTG CCAGAAGTGG AGCCTGGCCT CACCGCCCGG GAGCAGGAGG
 661 CCACCCCCCG ACCCAGGGAG ACCACACAGC TCCCGACCAC TCATCAGGCC TCAACGACCA
 721 CAGCCACCAC GGCCCAGGAG CCCGCCACCT CCCACCCCCA CAGGGACATG CAGCCTGGCC
 781 ACCATGAGAC CTCAACCCCT GCAGGACCCA GCCAAGCTGA CCTTCACACT CCCCACACAG
 841 AGGATGGAGG TCCTTCTGCC ACCGAGAGGG CTGCTGAGGA TGGAGCCTCC AGTCAGCTCC
 901 CAGCAGCAGA GGGCTCTGGG GAGCAGGACT TCACCTTTGA AACCTCGGGG GAGAATACGG
 961 CTGTA**ATGGT GAGCAAGGGC GAGGAGACCA CAATGGGCGT AATCAAGCCC GACATGAAGA**
1021 **TCAAGCTGAA GATGGAGGGC AACGTGAATG GCCACGCCTT CGTGATCGAG GGCGAGGGCG**
1081 **AGGGCAAGCC CTACGACGGC ACCAACACCA TCAACCTGGA GGTGAAGGAG GGAGCCCCCC**
1141 **TGCCCTTCTC CTACGACATT CTGACCACCG CGTTCGCCTA CGGCAACAGG GCCTTCACCA**
1201 **AGTACCCCGA CGACATCCCC AACTACTTCA AGCAGTCCTT CCCCGAGGGC TACTCTTGGG**
1261 **AGCGCACCAT GACCTTCGAG GACAAGGGCA TCGTGAAGGT GAAGTCCGAC ATCTCCATGG**
1321 **AGGAGGACTC CTTCATCTAC GAGATACACC TCAAGGGCGA GAACTTCCCC CCCAACGGCC**
1381 **CCGTGATGCA GAAGAAGACC ACCGGCTGGG ACGCCTCCAC CGAGAGGATG TACGTGCGCG**
1441 **ACGGCGTGCT GAAGGGCGAC GTCAAGCACA AGCTGCTGCT GGAGGGCGGC GGCCACCACC**
1501 **GCGTTGACTT CAAGACCATC TACAGGGCCA AGAAGGCGGT GAAGCTGCCC GACTATCACT**
1561 **TTGTGGACCA CCGCATCGAG ATCCTGAACC ACGACAAGGA CTACAACAAG GTGACCGTTT**
1621 **ACGAGAGCGC CGTGGCCCGC AACTCCACCG ACGGCATGGA CGAGCTGTAC AAGGGGCCAG**
1681 **GTGGTGCAGG GCCAGGTGGT GCAGGGCCAG GTGGTGCAGG GCCAGGTGGT GCAGGGCCCG**
1741 **GTGGTGCAGG TCCAGGTGGT GCAGGTCCAG GTGGTGCAGG TCCAGGTGGT GCTATGGTGA**
1801 **GCAAGGGCGA GGAGCTGTTC ACCGGGGTGG TGCCCATCCT GGTCGAGCTG GACGGCGACG**
1861 **TAAACGGCCA CAAGTTCAGC GTGTCCGGCG AGGGCGAGGG CGATGCCACC TACGGCAAGC**
1921 **TGACCCTGAA GCTGATCTGC ACCACCGGCA AGCTGCCCGT GCCCTGGCCC ACCCTCGTGA**
1981 **CCACCCTGGG CTACGGCCTG CAGTGCTTCG CCCGCTACCC CGACCACATG AAGCAGCACG**
2041 **ACTTCTTCAA GTCCGCCATG CCCGAAGGCT ACGTCCAGGA GCGCACCATC TTCTTCAAGG**
2101 **ACGACGGCAA CTACAAGACC CGCGCCGAGG TGAAGTTCGA GGGCGACACC CTGGTGAACC**
2161 **GCATCGAGCT GAAGGGCATC GACTTCAAGG AGGACGGCAA CATCCTGGGG CACAAGCTGG**
2221 **AGTACAACTA CAACAGCCAC AACGTCTATA TCACCGCCGA CAAGCAGAAG AACGGCATCA**
2281 **AGGCCAACTT CAAGATCCGC CACAACATCG AGGACGGCGG CGTGCAGCTC GCCGACCACT**
2341 **ACCAGCAGAA CACCCCCATC GGCGACGGCC CCGTGCTGCT GCCCGACAAC CACTACCTGA**
2401 **GCTACCAGTC CAAGCTGAGC AAAGACCCCA ACGAGAAGCG CGATCACATG GTCCTGCTGG**
2461 **AGTTCGTGAC CGCCGCCGGG ATCACTCTCG GCATGGACGA GCTGTACAAG TAA**GTGGCCG
2521 TGGAGCCTGA CCGCCGGAAC CAGTCCCCAG TGGATCAGGG GGCCACGGGG GCCTCACAGG
2581 GCCTCCTGGA CAGGAAAGAG GTGCTGGGAG GGGTCATTGC CGGAGGCCTC GTGGGGCTCA
2641 TCTTTGCTGT GTGCCTGGTG GGTTTCATGC TGTACCGCAT GAAGAAGAAG GACGAAGGCA
2701 GCTACTCCTT GGAGGAGCCG AAACAAGCCA ACGGCGGGGC CTACCAGAAG CCCACCAAAC
2761 AGGAGGAATT CTATGCCTGA CGCGGGAGCC ATGCGCCCCC TCCGCCCTGC CACTCACTAG
2821 GCCCCCACTT GCCTCTTCCT TGAAGAACTG CAGGCCCTGG CCTCCCCTGC CACCAGGCCA
2881 CCTCCCCAGC ATTCCAGCCC CTCTGGTCGC TCCTGCCCAC GGAGTCGTGG GGTGTGCTGG
2941 GAGCTCCACT CTGCTTCTCT GACTTCTGCC TGGAGACTTA GGGCACCAGG GGTTTCTCGC
3001 ATAGGACCTT TCCACCACAG CCAGCACCTG GCATCGCACC ATTCTGACTC GGTTTCTCCA
3061 AACTGAAGCA GCCTCTCCCC AGGTCCAGCT CTGGAGGGGA GGGGGATCCG ACTGCTTTGG
```

```
3121 ACCTAAATGG CCTCATGTGG CTGGAAGATC CTGCGGGTGG GGCTTGGGGC TCACACACCT
3181 GTAGCACTTA CTGGTAGGAC CAAGCATCTT GGGGGGGTGG CCGCTGAGTG GCAGGGGACA
3241 GGAGTCCACT TTGTTTCGTG GGGAGGTCTA ATCTAGATAT CGACTTGTTT TTGCACATGT
3301 TTCCTCTAGT TCTTTGTTCA TAGCCCAGTA GACCTTGTTA CTTCTGAGGT AAGTTAAGTA
3361 AGTTGATTCG GTATCCCCCC ATCTTGCTTC CCTAATCTAT GGTCGGGAGA CAGCATCAGG
3421 GTTAAGAAGA CTTTTTTTTT TTTTTTTTAA ACTAGGAGAA CCAAATCTGG AAGCCAAAAT
3481 GTAGGCTTAG TTTGTGTGTT GTCTCTTGAG TTTGTCGCTC ATGTGTGCAA CAGGGTATGG
3541 ACTATCTGTC TGGTGGCCCC GTTTCTGGTG GTCTGTTGGC AGGCTGGCCA GTCCAGGCTG
3601 CCGTGGGGCC GCCGCCTCTT TCAAGCAGTC GTGCCTGTGT CCATGCGCTC AGGGCCATGC
3661 TGAGGCCTGG GCCGCTGCCA CGTTGGAGAA GCCCGTGTGA GAAGTGAATG CTGGGACTCA
3721 GCCTTCAGAC AGAGAGGACT GTAGGGAGGG CGGCAGGGGC CTGGAGATCC TCCTGCAGAC
3781 CACGCCCGTC CTGCCTGTGG CGCCGTCTCC AGGGGCTGCT TCCTCCTGGA AATTGACGAG
3841 GGGTGTCTTG GGCAGAGCTG GCTCTGAGCG CCTCCATCCA AGGCCAGGTT CTCCGTTAGC
3901 TCCTGTGGCC CCACCCTGGG CCCTGGGCTG GAATCAGGAA TATTTTCCAA AGAGTGATAG
3961 TCTTTTGCTT TTGGCAAAAC TCTACTTAAT CCAATGGGTT TTTCCCTGTA CAGTAGATTT
4021 TCCAAATGTA ATAAACTTTA ATATAAAGTA GTCCTGTGAA TGCCACTGCC TTCGCTTCTT
4081 GCCTCTGTGC TGTGTGTGAC GTGACCGGAC TTTTCTGCAA ACACCAACAT GTTGGGAAAC
4141 TTGGCTCGAA TCTCTGTGCC TTCGTCTTTC CCATGGGGAG GGATTCTGGT TCCAGGGTCC
4201 CTCTGTGTAT TTGCTTTTTT GTTTTGGCTG AAATTCTCCT GGAGGTCGGT AGGTTCAGCC
4261 AAGGTTTTAT AAGGCTGATG TCAATTTCTG TGTTGCCAAG CTCCAAGCCC CATCTTCTAA
4321 ATGGCAAAGG AAGGTGGATG GCCCCAGCAC AGCTTGACCT GAGGCTGTGG TCACAGCGGA
4381 GGTGTGGAGC CGAGGCCTAC CCCGCAGACA CCTTGGACAT CCTCCTCCCA CCCGGCTGCA
4441 GAGGCCAGAG GCCCCCAGCC CAGGGCTCCT GCACTTACTT GCTTATTTGA CAACGTTTCA
4501 GCGACTCCGT TGGCCACTCC GAGAGGTGGG CCAGTCTGTG GATCAGAGAT GCACCACCAA
4561 GCCAAGGGAA CCTGTGTCCG GTATTCGATA CTGCGACTTT CTGCCTGGAG TGTATGACTG
4621 CACATGACTC GGGGGTGGGG AAAGGGGTCG GCTGACCATG CTCATCTGCT GGTCCGTGGG
4681 ACGGTGCCCA AGCCAGAGGC TGGGTTCATT TGTGTAACGA CAATAAACGG TACTTGTCAT
4741 TTCGGGCAAA AAAAAAAAAA AAAAA
```

Appendix B. Sequence of Syndecan-1 Tension Sensor Expression Clone

Name: EX-Z5956-Lv105
Vector: pEZ-Lv105

```
   1 AAAGTGGTTG ATCGCGTGCA TGCGACGTCA TAGCTCTCTC CCAATTCTCG ACCTCGAGAC
  61 AAATGGCAGT ATTCATCCAC AATTTTAAAA GAAAAGGGGG GATTGGGGGG TACAGTGCAG
 121 GGGAAAGAAT AGTAGACATA ATAGCAACAG ACATACAAAC TAAAGAATTA CAAAAACAAA
 181 TTACAAAAAT TCAAAATTTT CGGGTTTATT ACAGGGACAG CAGAGATCCA GTTTGGCCGC
 241 GGCTCGAGGG GGTTGGGGTT GCGCCTTTTC CAAGGCAGCC CTGGGTTTGC GCAGGGACGC
 301 GGCTGCTCTG GGCGTGGTTC CGGGAAACGC AGCGGCGCCG ACCCTGGGTC TCGCACATTC
 361 TTCACGTCCG TTCGCAGCGT CACCCGGATC TTCGCCGCTA CCCTTGTGGG CCCCCCGGCG
 421 ACGCTTCCTG CTCCGCCCCT AAGTCGGGAA GGTTCCTTGC GGTTCGCGGC GTGCCGGACG
 481 TGACAAACGG AAGCCGCACG TCTCACTAGT ACCCTCGCAG ACGGACAGCG CCAGGGAGCA
 541 ATGGCAGCGC GCCGACCGCG ATGGGCTGTG GCCAATAGCG GCTGCTCAGC AGGGCGCGCC
 601 GAGAGCAGCG GCCGGGAAGG GGCGGTGCGG GAGGCGGGGT GTGGGGCGGT AGTGTGGGCC
 661 CTGTTCCTGC CCGCGCGGTG TTCCGCATTC TGCAAGCCTC CGGAGCGCAC GTCGGCAGTC
 721 GGCTCCCTCG TTGACCGAAT CACCGACCTC TCTCCCCAGG GGGATCCACC GGAGCTTACC
 781 ATGACCGAGT ACAAGCCCAC GGTGCGCCTC GCCACCCGCG ACGACGTCCC CAGGGCGGTA
 841 CGCACCCTCG CCGCCGCGTT CGCCGACTAC CCCGCCACGC GCCACACCGT CGATCCGGAC
 901 CGCCACATCG AGCGGGTCAC CGAGCTGCAA GAACTCTTCC TCACGCGCGT CGGGCTCGAC
 961 ATCGGCAAGG TGTGGGTCGC GGACGACGGC GCCGCGGTGG CGGTCTGGAC CACGCCGGAG
1021 AGCGTCGAAG CGGGGGCGGT GTTCGCCGAG ATCGGCCCGC GCATGGCCGA GTTGAGCGGT
1081 TCCCGGCTGG CCGCGCAGCA ACAGATGGAA GGCCTCCTGG CGCCGCACCG GCCCAAGGAG
1141 CCCGCGTGGT TCCTGGCCAC CGTCGGCGTC TCGCCCGACC ACCAGGGCAA GGGTCTGGGC
1201 AGCGCCGTCG TGCTCCCCGG AGTGGAGGCG GCCGAGCGCG CCGGGGTGCC CGCCTTCCTG
1261 GAGACCTCCG CGCCCCGCAA CCTCCCCTTC TACGAGCGGC TCGGCTTCAC CGTCACCGCC
1321 GACGTCGAGG TGCCCGAAGG ACCGCGCACC TGGTGCATGA CCCGCAAGCC CGGTGCCTGA
1381 CGCCCGCCCC ACGACCCGCA GCGCCCGACC GAAAGGAGCG CACGACCCCA TGCATCGGTA
1441 CCTTTAAGAC CAATGACTTA CAAGGCAGCT GTAGATCTTA GCCACTTTTT AAAAGAAAAG
1501 GGGGGACTGG AAGGGCTAAT TCACTCCCAA CGAAGACAAG ATCTGCTTTT TGCTTGTACT
1561 GGGTCTCTCT GGTTAGACCA GATCTGAGCC TGGGAGCTCT CTGGCTAACT AGGGAACCCA
1621 CTGCTTAAGC CTCAATAAAG CTTGCCTTGA GTGCTTCAAG TAGTGTGTGC CCGTCTGTTG
1681 TGTGACTCTG GTAACTAGAG ATCCCTCAGA CCCTTTTAGT CAGTGTGGAA AATCTCTAGC
1741 AGTAGTAGTT CATGTCATCT TATTATTCAG TATTTATAAC TTGCAAAGAA ATGAATATCA
1801 GAGAGTGAGA GGAACTTGTT TATTGCAGCT TATAATGGTT ACAAATAAAG CAATAGCATC
1861 ACAAATTTCA CAAATAAAGC ATTTTTTTCA CTGCATTCTA GTTGTGGTTT GTCCAAACTC
1921 ATCAATGTAT CTTATCATGT CTGGCTCTAG CTATCCCGCC CCTAACTCCG CCCATCCCGC
1981 CCCTAACTCC GCCCAGTTCC GCCCATTCTC CGCCCCATGG CTGACTAATT TTTTTTATTT
2041 ATGCAGAGGC CGAGGCCGCC TCGGCCTCTG AGCTATTCCA GAAGTAGTGA GGAGGCTTTT
2101 TTGGAGGCCT AGGGACGTAC CCAATTCGCC CTATAGTGAG TCGTATTACG CGCGCTCACT
2161 GGCCGTCGTT TTACAACGTC GTGACTGGGA AAACCCTGGC GTTACCCAAC TTAATCGCCT
2221 TGCAGCACAT CCCCCTTTCG CCAGCTGGCG TAATAGCGAA GAGGCCCGCA CCGATCGCCC
2281 TTCCCAACAG TTGCGCAGCC TGAATGGCGA ATGGGACGCG CCCTGTAGCG GCGCATTAAG
2341 CGCGGCGGGT GTGGTGGTTA CGCGCAGCGT GACCGCTACA CTTGCCAGCG CCCTAGCGCC
2401 CGCTCCTTTC GCTTTCTTCC CTTCCTTTCT CGCCACGTTC GCCGGCTTTC CCCGTCAAGC
2461 TCTAAATCGG GGGCTCCCTT TAGGGTTCCG ATTTAGTGCT TTACGGCACC TCGACCCCAA
2521 AAAACTTGAT TAGGGTGATG GTTCACGTAG TGGGCCATCG CCCTGATAGA CGGTTTTTCG
2581 CCCTTTGACG TTGGAGTCCA CGTTCTTTAA TAGTGGACTC TTGTTCCAAA CTGGAACAAC
2641 ACTCAACCCT ATCTCGGTCT ATTCTTTTGA TTTATAAGGG ATTTTGCCGA TTTCGGCCTA
2701 TTGGTTAAAA AATGAGCTGA TTTAACAAAA ATTTAACGCG AATTTTAACA AAATATTAAC
2761 GCTTACAATT TAGGTGGCAC TTTTCGGGGA AATGTGCGCG GAACCCCTAT TTGTTTATTT
2821 TTCTAAATAC ATTCAAATAT GTATCCGCTC ATGAGACAAT AACCCTGATA AATGCTTCAA
2881 TAATATTGAA AAAGGAAGAG TATGAGTATT CAACATTTCC GTGTCGCCCT TATTCCCTTT
2941 TTTGCGGCAT TTTGCCTTCC TGTTTTTGCT CACCCAGAAA CGCTGGTGAA AGTAAAAGAT
3001 GCTGAAGATC AGTTGGGTGC ACGAGTGGGT TACATCGAAC TGGATCTCAA CAGCGGTAAG
3061 ATCCTTGAGA GTTTTCGCCC CGAAGAACGT TTTCCAATGA TGAGCACTTT TAAAGTTCTG
```

3121 CTATGTGGCG CGGTATTATC CCGTATTGAC GCCGGGCAAG AGCAACTCGG TCGCCGCATA
3181 CACTATTCTC AGAATGACTT GGTTGAGTAC TCACCAGTCA CAGAAAAGCA TCTTACGGAT
3241 GGCATGACAG TAAGAGAATT ATGCAGTGCT GCCATAACCA TGAGTGATAA CACTGCGGCC
3301 AACTTACTTC TGACAACGAT CGGAGGACCG AAGGAGCTAA CCGCTTTTTT GCACAACATG
3361 GGGGATCATG TAACTCGCCT TGATCGTTGG GAACCGGAGC TGAATGAAGC CATACCAAAC
3421 GACGAGCGTG ACACCACGAT GCCTGTAGCA ATGGCAACAA CGTTGCGCAA ACTATTAACT
3481 GGCGAACTAC TTACTCTAGC TTCCCGGCAA CAATTAATAG ACTGGATGGA GGCGGATAAA
3541 GTTGCAGGAC CACTTCTGCG CTCGGCCCTT CCGGCTGGCT GGTTTATTGC TGATAAATCT
3601 GGAGCCGGTG AGCGTGGGTC TCGCGGTATC ATTGCAGCAC TGGGGCCAGA TGGTAAGCCC
3661 TCCCGTATCG TAGTTATCTA CACGACGGGG AGTCAGGCAA CTATGGATGA ACGAAATAGA
3721 CAGATCGCTG AGATAGGTGC CTCACTGATT AAGCATTGGT AACTGTCAGA CCAAGTTTAC
3781 TCATATATAC TTTAGATTGA TTTAAAACTT CATTTTTAAT TTAAAAGGAT CTAGGTGAAG
3841 ATCCTTTTTG ATAATCTCAT GACCAAAATC CCTTAACGTG AGTTTTCGTT CCACTGAGCG
3901 TCAGACCCCG TAGAAAAGAT CAAAGGATCT TCTTGAGATC CTTTTTTTCT GCGCGTAATC
3961 TGCTGCTTGC AAACAAAAAA ACCACCGCTA CCAGCGGTGG TTTGTTTGCC GGATCAAGAG
4021 CTACCAACTC TTTTTCCGAA GGTAACTGGC TTCAGCAGAG CGCAGATACC AAATACTGTT
4081 CTTCTAGTGT AGCCGTAGTT AGGCCACCAC TTCAAGAACT CTGTAGCACC GCCTACATAC
4141 CTCGCTCTGC TAATCCTGTT ACCAGTGGCT GCTGCCAGTG GCGATAAGTC GTGTCTTACC
4201 GGGTTGGACT CAAGACGATA GTTACCGGAT AAGGCGCAGC GGTCGGGCTG AACGGGGGGT
4261 TCGTGCACAC AGCCCAGCTT GGAGCGAACG ACCTACACCG AACTGAGATA CCTACAGCGT
4321 GAGCTATGAG AAAGCGCCAC GCTTCCCGAA GGGAGAAAGG CGGACAGGTA TCCGGTAAGC
4381 GGCAGGGTCG GAACAGGAGA GCGCACGAGG GAGCTTCCAG GGGGAAACGC CTGGTATCTT
4441 TATAGTCCTG TCGGGTTTCG CCACCTCTGA CTTGAGCGTC GATTTTTGTG ATGCTCGTCA
4501 GGGGGGCGGA GCCTATGGAA AAACGCCAGC AACGCGGCCT TTTTACGGTT CCTGGCCTTT
4561 TGCTGGCCTT TTGCTCACAT GTTCTTTCCT GCGTTATCCC CTGATTCTGT GGATAACCGT
4621 ATTACCGCCT TTGAGTGAGC TGATACCGCT CGCCGCAGCC GAACGACCGA GCGCAGCGAG
4681 TCAGTGAGCG AGGAAGCGGA AGAGCGCCCT TTGAGTGAGC TGATACCGCT CGCCGCAGCC
4741 GAACGACCGA GCGCAGCGAG TCAGTGAGCG AGGAAGCGGA AGAGCGCCCA ATACGCAAAC
4801 CGCCTCTCCC CGCGCGTTGG CCGATTCATT AATGCAGCTG GCACGACAGG TTTCCCGACT
4861 GGAAAGCGGG CAGTGAGCGC AACGCAAAAT GTGAGTTAGC TCACTCATTA GGCACCCCAG
4921 GCTTTACACT TTATGCTTCC GGCTCGTATG TTGTGTGGAA TTGTGAGCGG ATAACAATTT
4981 CACACAGGAA ACAGCTATGA CCATGATTAC GCCAAGCGCG CAATTAACCC TCACTAAAGG
5041 GAACAAAAGC TGGAGCTGCA AGCTTAATGT AGTCTTATGC AATACTCTTG TAGTCTTGCA
5101 ACATGGTAAC GATGAGTTAG CAACATGCCT TACAAGGAGA GAAAAAGCAC CGTGCATGCC
5161 GATTGGTGGA AGTAAGGTGG TACGATCGTG CCTTATTAGG AAGGCAACAG ACGGGTCTGA
5221 CATGGATTGG ACGAACCACT GAATTGCCGC ATTGCAGAGA TATTGTATTT AAGTGCCTAG
5281 CTCGATACAT AAACGGGTCT CTCTGGTTAG ACCAGATCTG AGCCTGGGAG CTCTCTGGCT
5341 AACTAGGGAA CCCACTGCTT AAGCCTCAAT AAAGCTTGCC TTGAGTGCTT CAAGTAGTGT
5401 GTGCCCGTCT GTTGTGTGAC TCTGGTAACT AGAGATCCCT CAGACCCTTT TAGTCAGTGT
5461 GGAAAATCTC TAGCAGTGGC GCCCGAACAG GGACTTGAAA GCGAAAGGGA AACCAGAGGA
5521 GCTCTCTCGA CGCAGGACTC GGCTTGCTGA AGCGCGCACG GCAAGAGGCG AGGGGCGGCG
5581 ACTGGTGAGT ACGCCAAAAA TTTTGACTAG CGGAGGCTAG AAGGAGAGAG ATGGGTGCGA
5641 GAGCGTCAGT ATTAAGCGGG GGAGAATTAG ATCGCGATGG GAAAAAATTC GGTTAAGGCC
5701 AGGGGGAAAG AAAAAATATA AATTAAAACA TATAGTATGG GCAAGCAGGG AGCTAGAACG
5761 ATTCGCAGTT AATCCTGGCC TGTTAGAAAC ATCAGAAGGC TGTAGACAAA TACTGGGACA
5821 GCTACAACCA TCCCTTCAGA CAGGATCAGA AGAACTTAGA TCATTATATA ATACAGTAGC
5881 AACCCTCTAT TGTGTGCATC AAAGGATAGA GATAAAAGAC ACCAAGGAAG CTTTAGACAA
5941 GATAGAGGAA GAGCAAAACA AAAGTAAGAC CACCGCACAG CAAGCGGCCG CTGATCTTCA
6001 GACCTGGAGG AGGAGATATG AGGGACAATT GGAGAAGTGA ATTATATAAA TATAAAGTAG
6061 TAAAAATTGA ACCATTAGGA GTAGCACCCA CCAAGGCAAA GAGAAGAGTG GTGCAGAGAG
6121 AAAAAAGAGC AGTGGGAATA GGAGCTTTGT TCCTTGGGTT CTTGGGAGCA GCAGGAAGCA
6181 CTATGGGCGC AGCGTCAATG ACGCTGACGG TACAGGCCAG ACAATTATTG TCTGGTATAG
6241 TGCAGCAGCA GAACAATTTG CTGAGGGCTA TTGAGGCGCA ACAGCATCTG TTGCAACTCA
6301 CAGTCTGGGG CATCAAGCAG CTCCAGGCAA GAATCCTGGC TGTGGAAAGA TACCTAAAGG
6361 ATCAACAGCT CCTGGGGATT TGGGGTTGCT CTGGAAAACT CATTTGCACC ACTGCTGTGC
6421 CTTGGAATGC TAGTTGGAGT AATAAATCTC TGGAACAGAT TTGGAATCAC ACGACCTGGA
6481 TGGAGTGGGA CAGAGAAATT AACAATTACA CAAGCTTAAT ACACTCCTTA ATTGAAGAAT
6541 CGCAAAACCA GCAAGAAAAG AATGAACAAG AATTATTGGA ATTAGATAAA TGGGCAAGTT
6601 TGTGGAATTG GTTTAACATA ACAAATTGGC TGTGGTATAT AAAATTATTC ATAATGATAG

```
 6661 TAGGAGGCTT GGTAGGTTTA AGAATAGTTT TTGCTGTACT TTCTATAGTG AATAGAGTTA
 6721 GGCAGGGATA TTCACCATTA TCGTTTCAGA CCCACCTCCC AACCCCGAGG GGACCCGACA
 6781 GGCCCGAAGG AATAGAAGAA GAAGGTGGAG AGAGAGACAG AGACAGATCC ATTCGATTAG
 6841 TGAACGGATC TCGACGGTAT CGATCACGAG ACTAGCCTCG AGCGGCCGCC CCCTTCACCG
 6901 AGGGCCTATT TCCCATGATT CCTTCATATT TGCATATACG ATACAAGGCT GTTAGAGAGA
 6961 TAATTGGAAT TAATTTGACT GTAAACACAA AGATATTAGT ACAAAATACG TGACGTAGAA
 7021 AGTAATAATT TCTTGGGTAG TTTGCAGTTT TAAAATTATG TTTTAAAATG GACTATCATA
 7081 TGCTTACCGT AACTTGAAAG TATTTCGATT TCTTGGCTTT ATATATCTTG TGGAAAGGAC
 7141 GAAACACCGG TGATCTATAC ATTGAATCAA TATTGGCAAT TAGCCATATT AGTCATTGGT
 7201 TATATAGCAT AAATCAATAT TGGCTATTGG CCATTGCATA CGTTGTATCT ATATCATAAT
 7261 ATGTACATTT ATATTGGCTC ATGTCCAATA TGACCGCCAT GTTGACATTG ATTATTGACT
 7321 AGTTATTAAT AGTAATCAAT TACGGGGTCA TTAGTTCATA GCCCATATAT GGAGTTCCGC
 7381 GTTACATAAC TTACGGTAAA TGGCCCGCCT GGCTGACCGC CCAACGACCC CCGCCCATTG
 7441 ACGTCAATAA TGACGTATGT TCCCATAGTA ACGCCAATAG GGACTTTCCA TTGACGTCAA
 7501 TGGGTGGAGT ATTTACGGTA AACTGCCCAC TTGGCAGTAC ATCAAGTGTA TCATATGCCA
 7561 AGTCCGCCCC CTATTGACGT CAATGACGGT AAATGGCCCG CCTGGCATTA TGCCCAGTAC
 7621 ATGACCTTAC GGGACTTTCC TACTTGGCAG TACATCTACG TATTAGTCAT CGCTATTACC
 7681 ATGGTGATGC GGTTTTGGCA GTACATCAAT GGGCGTGGAT AGCGGTTTGA CTCACGGGGA
 7741 TTTCCAAGTC TCCACCCCAT TGACGTCAAT GGGAGTTTGT TTTGGCACCA AAATCAACGG
 7801 GACTTTCCAA AATGTCGTAA CAACTCCGCC CCATTGACGC AAATGGGCGG TAGGCGTGTA
 7861 CGGTGGGAGG TCTATATAAG CAGAGCTCGT TTAGTGAACC GTCAGATCGC CTGGAGACGC
 7921 CATCCACGCT GTTTTGACCT CCATAGAAGA TTCTAGATTC GAAGAACAAG TTTGTACAAA
 7981 AAAGCAGGCT CCACCATGAG GCGCGCGGCG CTCTGGCTCT GGCTGTGCGC GCTGGCGCTG
 8041 AGCCTGCAGC CGGCCCTGCC GCAAATTGTG GCTACTAATT TGCCCCCTGA AGATCAAGAT
 8101 GGCTCTGGGG ATGACTCTGA CAACTTCTCC GGCTCAGGTG CAGGTGCTTT GCAAGATATC
 8161 ACCTTGTCAC AGCAGACCCC CTCCACTTGG AAGGACACGC AGCTCCTGAC GGCTATTCCC
 8221 ACGTCTCCAG AACCCACCGG CCTGGAGGCT ACAGCTGCCT CCACCTCCAC CCTGCCGGCT
 8281 GGAGAGGGGC CCAAGGAGGG AGAGGCTGTA GTCCTGCCAG AAGTGGAGCC TGGCCTCACC
 8341 GCCCGGGAGC AGGAGGCCAC CCCCCGACCC AGGGAGACCA CACAGCTCCC GACCACTCAT
 8401 CAGGCCTCAA CGACCACAGC CACCACGGCC CAGGAGCCCG CCACCTCCCA CCCCCACAGG
 8461 GACATGCAGC CTGGCCACCA TGAGACCTCA ACCCCTGCAG GACCCAGCCA AGCTGACCTT
 8521 CACACTCCCC ACACAGAGGA TGGAGGTCCT TCTGCCACCG AGAGGGCTGC TGAGGATGGA
 8581 GCCTCCAGTC AGCTCCCAGC AGCAGAGGGC TCTGGGGAGC AGGACTTCAC CTTTGAAACC
 8641 TCGGGGGAGA ATACGGCTGT AATGGTGAGC AAGGGCGAGG AGACCACAAT GGGCGTAATC
 8701 AAGCCCGACA TGAAGATCAA GCTGAAGATG GAGGGCAACG TGAATGGCCA CGCCTTCGTG
 8761 ATCGAGGGCG AGGGCGAGGG CAAGCCCTAC GACGGCACCA ACACCATCAA CCTGGAGGTG
 8821 AAGGAGGGAG CCCCCCTGCC CTTCTCCTAC GACATTCTGA CCACCGCGTT CGCCTACGGC
 8881 AACAGGGCCT TCACCAAGTA CCCCGACGAC ATCCCCAACT ACTTCAAGCA GTCCTTCCCC
 8941 GAGGGCTACT CTTGGGAGCG CACCATGACC TTCGAGGACA AGGGCATCGT GAAGGTGAAG
 9001 TCCGACATCT CCATGGAGGA GGACTCCTTC ATCTACGAGA TACACCTCAA GGGCGAGAAC
 9061 TTCCCCCCCA ACGGCCCCGT GATGCAGAAG AAGACCACCG GCTGGGACGC CTCCACCGAG
 9121 AGGATGTACG TGCGCGACGG CGTGCTGAAG GGCGACGTCA AGCACAAGCT GCTGCTGGAG
 9181 GGCGGCGGCC ACCACCGCGT TGACTTCAAG ACCATCTACA GGGCCAAGAA GGCGGTGAAG
 9241 CTGCCCGACT ATCACTTTGT GGACCACCGC ATCGAGATCC TGAACCACGA CAAGGACTAC
 9301 AACAAGGTGA CCGTTTACGA GAGCGCCGTG GCCCGCAACT CCACCGACGG CATGGACGAG
 9361 CTGTACAAGG GGCCAGGTGG TGCAGGGCCA GGTGGTGCAG GGCCAGGTGG TGCAGGGCCA
 9421 GGTGGTGCAG GGCCCGGTGG TGCAGGTCCA GGTGGTGCAG GTCCAGGTGG TGCAGGTCCA
 9481 GGTGGTGCTA TGGTGAGCAA GGGCGAGGAG CTGTTCACCG GGGTGGTGCC CATCCTGGTC
 9541 GAGCTGGACG GCGACGTAAA CGGCCACAAG TTCAGCGTGT CCGGCGAGGG CGAGGGCGAT
 9601 GCCACCTACG GCAAGCTGAC CCTGAAGCTG ATCTGCACCA CCGGCAAGCT GCCCGTGCCC
 9661 TGGCCCACCC TCGTGACCAC CCTGGGCTAC GGCCTGCAGT GCTTCGCCCG CTACCCCGAC
 9721 CACATGAAGC AGCACGACTT CTTCAAGTCC GCCATGCCCG AAGGCTACGT CCAGGAGCGC
 9781 ACCATCTTCT TCAAGGACGA CGGCAACTAC AAGACCCGCG CCGAGGTGAA GTTCGAGGGC
 9841 GACACCCTGG TGAACCGCAT CGAGCTGAAG GGCATCGACT TCAAGGAGGA CGGCAACATC
 9901 CTGGGGCACA AGCTGGAGTA CAACTACAAC AGCCACAACG TCTATATCAC CGCCGACAAG
 9961 CAGAAGAACG GCATCAAGGC CAACTTCAAG ATCCGCCACA ACATCGAGGA CGGCGGCGTG
10021 CAGCTCGCCG ACCACTACCA GCAGAACACC CCCATCGGCG ACGGCCCCGT GCTGCTGCCC
10081 GACAACCACT ACCTGAGCTA CCAGTCCAAG CTGAGCAAAG ACCCCAACGA GAAGCGCGAT
10141 CACATGGTCC TGCTGGAGTT CGTGACCGCC GCCGGGATCA CTCTCGGCAT GGACGAGCTG
```

```
10201 TACAAGTAAG TGGCCGTGGA GCCTGACCGC CGGAACCAGT CCCCAGTGGA TCAGGGGGCC
10261 ACGGGGGCCT CACAGGGCCT CCTGGACAGG AAAGAGGTGC TGGGAGGGGT CATTGCCGTA
10321 GGCCTCGTGG GGCTCATCTT TGCTGTGTGC CTGGTGGGTT TCATGCTGTA CCGCATGAAG
10381 AAGAAGGACG AAGGCAGCTA CTCCTTGGAG GAGCCGAAAC AAGCCAACGG CGGGGCCTAC
 10441 CAGAAGCCCA CCAAACAGGA GGAATTCTAT GCCTAGGACC CAGCTTTCTT GTAC
```

Bibliography

Abbott, W. M., Megerman, J., Hasson, J. E., L'Italien, G., & Warnock, D. F. (1987). Effect of compliance mismatch on vascular graft patency. *J Vasc Surg, 5*(2), 376-382.

Abrams, G., Schaus, S., Goodman, S., Nealey, P., & Murphy, C. (2000). Nanoscale topography of the corneal epithelial basement membrane and Descemet's membrane of the human. *Cornea, 19*(1), 57-64.

Abrams, G. A., Bentley, E., Nealey, P. F., & Murphy, C. J. (2002). Electron microscopy of the canine corneal basement membranes. *Cells Tissues Organs, 170*(4), 251-257.

Ahmad, P. J., Osborne, L. R., & Bendeck, M. P. (2007). Bouncing Back From Elastin Deficiency. *Circulation Research, 101*(5), 439-440. doi:10.1161/circresaha.107.160358

Ahn, E. H., Kim, Y., Kshitiz, An, S. S., Afzal, J., Lee, S., . . . Levchenko, A. (2014). Spatial control of adult stem cell fate using nanotopographic cues. *Biomaterials, 35*(8), 2401-2410. doi:10.1016/j.biomaterials.2013.11.037

Ai, H. W., Henderson, J. N., Remington, S. J., & Campbell, R. E. (2006). Directed evolution of a monomeric, bright and photostable version of Clavularia cyan fluorescent protein: structural characterization and applications in fluorescence imaging. *Biochemical Journal, 400*, 531-540. doi:10.1042/Bj20060874

Alexander, C. M., Reichsman, F., Hinkes, M. T., Lincecum, J., Becker, K. A., Cumberledge, S., & Bernfield, M. (2000). Syndecan-1 is required for Wnt-1-induced mammary tumorigenesis in mice. *Nat Genet, 25*(3), 329-332. doi:10.1038/77108

Altemeier, W. A., Schlesinger, S. Y., Buell, C. A., Parks, W. C., & Chen, P. (2012). Syndecan-1 controls cell migration by activating Rap1 to regulate focal adhesion disassembly. *J Cell Sci, 125*(Pt 21), 5188-5195. doi:10.1242/jcs.109884

Angsana, J., Chen, J., Smith, S., Xiao, J., Wen, J., Liu, L., . . . Chaikof, E. L. (2015). Syndecan-1 modulates the motility and resolution responses of macrophages. *Arterioscler Thromb Vasc Biol, 35*(2), 332-340. doi:10.1161/ATVBAHA.114.304720

Aoki, K., Kamioka, Y., & Matsuda, M. (2013). Fluorescence resonance energy transfer imaging of cell signaling from in vitro to in vivo: basis of biosensor construction, live imaging, and image processing. *Dev Growth Differ, 55*(4), 515-522. doi:10.1111/dgd.12039

Arnold, M., Cavalcanti-Adam, E. A., Glass, R., Blummel, J., Eck, W., Kantlehner, M., . . . Spatz, J. P. (2004). Activation of integrin function by nanopatterned adhesive interfaces. *Chemphyschem, 5*(3), 383-388. doi:10.1002/cphc.200301014

Arnold, M., Schwieder, M., Blummel, J., Cavalcanti-Adam, E. A., Lopez-Garcia, M., Kessler, H., . . . Spatz, J. P. (2009). Cell interactions with hierarchically structured nano-patterned adhesive surfaces. *Soft Matter, 5*(1), 72-77. doi:10.1039/B815634D

Autieri, M. V., Kelemen, S. E., & Wendt, K. W. (2003). AIF-1 is an actin-polymerizing and Rac1-activating protein that promotes vascular smooth muscle cell migration. *Circ Res, 92*(10), 1107-1114. doi:10.1161/01.RES.0000074000.03562.CC

Baeyens, N., Mulligan-Kehoe, M. J., Corti, F., Simon, D. D., Ross, T. D., Rhodes, J. M., . . . Schwartz, M. A. (2014). Syndecan 4 is required for endothelial alignment in flow and atheroprotective signaling. *Proc Natl Acad Sci U S A, 111*(48), 17308-17313. doi:10.1073/pnas.1413725111

Baeyens, N., Nicoli, S., Coon, B. G., Ross, T. D., Van den Dries, K., Han, J., . . . Schwartz, M. A. (2015). Vascular remodeling is governed by a VEGFR3-dependent fluid shear stress set point. *Elife, 4*. doi:10.7554/eLife.04645

Bajar, B. T., Wang, E. S., Zhang, S., Lin, M. Z., & Chu, J. (2016). A Guide to Fluorescent Protein FRET Pairs. *Sensors, 16*(9). doi:ARTN 1488
10.3390/s16091488

Baker, A. B., Ettenson, D. S., Jonas, M., Nugent, M. A., Iozzo, R. V., & Edelman, E. R. (2008). Endothelial cells provide feedback control for vascular remodeling through a mechanosensitive autocrine TGF-beta signaling pathway. *Circ Res, 103*(3), 289-297. doi:10.1161/CIRCRESAHA.108.179465

Barreto-Ortiz, S. F., Zhang, S., Davenport, M., Fradkin, J., Ginn, B., Mao, H. Q., & Gerecht, S. (2013). A novel in vitro model for microvasculature reveals regulation of circumferential ECM organization by curvature. *PLoS One, 8*(11), e81061. doi:10.1371/journal.pone.0081061

Barry, A. K., Wang, N., & Leckband, D. E. (2015). Local VE-cadherin mechanotransduction triggers long-ranged remodeling of endothelial monolayers. *J Cell Sci, 128*(7), 1341-1351. doi:10.1242/jcs.159954

Beauvais, D. M., Burbach, B. J., & Rapraeger, A. C. (2004). The syndecan-1 ectodomain regulates alphavbeta3 integrin activity in human mammary carcinoma cells. *J Cell Biol, 167*(1), 171-181. doi:10.1083/jcb.200404171

Beauvais, D. M., Ell, B. J., McWhorter, A. R., & Rapraeger, A. C. (2009). Syndecan-1 regulates alphavbeta3 and alphavbeta5 integrin activation during angiogenesis and is blocked by synstatin, a novel peptide inhibitor. *J Exp Med, 206*(3), 691-705. doi:10.1084/jem.20081278

Beauvais, D. M., & Rapraeger, A. C. (2003). Syndecan-1-mediated cell spreading requires signaling by alphavbeta3 integrins in human breast carcinoma cells. *Exp Cell Res, 286*(2), 219-232. doi:10.1016/s0014-4827(03)00126-5

Bernfield, M., Kokenyesi, R., Kato, M., Hinkes, M. T., Spring, J., Gallo, R. L., & Lose, E. J. (1992). Biology of the syndecans: a family of transmembrane heparan sulfate proteoglycans. *Annu Rev Cell Biol, 8*, 365-393. doi:10.1146/annurev.cb.08.110192.002053

Bettinger, C. J., Langer, R., & Borenstein, J. T. (2009). Engineering Substrate Topography at the Micro- and Nanoscale to Control Cell Function. *Angewandte Chemie-International Edition, 48*(30), 5406-5415. doi:10.1002/anie.200805179

Borghi, N., Sorokina, M., Shcherbakova, O. G., Weis, W. I., Pruitt, B. L., Nelson, W. J., & Dunn, A. R. (2012). E-cadherin is under constitutive actomyosin-generated tension that is increased at cell-cell contacts upon externally applied stretch. *Proc Natl Acad Sci U S A, 109*(31), 12568-12573. doi:10.1073/pnas.1204390109

Bustelo, X. R., Sauzeau, V., & Berenjeno, I. M. (2007). GTP-binding proteins of the Rho/Rac family: regulation, effectors and functions in vivo. *Bioessays, 29*(4), 356-370. doi:10.1002/bies.20558

Carey, D. J., Bendt, K. M., & Stahl, R. C. (1996). The cytoplasmic domain of syndecan-1 is required for cytoskeleton association but not detergent insolubility - Identification of essential cytoplasmic domain residues. *Journal of Biological Chemistry, 271*(25), 15253-15260. doi:DOI 10.1074/jbc.271.25.15253

Carson, D., Hnilova, M., Yang, X., Nemeth, C. L., Tsui, J. H., Smith, A. S., . . . Kim, D. H. (2016). Nanotopography-Induced Structural Anisotropy and Sarcomere Development in Human Cardiomyocytes Derived from Induced Pluripotent Stem Cells. *ACS Appl Mater Interfaces*. doi:10.1021/acsami.5b11671

Chakravarti, R., & Adams, J. C. (2006). Comparative genomics of the syndecans defines an ancestral genomic context associated with matrilins in vertebrates. *BMC Genomics, 7*, 83. doi:10.1186/1471-2164-7-83

Chan, B., & Leong, K. (2008). Scaffolding in tissue engineering: general approaches and tissue-specific considerations. *European spine journal, 17*(4), 467-479.

Chaterji, S., Kim, P., Choe, S. H., Tsui, J. H., Lam, C. H., Ho, D. S., . . . Kim, D. H. (2014). Synergistic effects of matrix nanotopography and stiffness on vascular smooth muscle cell function. *Tissue Eng Part A, 20*(15-16), 2115-2126. doi:10.1089/ten.tea.2013.0455

Chaterji, S., Lam, C. H., Ho, D. S., Proske, D. C., & Baker, A. B. (2014). Syndecan-1 regulates vascular smooth muscle cell phenotype. *PLoS One, 9*(2), e89824. doi:10.1371/journal.pone.0089824

Chen, J., Green, J., Yurdagul, A., Jr., Albert, P., McInnis, M. C., & Orr, A. W. (2015). alphavbeta3 Integrins Mediate Flow-Induced NF-kappaB Activation, Proinflammatory Gene Expression, and Early Atherogenic Inflammation. *Am J Pathol, 185*(9), 2575-2589. doi:10.1016/j.ajpath.2015.05.013

Chervin-Petinot, A., Courcon, M., Almagro, S., Nicolas, A., Grichine, A., Grunwald, D., . . . Gulino-Debrac, D. (2012). Epithelial protein lost in neoplasm (EPLIN) interacts with alpha-catenin and actin filaments in endothelial cells and stabilizes vascular capillary network in vitro. *J Biol Chem, 287*(10), 7556-7572. doi:10.1074/jbc.M111.328682

Chute, C., Keely, P., Alexander, C., & Friedl, A. (2013). Abstract B71: Syndecan-1 promotes breast cancer metastasis by modulating tissue stiffness. *Cancer Research*. doi:10.1158/1538-7445.TIM2013-B71

Chute, C., Yang, X., Meyer, K., Yang, N., O'Neil, K., Kasza, I., . . . Friedl, A. (2018). Syndecan-1 induction in lung microenvironment supports the establishment of breast tumor metastases. *Breast Cancer Res, 20*(1), 66. doi:10.1186/s13058-018-0995-x

Cluzel, C., Saltel, F., Lussi, J., Paulhe, F., Imhof, B. A., & Wehrle-Haller, B. (2005). The mechanisms and dynamics of (alpha)v(beta)3 integrin clustering in living cells. *J Cell Biol, 171*(2), 383-392. doi:10.1083/jcb.200503017

Conway, D. E., Breckenridge, M. T., Hinde, E., Gratton, E., Chen, C. S., & Schwartz, M. A. (2013). Fluid shear stress on endothelial cells modulates mechanical tension across VE-cadherin and PECAM-1. *Curr Biol, 23*(11), 1024-1030. doi:10.1016/j.cub.2013.04.049

Dalby, M. J., Gadegaard, N., & Oreffo, R. O. (2014). Harnessing nanotopography and integrin-matrix interactions to influence stem cell fate. *Nat Mater, 13*(6), 558-569. doi:10.1038/nmat3980

Dang, J. M., & Leong, K. W. (2007). Myogenic induction of aligned mesenchymal stem cell sheets by culture on thermally responsive electrospun nanofibers. *Advanced Materials, 19*(19), 2775-2779.

Day, R. N., Booker, C. F., & Periasamy, A. (2008). Characterization of an improved donor fluorescent protein for Forster resonance energy transfer microscopy. *J Biomed Opt, 13*(3), 031203. doi:10.1117/1.2939094

Diekman, B. O., & Guilak, F. (2013). Stem cell-based therapies for osteoarthritis: challenges and opportunities. *Current opinion in rheumatology, 25*(1), 119-126.

Discher, D. E., Janmey, P., & Wang, Y. L. (2005). Tissue cells feel and respond to the stiffness of their substrate. *Science, 310*(5751), 1139-1143. doi:10.1126/science.1116995

Dixit, P., Hern-Anderson, D., Ranieri, J., & Schmidt, C. E. (2001). Vascular graft endothelialization: comparative analysis of canine and human endothelial cell migration on natural biomaterials. *J Biomed Mater Res, 56*(4), 545-555.

Dreier, B., Gasiorowski, J. Z., Morgan, J. T., Nealey, P. F., Russell, P., & Murphy, C. J. (2013). Early responses of vascular endothelial cells to topographic cues. *Am J Physiol Cell Physiol, 305*(3), C290-298. doi:10.1152/ajpcell.00264.2012

Dreier, B., Raghunathan, V. K., Russell, P., & Murphy, C. J. (2012). Focal adhesion kinase knockdown modulates the response of human corneal epithelial cells to topographic cues. *Acta Biomater, 8*(12), 4285-4294. doi:10.1016/j.actbio.2012.07.004

Dupont, S., Morsut, L., Aragona, M., Enzo, E., Giulitti, S., Cordenonsi, M., . . . Piccolo, S. (2011). Role of YAP/TAZ in mechanotransduction. *Nature, 474*(7350), 179-183. doi:10.1038/nature10137

Ebong, E. E., Lopez-Quintero, S. V., Rizzo, V., Spray, D. C., & Tarbell, J. M. (2014). Shear-induced endothelial NOS activation and remodeling via heparan sulfate, glypican-1, and syndecan-1. *Integr Biol (Camb), 6*(3), 338-347. doi:10.1039/c3ib40199e

Engler, A. J., Sen, S., Sweeney, H. L., & Discher, D. E. (2006). Matrix elasticity directs stem cell lineage specification. *Cell, 126*(4), 677-689. doi:10.1016/j.cell.2006.06.044

Eriksson, A. S., & Spillmann, D. (2012). The mutual impact of syndecan-1 and its glycosaminoglycan chains--a multivariable puzzle. *J Histochem Cytochem, 60*(12), 936-942. doi:10.1369/0022155412460242

Farhadian, F., Contard, F., Sabri, A., Samuel, J., & Rappaport, L. (1996). Fibronectin and basement membrane in cardiovascular organogenesis and disease pathogenesis. *Cardiovascular Research, 32*(3), 433-442.

Faulkner, A., Purcell, R., Hibbert, A., Latham, S., Thomson, S., Hall, W. L., . . . Bishop-Bailey, D. (2014). A thin layer angiogenesis assay: a modified basement matrix assay for

assessment of endothelial cell differentiation. *BMC Cell Biol, 15*, 41. doi:10.1186/s12860-014-0041-5

Frontini, M. J., Nong, Z., Gros, R., Drangova, M., O'Neil, C., Rahman, M. N., . . . Pickering, J. G. (2011). Fibroblast growth factor 9 delivery during angiogenesis produces durable, vasoresponsive microvessels wrapped by smooth muscle cells. *Nature biotechnology, 29*(5), 421-427.

Fu, B. M., & Tarbell, J. M. (2013). Mechano-sensing and transduction by endothelial surface glycocalyx: composition, structure, and function. *Wiley Interdiscip Rev Syst Biol Med, 5*(3), 381-390. doi:10.1002/wsbm.1211

Fu, X., Gong, M. C., Jia, T., Somlyo, A. V., & Somlyo, A. P. (1998). The effects of the Rho-kinase inhibitor Y-27632 on arachidonic acid-, GTPgammaS-, and phorbol ester-induced Ca2+-sensitization of smooth muscle. *FEBS Lett, 440*(1-2), 183-187.

Givens, C., & Tzima, E. (2016). Endothelial Mechanosignaling: Does One Sensor Fit All? *Antioxid Redox Signal, 25*(7), 373-388. doi:10.1089/ars.2015.6493

Golubovskaya, V. M., Figel, S., Ho, B. T., Johnson, C. P., Yemma, M., Huang, G., . . . Cance, W. G. (2012). A small molecule focal adhesion kinase (FAK) inhibitor, targeting Y397 site: 1-(2-hydroxyethyl)-3, 5, 7-triaza-1-azoniatricyclo [3.3.1.1(3,7)]decane; bromide effectively inhibits FAK autophosphorylation activity and decreases cancer cell viability, clonogenicity and tumor growth in vivo. *Carcinogenesis, 33*(5), 1004-1013. doi:10.1093/carcin/bgs120

Grashoff, C., Hoffman, B. D., Brenner, M. D., Zhou, R., Parsons, M., Yang, M. T., . . . Schwartz, M. A. (2010a). Measuring mechanical tension across vinculin reveals regulation of focal adhesion dynamics. *Nature, 466*(7303), 263-266. doi:10.1038/nature09198

Grashoff, C., Hoffman, B. D., Brenner, M. D., Zhou, R. B., Parsons, M., Yang, M. T., . . . Schwartz, M. A. (2010b). Measuring mechanical tension across vinculin reveals regulation of focal adhesion dynamics. *Nature, 466*(7303), 263-U143. doi:10.1038/nature09198

Gray, K. M., & Stroka, K. M. (2017). Vascular endothelial cell mechanosensing: New insights gained from biomimetic microfluidic models. *Semin Cell Dev Biol, 71*, 106-117. doi:10.1016/j.semcdb.2017.06.002

Greisler, H. P. (1990). Interactions at the blood/material interface. *Ann Vasc Surg, 4*(1), 98-103. doi:10.1007/BF02042699

Hachet-Haas, M., Converset, N., Marchal, O., Matthes, H., Gioria, S., Galzi, J. L., & Lecat, S. (2006). FRET and colocalization analyzer--a method to validate measurements of

sensitized emission FRET acquired by confocal microscopy and available as an ImageJ Plug-in. *Microsc Res Tech, 69*(12), 941-956. doi:10.1002/jemt.20376

Haga, J. H., Li, Y. S., & Chien, S. (2007). Molecular basis of the effects of mechanical stretch on vascular smooth muscle cells. *J Biomech, 40*(5), 947-960. doi:10.1016/j.jbiomech.2006.04.011

Hahn, C., & Schwartz, M. A. (2009). Mechanotransduction in vascular physiology and atherogenesis. *Nat Rev Mol Cell Biol, 10*(1), 53-62. doi:10.1038/nrm2596

Hayashida, K., Johnston, D. R., Goldberger, O., & Park, P. W. (2006). Syndecan-1 expression in epithelial cells is induced by transforming growth factor beta through a PKA-dependent pathway. *J Biol Chem, 281*(34), 24365-24374. doi:10.1074/jbc.M509320200

Hedin, U., Roy, J., Tran, P. K., Lundmark, K., & Rahman, A. (2000). Control of smooth muscle cell proliferation-the role of the basement membrane. *THROMBOSIS AND HAEMOSTASIS-STUTTGART-, 82*, 23-26.

Hill, E., Boontheekul, T., & Mooney, D. J. (2006). Regulating activation of transplanted cells controls tissue regeneration. *Proceedings of the National Academy of Sciences of the United States of America, 103*(8), 2494-2499.

Ho, B., Hou, G., Pickering, J. G., Hannigan, G., Langille, B. L., & Bendeck, M. P. (2008). Integrin-linked kinase in the vascular smooth muscle cell response to injury. *Am J Pathol, 173*(1), 278-288. doi:10.2353/ajpath.2008.071046

Hoenig, M. R., Campbell, G. R., Rolfe, B. E., & Campbell, J. H. (2005). Tissue-Engineered Blood Vessels: Alternative to Autologous Grafts? *Arteriosclerosis, thrombosis, and vascular biology, 25*(6), 1128-1134. doi:10.1161/01.atv.0000158996.03867.72

Hu, W., Yim, E. K., Reano, R. M., Leong, K. W., & Pang, S. W. (2005). Effects of nanoimprinted patterns in tissue-culture polystyrene on cell behavior. *J Vac Sci Technol A, 23*(6), 2984-2989. doi:10.1116/1.2121729

Huang, J., Davis, E. C., Chapman, S. L., Budatha, M., Marmorstein, L. Y., Word, R. A., & Yanagisawa, H. (2010). Fibulin-4 deficiency results in ascending aortic aneurysms: a potential link between abnormal smooth muscle cell phenotype and aneurysm progression. *Circ Res, 106*(3), 583-592. doi:10.1161/CIRCRESAHA.109.207852

Ibrahim, S. A., Yip, G. W., Stock, C., Pan, J. W., Neubauer, C., Poeter, M., . . . Gotte, M. (2012). Targeting of syndecan-1 by microRNA miR-10b promotes breast cancer cell motility and invasiveness via a Rho-GTPase- and E-cadherin-dependent mechanism. *Int J Cancer, 131*(6), E884-896. doi:10.1002/ijc.27629

Isenberg, B. C., & Wong, J. Y. (2006). Building structure into engineered tissues. *Materials Today, 9*(12), 54-60. doi:http://dx.doi.org/10.1016/S1369-7021(06)71743-6

Ishikawa, T., & Kramer, R. H. (2010). Sdc1 negatively modulates carcinoma cell motility and invasion. *Exp Cell Res, 316*(6), 951-965. doi:10.1016/j.yexcr.2009.12.013

Jenkins, L. M., Horst, B., Lancaster, C. L., & Mythreye, K. (2018). Dually modified transmembrane proteoglycans in development and disease. *Cytokine Growth Factor Rev, 39*, 124-136. doi:10.1016/j.cytogfr.2017.12.003

Jiang, G., Huang, A. H., Cai, Y., Tanase, M., & Sheetz, M. P. (2006). Rigidity sensing at the leading edge through alphavbeta3 integrins and RPTPalpha. *Biophys J, 90*(5), 1804-1809. doi:10.1529/biophysj.105.072462

Kalluri, R. (2003). Basement membranes: structure, assembly and role in tumour angiogenesis. *Nat Rev Cancer, 3*(6), 422-433.

Karp, J. M., & Langer, R. (2007). Development and therapeutic applications of advanced biomaterials. *Current Opinion in Biotechnology, 18*(5), 454-459. doi:http://dx.doi.org/10.1016/j.copbio.2007.09.008

Kato, R. B., Roy, B., De Oliveira, F. S., Ferraz, E. P., De Oliveira, P. T., Kemper, A. G., . . . Beloti, M. M. (2014). Nanotopography directs mesenchymal stem cells to osteoblast lineage through regulation of microRNA-SMAD-BMP-2 circuit. *J Cell Physiol, 229*(11), 1690-1696. doi:10.1002/jcp.24614

Katsumi, A., Naoe, T., Matsushita, T., Kaibuchi, K., & Schwartz, M. A. (2005). Integrin activation and matrix binding mediate cellular responses to mechanical stretch. *J Biol Chem, 280*(17), 16546-16549. doi:10.1074/jbc.C400455200

Khotskaya, Y. B., Dai, Y., Ritchie, J. P., MacLeod, V., Yang, Y., Zinn, K., & Sanderson, R. D. (2009). Syndecan-1 is required for robust growth, vascularization, and metastasis of myeloma tumors in vivo. *J Biol Chem, 284*(38), 26085-26095. doi:10.1074/jbc.M109.018473

Kim, D. H., Han, K., Gupta, K., Kwon, K. W., Suh, K. Y., & Levchenko, A. (2009). Mechanosensitivity of fibroblast cell shape and movement to anisotropic substratum topography gradients. *Biomaterials, 30*(29), 5433-5444. doi:10.1016/j.biomaterials.2009.06.042

Kim, D. H., Kshitiz, Smith, R. R., Kim, P., Ahn, E. H., Kim, H. N., . . . Levchenko, A. (2012). Nanopatterned cardiac cell patches promote stem cell niche formation and myocardial regeneration. *Integr Biol (Camb), 4*(9), 1019-1033. doi:10.1039/c2ib20067h

Kim, D. H., Provenzano, P. P., Smith, C. L., & Levchenko, A. (2012a). Matrix nanotopography as a regulator of cell function. *Journal of Cell Biology, 197*(3), 351-360. doi:10.1083/jcb.201108062

Kim, D. H., Provenzano, P. P., Smith, C. L., & Levchenko, A. (2012b). Matrix nanotopography as a regulator of cell function. *J Cell Biol, 197*(3), 351-360. doi:10.1083/jcb.201108062

Kim, H. N., Jiao, A., Hwang, N. S., Kim, M. S., Kang, D. H., Kim, D. H., & Suh, K. Y. (2013). Nanotopography-guided tissue engineering and regenerative medicine. *Adv Drug Deliv Rev, 65*(4), 536-558. doi:10.1016/j.addr.2012.07.014

Koda, J. E., Rapraeger, A., & Bernfield, M. (1985). Heparan sulfate proteoglycans from mouse mammary epithelial cells. Cell surface proteoglycan as a receptor for interstitial collagens. *J Biol Chem, 260*(13), 8157-8162.

Kogata, N., Tribe, R. M., Fassler, R., Way, M., & Adams, R. H. (2009). Integrin-linked kinase controls vascular wall formation by negatively regulating Rho/ROCK-mediated vascular smooth muscle cell contraction. *Genes Dev, 23*(19), 2278-2283. doi:10.1101/gad.535409

Krieg, M., Dunn, A. R., & Goodman, M. B. (2014). Mechanical control of the sense of touch by beta-spectrin. *Nat Cell Biol, 16*(3), 224-233. doi:10.1038/ncb2915

Kumar, A., Ouyang, M., Van den Dries, K., McGhee, E. J., Tanaka, K., Anderson, M. D., . . . Schwartz, M. A. (2016a). Correction: Talin tension sensor reveals novel features of focal adhesion force transmission and mechanosensitivity. *J Cell Biol, 214*(2), 231. doi:10.1083/jcb.201510012070620160c

Kumar, A., Ouyang, M., Van den Dries, K., McGhee, E. J., Tanaka, K., Anderson, M. D., . . . Schwartz, M. A. (2016b). Talin tension sensor reveals novel features of focal adhesion force transmission and mechanosensitivity. *J Cell Biol, 213*(3), 371-383. doi:10.1083/jcb.201510012

Langford, J. K., Stanley, M. J., Cao, D., & Sanderson, R. D. (1998). Multiple heparan sulfate chains are required for optimal syndecan-1 function. *J Biol Chem, 273*(45), 29965-29971. doi:10.1074/jbc.273.45.29965

Le, V., Lee, J., Chaterji, S., Spencer, A., Liu, Y. L., Kim, P., . . . Baker, A. B. (2018). Syndecan-1 in mechanosensing of nanotopological cues in engineered materials. *Biomaterials, 155*, 13-24. doi:10.1016/j.biomaterials.2017.11.007

Lesauskaite, V., Tanganelli, P., Sassi, C., Neri, E., Diciolla, F., Ivanoviene, L., . . . Spina, D. (2001). Smooth muscle cells of the media in the dilatative pathology of ascending thoracic aorta: morphology, immunoreactivity for osteopontin, matrix metalloproteinases, and their inhibitors. *Hum Pathol, 32*(9), 1003-1011. doi:10.1053/hupa.2001.27107

Lesman, A., Gepstein, L., & Levenberg, S. (2010). Vascularization shaping the heart. *Annals of the New York Academy of Sciences, 1188*(1), 46-51. doi:10.1111/j.1749-6632.2009.05082.x

Liliensiek, S. J., Wood, J. A., Yong, J., Auerbach, R., Nealey, P. F., & Murphy, C. J. (2010). Modulation of human vascular endothelial cell behaviors by nanotopographic cues. *Biomaterials, 31*(20), 5418-5426. doi:10.1016/j.biomaterials.2010.03.045

Lin, Y.-D., Luo, C.-Y., Hu, Y.-N., Yeh, M.-L., Hsueh, Y.-C., Chang, M.-Y., . . . Hsieh, P. C. H. (2012). Instructive Nanofiber Scaffolds with VEGF Create a Microenvironment for Arteriogenesis and Cardiac Repair. *Science Translational Medicine, 4*(146), 146ra109. doi:10.1126/scitranslmed.3003841

Loesberg, W. A., te Riet, J., van Delft, F. C., Schon, P., Figdor, C. G., Speller, S., . . . Jansen, J. A. (2007). The threshold at which substrate nanogroove dimensions may influence fibroblast alignment and adhesion. *Biomaterials, 28*(27), 3944-3951. doi:10.1016/j.biomaterials.2007.05.030

Lu, D., & Kassab, G. S. (2011). Role of shear stress and stretch in vascular mechanobiology. *J R Soc Interface, 8*(63), 1379-1385. doi:10.1098/rsif.2011.0177

Luo, T., Mohan, K., Iglesias, P. A., & Robinson, D. N. (2013). Molecular mechanisms of cellular mechanosensing. *Nat Mater, 12*(11), 1064-1071. doi:10.1038/nmat3772

Lutolf, M., & Hubbell, J. (2005). Synthetic biomaterials as instructive extracellular microenvironments for morphogenesis in tissue engineering. *Nature biotechnology, 23*(1), 47-55.

Maeda, T., Sakabe, T., Sunaga, A., Sakai, K., Rivera, A. L., Keene, D. R., . . . Sakai, T. (2011). Conversion of mechanical force into TGF-beta-mediated biochemical signals. *Curr Biol, 21*(11), 933-941. doi:10.1016/j.cub.2011.04.007

Martino, F., Perestrelo, A. R., Vinarsky, V., Pagliari, S., & Forte, G. (2018). Cellular Mechanotransduction: From Tension to Function. *Front Physiol, 9*, 824. doi:10.3389/fphys.2018.00824

Mason, T. G., Ganesan, K., van Zanten, J. H., Wirtz, D., & Kuo, S. C. (1997). Particle tracking microrheology of complex fluids. *Phys Rev Lett, 79*(17), 3282.

Mattson, J. M., Turcotte, R., & Zhang, Y. (2017). Glycosaminoglycans contribute to extracellular matrix fiber recruitment and arterial wall mechanics. *Biomech Model Mechanobiol, 16*(1), 213-225. doi:10.1007/s10237-016-0811-4

McQuade, K. J., Beauvais, D. M., Burbach, B. J., & Rapraeger, A. C. (2006). Syndecan-1 regulates alphavbeta5 integrin activity in B82L fibroblasts. *J Cell Sci, 119*(Pt 12), 2445-2456. doi:10.1242/jcs.02970

Mengsteab, P. Y., Uto, K., Smith, A. S., Frankel, S., Fisher, E., Nawas, Z., . . . Kim, D. H. (2016). Spatiotemporal control of cardiac anisotropy using dynamic nanotopographic cues. *Biomaterials, 86*, 1-10. doi:10.1016/j.biomaterials.2016.01.062

Miettinen, H. M., Edwards, S. N., & Jalkanen, M. (1994). Analysis of transport and targeting of syndecan-1: effect of cytoplasmic tail deletions. *Mol Biol Cell, 5*(12), 1325-1339. doi:10.1091/mbc.5.12.1325

Morgan, M. R., Humphries, M. J., & Bass, M. D. (2007). Synergistic control of cell adhesion by integrins and syndecans. *Nat Rev Mol Cell Biol, 8*(12), 957-969. doi:10.1038/nrm2289

Mould, A. P., Askari, J. A., Barton, S., Kline, A. D., McEwan, P. A., Craig, S. E., & Humphries, M. J. (2002). Integrin activation involves a conformational change in the alpha 1 helix of the beta subunit A-domain. *J Biol Chem, 277*(22), 19800-19805. doi:10.1074/jbc.M201571200

Murakami, M., & Simons, M. (2009). Regulation of vascular integrity. *Journal of molecular medicine, 87*(6), 571-582.
Mythreye, K., & Blobe, G. C. (2009). Proteoglycan signaling co-receptors: roles in cell adhesion, migration and invasion. *Cell Signal, 21*(11), 1548-1558. doi:10.1016/j.cellsig.2009.05.001

Nagai, T., Ibata, K., Park, E. S., Kubota, M., Mikoshiba, K., & Miyawaki, A. (2002). A variant of yellow fluorescent protein with fast and efficient maturation for cell-biological applications. *Nat Biotechnol, 20*(1), 87-90. doi:10.1038/nbt0102-87

Nerlich, A., Rohde, M., Talay, S. R., Genth, H., Just, I., & Chhatwal, G. S. (2009). Invasion of endothelial cells by tissue-invasive M3 type group A streptococci requires Src kinase and activation of Rac1 by a phosphatidylinositol 3-kinase-independent mechanism. *J Biol Chem, 284*(30), 20319-20328. doi:10.1074/jbc.M109.016501

Nikolova, G., Strilic, B., & Lammert, E. (2007). The vascular niche and its basement membrane. *Trends in cell biology, 17*(1), 19-25. doi:http://dx.doi.org/10.1016/j.tcb.2006.11.005

Ogawa, T., Tsubota, Y., Hashimoto, J., Kariya, Y., & Miyazaki, K. (2007). The short arm of laminin gamma2 chain of laminin-5 (laminin-332) binds syndecan-1 and regulates cellular adhesion and migration by suppressing phosphorylation of integrin beta4 chain. *Mol Biol Cell, 18*(5), 1621-1633. doi:10.1091/mbc.E06-09-0806

Orlandini, M., Nucciotti, S., Galvagni, F., Bardelli, M., Rocchigiani, M., Petraglia, F., & Oliviero, S. (2008). Morphogenesis of human endothelial cells is inhibited by DAB2 via Src. *FEBS Lett, 582*(17), 2542-2548. doi:10.1016/j.febslet.2008.06.025

Osawa, M., Masuda, M., Kusano, K., & Fujiwara, K. (2002). Evidence for a role of platelet endothelial cell adhesion molecule-1 in endothelial cell mechanosignal transduction: is it a mechanoresponsive molecule? *J Cell Biol, 158*(4), 773-785. doi:10.1083/jcb.200205049

Paszek, M. J., DuFort, C. C., Rossier, O., Bainer, R., Mouw, J. K., Godula, K., . . . Weaver, V. M. (2014). The cancer glycocalyx mechanically primes integrin-mediated growth and survival. *Nature, 511*(7509), 319-+. doi:10.1038/nature13535

Patterson, J. T., Gilliland, T., Maxfield, M. W., Church, S., Naito, Y., Shinoka, T., & Breuer, C. K. (2012). Tissue-engineered vascular grafts for use in the treatment of congenital heart disease: from the bench to the clinic and back again. *Regenerative medicine, 7*(3), 409-419.

Peng, G., Wang, J., Lu, W., & Ran, P. (2010). Isolation and primary culture of rat distal pulmonary venous smooth muscle cells. *Hypertens Res, 33*(4), 308-313. doi:10.1038/hr.2009.234

Perillo, E. P., Liu, Y. L., Huynh, K., Liu, C., Chou, C. K., Hung, M. C., . . . Dunn, A. K. (2015). Deep and high-resolution three-dimensional tracking of single particles using nonlinear and multiplexed illumination. *Nat Commun, 6*, 7874. doi:10.1038/ncomms8874

Peyton, S. R., & Putnam, A. J. (2005). Extracellular matrix rigidity governs smooth muscle cell motility in a biphasic fashion. *J Cell Physiol, 204*(1), 198-209. doi:10.1002/jcp.20274

Rapraeger, A. C. (2013). Synstatin: a selective inhibitor of the syndecan-1-coupled IGF1R-alphavbeta3 integrin complex in tumorigenesis and angiogenesis. *FEBS J, 280*(10), 2207-2215. doi:10.1111/febs.12160

Roper, J. A., Williamson, R. C., & Bass, M. D. (2012). Syndecan and integrin interactomes: large complexes in small spaces. *Curr Opin Struct Biol, 22*(5), 583-590. doi:10.1016/j.sbi.2012.07.003

Ruiz-Ortega, M., Rodriguez-Vita, J., Sanchez-Lopez, E., Carvajal, G., & Egido, J. (2007). TGF-beta signaling in vascular fibrosis. *Cardiovasc Res, 74*(2), 196-206. doi:10.1016/j.cardiores.2007.02.008

Sakai, T., Li, S., Docheva, D., Grashoff, C., Sakai, K., Kostka, G., . . . Fassler, R. (2003). Integrin-linked kinase (ILK) is required for polarizing the epiblast, cell adhesion, and controlling actin accumulation. *Genes Dev, 17*(7), 926-940. doi:10.1101/gad.255603

Samuel, R., Daheron, L., Liao, S., Vardam, T., Kamoun, W. S., Batista, A., . . . Au, P. (2013). Generation of functionally competent and durable engineered blood vessels from human induced pluripotent stem cells. *Proceedings of the National Academy of Sciences, 110*(31), 12774-12779.

Shin'oka, T., Imai, Y., & Ikada, Y. (2001). Transplantation of a tissue-engineered pulmonary artery. *New England Journal of Medicine, 344*(7), 532-533.
Stepp, M. A., Gibson, H. E., Gala, P. H., Iglesia, D. D., Pajoohesh-Ganji, A., Pal-Ghosh, S., . . . Bernfield, M. (2002). Defects in keratinocyte activation during wound healing in the syndecan-1-deficient mouse. *J Cell Sci, 115*(Pt 23), 4517-4531. doi:10.1242/jcs.00128

Stewart, M. D., Ramani, V. C., & Sanderson, R. D. (2015). Shed syndecan-1 translocates to the nucleus of cells delivering growth factors and inhibiting histone acetylation: a novel mechanism of tumor-host cross-talk. *J Biol Chem, 290*(2), 941-949. doi:10.1074/jbc.M114.608455

Su, G., Blaine, S. A., Qiao, D., & Friedl, A. (2007). Shedding of syndecan-1 by stromal fibroblasts stimulates human breast cancer cell proliferation via FGF2 activation. *J Biol Chem, 282*(20), 14906-14915. doi:10.1074/jbc.M611739200
Suh, K.-Y., Park, M. C., & Kim, P. (2009). Capillary Force Lithography: A Versatile Tool for Structured Biomaterials Interface Towards Cell and Tissue Engineering. *Advanced Functional Materials, 19*(17), 2699-2712. doi:10.1002/adfm.200900771

Swift, J., Ivanovska, I. L., Buxboim, A., Harada, T., Dingal, P. C., Pinter, J., . . . Discher, D. E. (2013). Nuclear lamin-A scales with tissue stiffness and enhances matrix-directed differentiation. *Science, 341*(6149), 1240104. doi:10.1126/science.1240104

Tarbell, J. M., Simon, S. I., & Curry, F. R. (2014). Mechanosensing at the vascular interface. *Annu Rev Biomed Eng, 16*, 505-532. doi:10.1146/annurev-bioeng-071813-104908

Tzima, E., del Pozo, M. A., Shattil, S. J., Chien, S., & Schwartz, M. A. (2001). Activation of integrins in endothelial cells by fluid shear stress mediates Rho-dependent cytoskeletal alignment. *EMBO J, 20*(17), 4639-4647. doi:10.1093/emboj/20.17.4639

Tzima, E., Irani-Tehrani, M., Kiosses, W. B., Dejana, E., Schultz, D. A., Engelhardt, B., . . . Schwartz, M. A. (2005). A mechanosensory complex that mediates the endothelial cell response to fluid shear stress. *Nature, 437*(7057), 426-431. doi:10.1038/nature03952

Varelas, X., Samavarchi-Tehrani, P., Narimatsu, M., Weiss, A., Cockburn, K., Larsen, B. G., . . . Wrana, J. L. (2010). The Crumbs complex couples cell density sensing to Hippo-dependent control of the TGF-beta-SMAD pathway. *Dev Cell, 19*(6), 831-844. doi:10.1016/j.devcel.2010.11.012

Voyvodic, P. L., Min, D., Liu, R., Williams, E., Chitalia, V., Dunn, A. K., & Baker, A. B. (2014). Loss of syndecan-1 induces a pro-inflammatory phenotype in endothelial cells with a dysregulated response to atheroprotective flow. *J Biol Chem, 289*(14), 9547-9559. doi:10.1074/jbc.M113.541573

Vuoriluoto, K., Jokinen, J., Kallio, K., Salmivirta, M., Heino, J., & Ivaska, J. (2008). Syndecan-1 supports integrin alpha2beta1-mediated adhesion to collagen. *Exp Cell Res, 314*(18), 3369-3381. doi:10.1016/j.yexcr.2008.07.005

Wang, N. (2017). Review of Cellular Mechanotransduction. *J Phys D Appl Phys, 50*(23).
Wang, Y., Shi, H., Qiao, J., Tian, Y., Wu, M., Zhang, W., . . . Huang, Y. (2014). Electrospun tubular scaffold with circumferentially aligned nanofibers for regulating smooth muscle cell growth. *ACS Appl Mater Interfaces, 6*(4), 2958-2962. doi:10.1021/am405556x

Wolinksy, H., & Glagov, S. (1967). A Lamellar Unit of Aortic Medial Structure and Function in Mammals. *Circulation Research, 20*(1), 99-111. doi:10.1161/01.res.20.1.99

Wood, J. A., Shah, N. M., McKee, C. T., Hughbanks, M. L., Liliensiek, S. J., Russell, P., & Murphy, C. J. (2011). The role of substratum compliance of hydrogels on vascular endothelial cell behavior. *Biomaterials, 32*(22), 5056-5064. doi:10.1016/j.biomaterials.2011.03.054

Woods, A. (2001). Syndecans: transmembrane modulators of adhesion and matrix assembly. *J Clin Invest, 107*(8), 935-941. doi:10.1172/JCI12802

Wu, P. H., Hale, C. M., Chen, W. C., Lee, J. S., Tseng, Y., & Wirtz, D. (2012). High-throughput ballistic injection nanorheology to measure cell mechanics. *Nat Protoc, 7*(1), 155-170. doi:10.1038/nprot.2011.436

Xia, N., Thodeti, C. K., Hunt, T. P., Xu, Q., Ho, M., Whitesides, G. M., . . . Ingber, D. E. (2008). Directional control of cell motility through focal adhesion positioning and spatial control of Rac activation. *FASEB J, 22*(6), 1649-1659. doi:10.1096/fj.07-090571

Xu, J., Viasnoff, V., & Wirtz, D. (1998). Compliance of actin filament networks measured by particle-tracking microrheology and diffusing wave spectroscopy. *Rheol Acta, 37*(4), 387-398.

Yang, N., & Friedl, A. (2016). Syndecan-1-Induced ECM Fiber Alignment Requires Integrin alphavbeta3 and Syndecan-1 Ectodomain and Heparan Sulfate Chains. *PLoS One, 11*(2), e0150132. doi:10.1371/journal.pone.0150132

Ye, G. J., Nesmith, A. P., & Parker, K. K. (2014). The role of mechanotransduction on vascular smooth muscle myocytes' [corrected] cytoskeleton and contractile function. *Anat Rec (Hoboken), 297*(9), 1758-1769. doi:10.1002/ar.22983

Yim, E., Reano, R., Pang, S., Yee, A., Chen, C., & Leong, K. (2005). Nanopattern-induced changes in morphology and motility of smooth muscle cells. *Biomaterials, 26*(26), 5405-5413. doi:10.1016/j.biomaterials.2005.01.058

Yim, E. K., Reano, R. M., Pang, S. W., Yee, A. F., Chen, C. S., & Leong, K. W. (2005). Nanopattern-induced changes in morphology and motility of smooth muscle cells. *Biomaterials, 26*(26), 5405-5413. doi:10.1016/j.biomaterials.2005.01.058

Yu, D., Makkar, G., Strickland, D. K., Blanpied, T. A., Stumpo, D. J., Blackshear, P. J., . . . Monahan, T. S. (2015). Myristoylated Alanine-Rich Protein Kinase Substrate (MARCKS) Regulates Small GTPase Rac1 and Cdc42 Activity and Is a Critical Mediator of Vascular Smooth Muscle Cell Migration in Intimal Hyperplasia Formation. *J Am Heart Assoc, 4*(10), e002255. doi:10.1161/JAHA.115.002255

Zacharias, D. A., Violin, J. D., Newton, A. C., & Tsien, R. Y. (2002). Partitioning of lipid-modified monomeric GFPs into membrane microdomains of live cells. *Science, 296*(5569), 913-916. doi:10.1126/science.1068539

Zhou, Q. H., Xie, J., Bao, M., Yuan, H. H., Ye, Z. Y., Lou, X. X., & Zhang, Y. Z. (2015). Engineering aligned electrospun PLLA microfibers with nano-porous surface nanotopography for modulating the responses of vascular smooth muscle cells. *Journal of Materials Chemistry B, 3*(21), 4439-4450. doi:10.1039/c5tb00051c

Zhu, L. H., Wang, L., Wang, D., Jiang, H., Tang, Q. Z., Yan, L., . . . Li, H. (2010). Puerarin attenuates high-glucose-and diabetes-induced vascular smooth muscle cell proliferation by blocking PKCbeta2/Rac1-dependent signaling. *Free Radic Biol Med, 48*(4), 471-482. doi:10.1016/j.freeradbiomed.2009.10.040

Zorlutuna, P., Elsheikh, A., & Hasirci, V. (2009). Nanopatterning of collagen scaffolds improve the mechanical properties of tissue engineered vascular grafts. *Biomacromolecules, 10*(4), 814-821. doi:10.1021/bm801307y